UNIVERSITEIT VAN AMSTERDAM

VU VRIJE UNIVERSITEIT AMSTERDAM

MSc Physics & Astronomy
Science for Energy and Sustainability

Eu^{3+} doped $CsPbBr_3$ for white LEDs

by
Linde van de Ven
10559051

Master thesis
60 EC
February 2021 - February 2022

Supervisor
prof. dr. Erik Garnett

Second examiner
prof. dr. Bruno Ehrler

SEABOROUGH
Giving Light Purpose

AMOLF physics of functional complex matter

Abstract

To combat climate change, electricity consumption has to be reduced. Light emitting diodes (LEDs) are an energy-saving alternative to energy intensive forms of lighting. White LEDs (wLEDs) give off an undesirable 'cool' blue hue. Efficient and narrow emission peak red emitters are needed for 'warm' wLEDs. Eu^{3+} was incorporated in the $CsPbBr_3$ perovskite lattice to investigate the qualities of green emitter $CsPbBr_3$ as a host material and energy donor for Eu^{3+} red emission. Eu^{3+} is a suitable material for use as a red phosphor in wLEDs because of its narrow emission peaks around 610 nm.

$CsPbBr_3$ was encapsulated in silica molecular sieve MCM-41 to improve stability. This protects the perovskite from the influence of oxygen, water, heat, and illumination. Eu^{3+} was effectively doped in the perovskite lattice. $CsPbBr_3$ emission was preserved, however, Eu^{3+} emission was not enhanced. Enhanced Eu^{3+} emission could be seen upon incorporation in a mesoporous yttria-stabilized zirconia (mYSZ) host. $CsPbBr_3$ was formed in the pores of mYSZ, and showed improved stability under the influence of oxygen and water. No enhanced Eu^{3+} emisison was detected when incorporating $CsPbBr_3$ in the pores of Eu^{3+} doped mYSZ. High intensity Eu^{3+} emission was found from Eu^{3+} β-diketonate complex $Eu(tta)_4P(Ph)_4$ with PLQY up to 52% under 405 nm illumination. Emission intensity of this complex was low under 460 nm excitation.

Contents

1 Introduction **3**

2 Theory **4**
2.1 White LEDs . . . 4
2.2 $CsPbBr_3$ as a green LED phosphor . . . 6
2.2.1 $CsPbX_3$ . . . 6
2.2.2 Stability of $CsPbBr_3$ . . . 7
2.2.3 $CsPbBr_3$ in silica mesoporous sieves . . . 8
2.3 Eu^{3+} as a red LED phosphor . . . 11
2.3.1 Lanthanides . . . 11
2.3.2 Electron configuration of Eu^{3+} . . . 11
2.3.3 Judd-Ofelt theory . . . 12
2.3.4 Emission . . . 13
2.3.5 Absorption . . . 15
2.4 Energy transfer to Eu^{3+} . . . 17
2.4.1 Dexter energy transfer and Förster Resonance Energy Transfer . . . 17
2.4.2 Dexter energy transfer in a Eu^{3+} β-diketonate complex . . . 18
2.4.3 Förster Resonance Energy Transfer from Tb^{3+} to Eu^{3+} . . . 19
2.5 Enhanced Eu^{3+} emission by doping in $CsPbBr_3$ . . . 20

3 Methods **22**

4 Results and Discussion **26**
4.1 $CsPbBr_3@SiO_2$ . . . 26
4.2 Stability of $CsPbBr_3@SiO_2$ . . . 27
4.2.1 Stability of $CsPbBr_3@SiO_2$ under industrial laser power . . . 28
4.3 Eu^{3+} doped $CsPbBr_3@SiO_2$ . . . 30
4.3.1 $CsPbBr_3$:$Eu^{3+}@SiO_2$ annealed at 900°C . . . 31
4.3.2 $CsPbBr_3$:$Eu^{3+}@SiO_2$ combined with red phosphor Y_2O_3:15%Eu^{3+} . . . 33
4.4 Mesoporous yttria-stabilized zirconia . . . 34
4.4.1 Encapsulating $CsPbBr_3$ with mesoporous yttria-stabilized zirconia . . . 34
4.4.2 Eu^{3+} doped mesoporous yttria-stabilized zirconia . . . 37
4.4.3 mYSZ:10%Eu^{3+} annealed at high temperature . . . 38
4.5 Eu^{3+} β-diketonate complex . . . 40
4.5.1 $CsPbBr_3@SiO_2$ combined with Eu^{3+} β-diketonate . . . 41

5 Conclusions and outlook **42**

Acknowledgements **44**

Bibliography **45**

A Appendix **52**
A.1 Setup for testing stability of $CsPbBr_3@SiO_2$ under heat and illumination . . . 52
A.2 PLQY measurements . . . 53
A.3 Lorentzian fit of $CsPbBr_3@SiO_2$ . . . 54

A.4 Tauc plot of $CsPbBr_3$@SiO_2 54
A.5 Y_2O_3:15%Eu^{3+} on $CsPbBr_3$ nanocubes 55
A.6 Luminescence of $CsPbBr_3$@mYSZ and mYSZ:10%Eu^{3+} in 1M HCl 56
A.7 Stability of the Eu^{3+} β-diketonate complex 57

Chapter 1

Introduction

Climate change causes periods of extreme drought and rainfall, leading to famines, floods, fires, and a loss of biodiversity [2]. Average temperatures have already increased by 1°C and the sea level has risen by 20 cm in the last 100 years [3]. Although the international Paris Agreement in 2015 aimed for a maximum temperature increase of 1.5°C, it is likely this will already be reached between 2030 and 2052 [3]. There has been a growing call for action to stop emitting greenhouse gasses and stop climate change.

Figure 1.1: a) the Creek Fire, Sierra National Forest in California, 2021. Many wildfires are directly caused by climate change [4]. In 2021, a record of wildfires spread across the globe. Photo from [4], b) at a climate protest in Amsterdam, thousands could be seen demonstrating. Photo from [5]

To stop human induced climate change, energy use has to drastically decline. Lighting is responsible for a large part of our energy use and is a large source of CO_2 emission. About 6% of global electricity is used for home lighting, and 10% for commercial lighting [6]. Therefore, an increase in lighting efficiency could have a vast impact on global emissions.

Light-emitting diodes (LEDs) provide a sustainable way of lighting. Compared to incandescent lighting, LEDs have a tenfold increase in efficiency [6], low heat loss, and a long device lifetime [7], making them more durable. Their low production cost also make them an attractive commercial option [7].

White LEDs (wLEDs) are crucial for lighting. Most wLEDs give off an undesirable 'cool' blue white light, which is unpleasant to eyes and can have adverse effects on health [8]. This underlines the need for wLEDs with a 'warm' color. For this purpose, efficient and narrow emission peak red emitters have to be found.

This thesis is aimed towards using Eu^{3+} as a red emitter because of its narrow emission peaks [9]. However, Eu^{3+} is not a good absorber [1]. To enhance emission, Eu^{3+} is doped in perovskite $CsPbBr_3$. By utilizing $CsPbBr_3$ as a host material, Eu^{3+} excitation could be enhanced, and energy could be transferred from the perovskite to Eu^{3+}. $CsPbBr_3$ is encapsulated in a mesoporous silica matrix to improve stability, and can also serve as a green phosphor. Energy transfer from $CsPbBr_3$ is also investigated by incorporating Eu^{3+} and $CsPbBr_3$ in a mesoporous yttria-stabilized zirconia host. Lastly, Eu^{3+} emission is improved by adding β-diketonate ligands.

Chapter 2

Theory

2.1 White LEDs

An LED consists of a semiconductor that emits photons upon electrical excitation. Electrons in an excited state radiatively recombine with electron holes and emit a photon. The wavelength of the emitted photon is dependent on the bandgap of the semiconductor, which is defined as the energy gap between the conduction and the valence band [10]. The bandgap varies between materials, and using different materials, LEDs are available in all colors.

A white LED can be made by combining a blue or ultraviolet LED-chip with a phosphor that can absorb this blue or UV light and downconvert it to other wavelengths (see Figure 2.1 b), c)) [7]. The light emitted by the LED-chip and by the phosphor combine to result in white light. Blue LED-chips are mostly made of indium gallium nitride (InGaN), a semiconductor with emission around 460 nm [11]. Blue LED-chips are more efficient and cost-effective compared to UV LED-chips, and more suited for use in lighting displays [6].

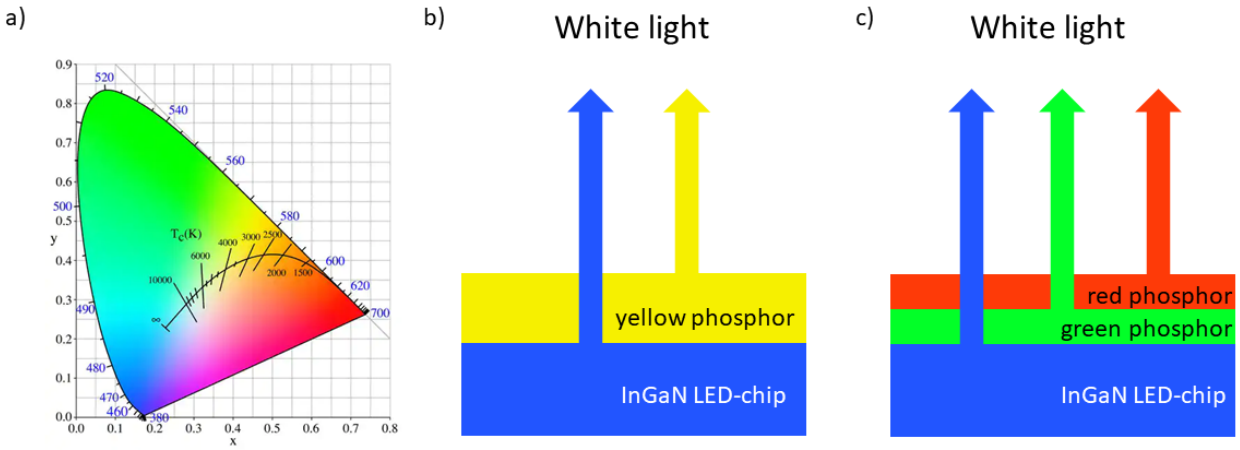

Figure 2.1: a) CIE 1931 chromaticity diagram with the CCT blackbody curve. Figure from [12], b) a blue LED-chip with a yellow downconverting phosphor, c) a blue LED chip with a red and a green downconverting phosphor

The color of wLEDs can be compared to that of an ideal black-body radiator through the correlated color temperature (CCT) [13]. A lower CCT corresponds to a 'warm' white light with a yellow hue, while a high CCT corresponds to a 'cool' blueish white light [14]. The CCT blackbody curve is shown in Figure 2.1 a). LED emission color can be depicted in a CIE 1931 color space chromaticity diagram (see Figure 2.1 a)) [13]. An emitter with high color purity is displayed on the edge of the diagram. For white LEDs, high purity color is desirable, which can be achieved by employing narrow-band emitters with low full-width-half-maximum (FWHM) [13]. The color gamut of an LED is the space between different colored emitters on the CIE chromaticity diagram. A warm white LED has a wide color gamut.

The human eye can detect light between 400 and 700 nm, with a large sensitivity to green light, but much less to blue and red light [14]. The emission spectrum of an wLED has to be adjusted accordingly. The most preferred spectrum has narrow bandwidth emission, with small FWHM [15]. A narrow-band red phosphor, a broader green and a blue InGaN LED-chip are experienced as favorable [14].

Often a single yellow phosphor is used, as is depicted in Figure 2.1 b). The most used phosphor is the yellow YAG ($Y_3Al_5O_{12}$:Ce^{3+}) phosphor, which can reach a photoluminescence quantum yield (PLQY) of 38.4% [16]. The PLQY is defined as the ratio between the amount of photons that are emitted divided by the amount of photons that are absorbed [14]. However, with only a single phosphor the color of the light cannot be tuned. The light from these LEDs appears very cool due to the absence of red light [17] and have a CCT above 4500, corresponding to a blueish cool color.

An LED with two phosphors can produce a wider color gamut. Both phosphors are able to absorb blue light, with one phosphor downconverting the light into green and the other into red light, as can be seen in Figure 2.1c)). By controlling the emission of these phosphors, color rendering can be optimized and white light can potentially have any hue. Research on these phosphors has yielded many different phosphors, like $Sr_2MgAl_{22}O_{36}$:Mn^{2+}, K_2SiF_6:Mn^{4+}, $Ba_2LiSi_7AlN_{12}$:Eu^{2+}, $SrLiAl_3N_4$:Eu^{2+} and more [18]. Many red phosphors have a broad red emission, which leads to a low color purity. Moreover, part of the emission spectrum lies outside of the range of the human eye, leading to a decrease in effectivity. Conventional red phosphors do not have a high PLQY and are expensive to synthesize [19].

LEDs have an operating temperature of around 80°C, with peak temperatures that can rise up to 120°C [7]. Most LEDs have an operating power of 1-3 W/mm^2, while high power or mini LEDs can reach powers of 10 W/mm^2 [20]. Phosphors must be able to withstand conditions in an LED encasing, with a lifetime of 50000 hours, similar to that of the LED-chip. Phosphors that are currently used are often not as stable as LED-chips, leading to a decrease in lifetime and unstable color purity of LEDs [14].

$CsPbX_3$ metal halide perovskites are promising candidates for LED phosphors [14], [18]. These materials have a high PLQY, narrow FWHM and tunable center wavelength [22]. $CsPbBr_3$ exhibits green emission, which makes it suited for use as a green phosphor. Eu^{3+} can be used as a red phosphor because of its extremely narrow FWHM and bright emission centered around 610 nm [1]. By doping Eu^{3+} in $CsPbBr_3$ these materials could serve as a double phosphor for wLEDs.

2.2 $CsPbBr_3$ as a green LED phosphor

2.2.1 $CsPbX_3$

Perovskites are a class of materials with possible applications in solar cells and LEDs. Since perovskites emerged as a research interest 25 years ago, research efforts have skyrocketed. This has resulted in an enormous growth in quantum efficiency [21].

Perovskite is a material with the same crystal structure as the mineral calcium titanium oxide ($CaTiO_3$). This structure consists of an A cation, a B cation, and a three X anions, and has formula ABX_3. A and B are of different sizes, A being larger than B [22]. These components are ordered in an octahedral structure (see Figure 2.2). Often used materials are caesium (Cs), methylammonium (MA) or formamidinium (FA) as A cation, lead (Pb) or tin (Sn) as B cation and chloride (Cl), bromide (Br) or iodide (I) as X anion.

$CsPbX_3$ (X = Br, Cl, I) inorganic metal lead-halide perovskites consist of a Cs A cation, a Pb B cation and halides Cl, Br or I as X anion.

The bandgap of inorganic metal lead-halide perovskites is tunable within the visible spectrum. The bandgap and emission peaks of $CsPbX_3$ range from 400-700 nm, depending on the halide. $CsPbX_3$ nanocrystals have emission spectra with FWHM between 12 and 42 nm [23]. Typical $CsPbX_3$ emission can be seen in Figure 2.3. In nanocrystals with a radius smaller than the Bohr exciton radius of $CsPbX_3$, around 3.5 nm, quantum confinement can blueshift the emission of $CsPbX_3$ [25], [26].

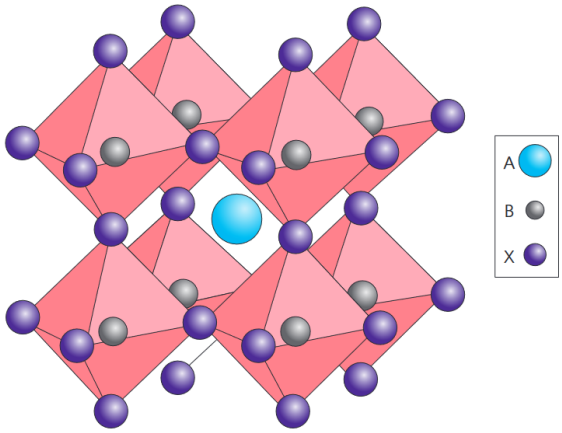

Figure 2.2: Perovskite ABX_3 structure. Figure from [22]

Inorganic metal lead-halide perovskite nanocrystals are good candidates for use as LED phosphor because of their tunable bandgaps, efficient absorption and emission, and near-unity PLQY [6], [18], [27], [28]. $CsPbX_3$ also has high defect tolerance, as trap states and defects mostly exist within the valence and conduction band, and not within the bandgap [29]. This makes electronic properties of perovskites appear as though the material is defect free, although many trap states, defects and vacancies in the perovskite structure can exist without influencing the absorption and emission [29], [30].

Compared to commercial phosphors with FWHM ~60 nm, perovskites have a narrow FWHM, which means a high color purity can be achieved [6]. Fast deposition processes like spin-coating, screen- or inkjet printing can be used in fabrication. This, together with low material costs makes the use of perovskites as LED phosphor cheap. Very thin layers of material can yield a high emission, which makes perovskites suitable for use on mini-LEDs. Perovskite nanocrystals are commercially available [31], but perovskite LED phosphors are not yet available on the market. $CsPbBr_3$ emits around 520 nm, making it suited for use as a green LED phosphor.

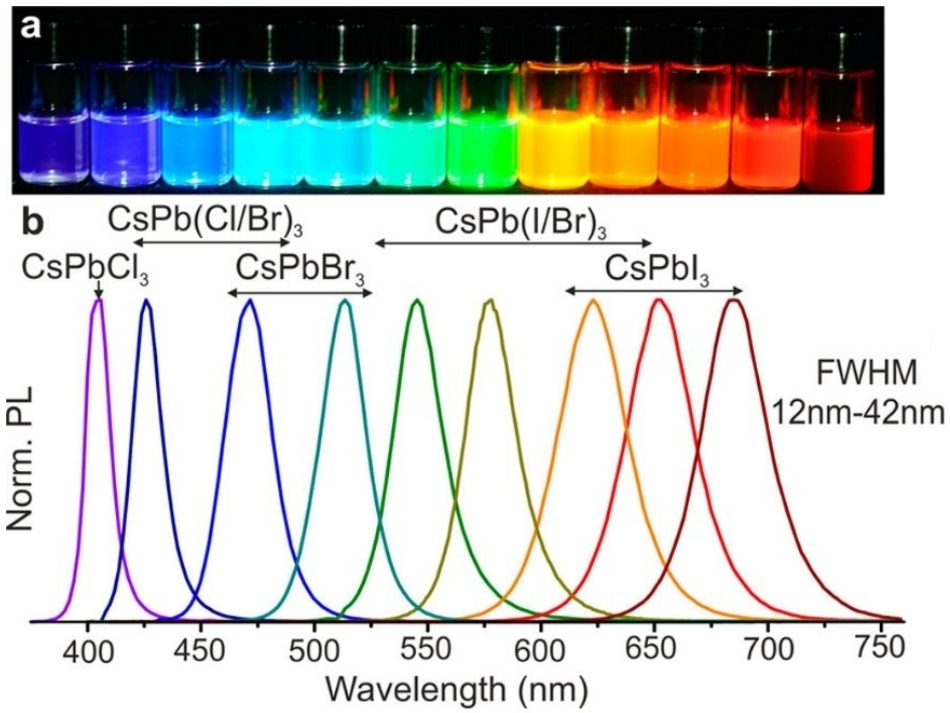

Figure 2.3: $CsPbX_3$ emission, a) colloidal $CsPbX_3$ under UV illumination, b) PL spectra of $CsPbX_3$ under 350-400 nm excitation. Figure from [23]

2.2.2 Stability of $CsPbBr_3$

One of the main obstacles to using $CsPbBr_3$ as LED phosphor is poor stability. Perovskites are sensitive to oxygen, (UV) light, water and thermal stress, with exposure leading to degradation within minutes [32].

The crystal structure and structural stability of perovskites can be estimated with the Goldschmidt tolerance factor

$$t = \frac{r_A + r_X}{\sqrt{2}(r_B + r_X)}$$

r_A, r_B and r_X correspond to the Goldschmidt ionic radii of the A cation, B cation and X anion respectively. The tolerance factor gives the ratio of the distance from cation A to anion X to the distance from cation B to anion X [22].

t predicts the deviation from the ideal perovskite structure which is indicated by $t = 1$ [27]. Materials with a tolerance factor $0.71<t<1$ are structurally stable. A tolerance factor between 0.9 and 1 indicates a cubic structure, and a tolerance factor below 0.9 indicates an orthorhombic structure [22]. $CsPbBr_3$ has a tolerance factor of 0.9, meaning that it is stable in the cubic phase.

When exposed to water, $CsPbBr_3$ will degrade within minutes. The melting point of the perovskite lies at 567°C, but it will undergo phase changes at lower temperature, rendering it useless as phosphor at temperatures above 177°C, although lower temperatures can also damage the perovskite [18], [33]. Under illumination of 0.03 W/mm^2, an order of magnitude smaller than LED-chip emission intensity, $CsPbBr_3$ will already lose 82% of its emission within 60 minutes [34]. Perovskites can exhibit self-healing behavior. After degradation, the perovskite can restore its structure within minutes to hours and recover its luminescent abilities [35], [36].

The perovskite must be stable for up to 50000 hours, with <10% drop in performance for use as an LED phosphor [7]. Oftentimes, stability is measured in rapid aging tests for 1000 hours [32]. Aging tests expose the perovskite to moisture, thermal stress and illumination, in order to simulate conditions in an LED.

The stability of $CsPbBr_3$ is inferior to that of often used ceramic phosphors [18]. In order to commercialize $CsPbBr_3$ LED phosphors, stabilizing steps have to be taken. Stability of $CsPbBr_3$ has been improved by adding ligands [29], by combining a 2D perovskite layer on top of a 3D bulk perovskite [37], or by passivating the surface [38].

One of the best ways of stabilizing perovskite is by encapsulation. To improve $CsPbBr_3$ stability optimally, the encapsulant has to be intrinsically stable, it cannot be porous, and it has to completely encapsulate the perovskite [18]. The matrix must be able to withstand LED operating conditions, so it has to be stable under illumination and heat. It also cannot absorb light emitted by the perovskite.

Many different materials have been used for encapsulation of perovskites. $CsPbBr_3$ has been implemented as core in a TiO_2 shell [39], inside of epoxies, coatings, alumina matrices, tellurite glass, polymers, and more [18], [34], [39]–[41]. $CsPbX_3$ perovskites have been protected by combining the perovskite with ZrO_2, improving stability and PLQY [42]–[44]. Most of these materials slow down the degradation of the perovskite, but do not completely stabilize it.

Silica is an encapsulant that is non-porous, and impermeable to oxygen and water. It is also transparent for visible light, and can withstand LED operating temperatures. This makes it a good candidate for stabilizing perovskites.

2.2.3 $CsPbBr_3$ in silica mesoporous sieves

Silica mesoporous sieves have pores of uniform size that can be tuned depending on the organic template they are produced with [45]. They are non-toxic, cheap, and made of earth abundant materials [11].

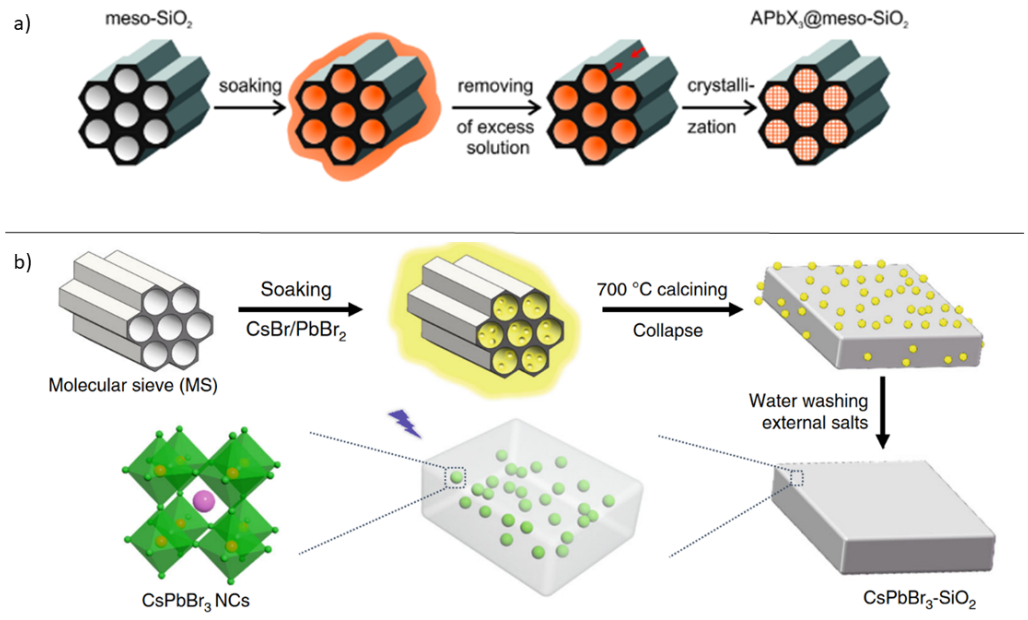

Figure 2.4: a) Perovskite precursors are soaked with a mesoporous sieve, excess solution is evaporated off, and $APbX_3$ is crystallized at 120°C in the pores. Figure from [28], b) Encapsulation of $CsPbBr_3$ in MCM-41. Figure from [18]

The group of Kovalenko soaked perovskite precursors in commercially available mesoporous sieves with pore sizes between 2.5 and 50 nm (see Figure 2.4 a)) [28]. Photoluminescence measurements showed perovskite emission with a narrow FWHM down to 22 nm, and PLQY above 50% [28]. However, this way of encapsulating does not completely protect the perovskites, as the pores are not sealed.

A paper by Zhang et al. (2020) presented MCM-41 as most suited template for encapsulation of $CsPbX_3$ perovskites, as the pores of this material collapse at high temperature [18]. MCM-41 is a silica molecular sieve with a pore size of 3.4 nm [45], [46]. The silica matrix was soaked in perovskite precursors and dried. Afterwards, the sample was annealed at 700°C. At temperatures above 600°C, the perovskite precursors sublimate into the pores of the molecular sieve. These pores collapse around 700°C, and when cooling down the sample, $CsPbBr_3$ nanocrystals are formed in the collapsed pores (see Figure 2.4 b)). A PLQY up to 71% was measured [24].

This process encapsulates the perovskite nanocrystals, and protects them from degrading influences of oxygen, water, heat and illumination. $CsPbBr_3$ encapsulated in MCM-41 ($CsPbBr_3$@SiO_2) showed slightly improved PLQY after 50 days in water (see Figure 2.5 a)). This material was installed on an LED-chip, and after 1000 hours, PL intensity survived completely. Under aging conditions of 85% humidity and 85°C, emission showed an initial rise, followed by a drop in intensity. The intensity did however not drop below initial intensity (Figure 2.5 b)). Compared to non-encapsulated $CsPbBr_3$, there is a large difference in stability. Compared to green phosphor Sr_2SiO_4:Eu^{2+} and red phosphor KSF, a significant improvement can be seen (see Figure 2.5 c)). This shows $CsPbBr_3$@SiO_2 has stability comparable to that of a commercial phosphor.

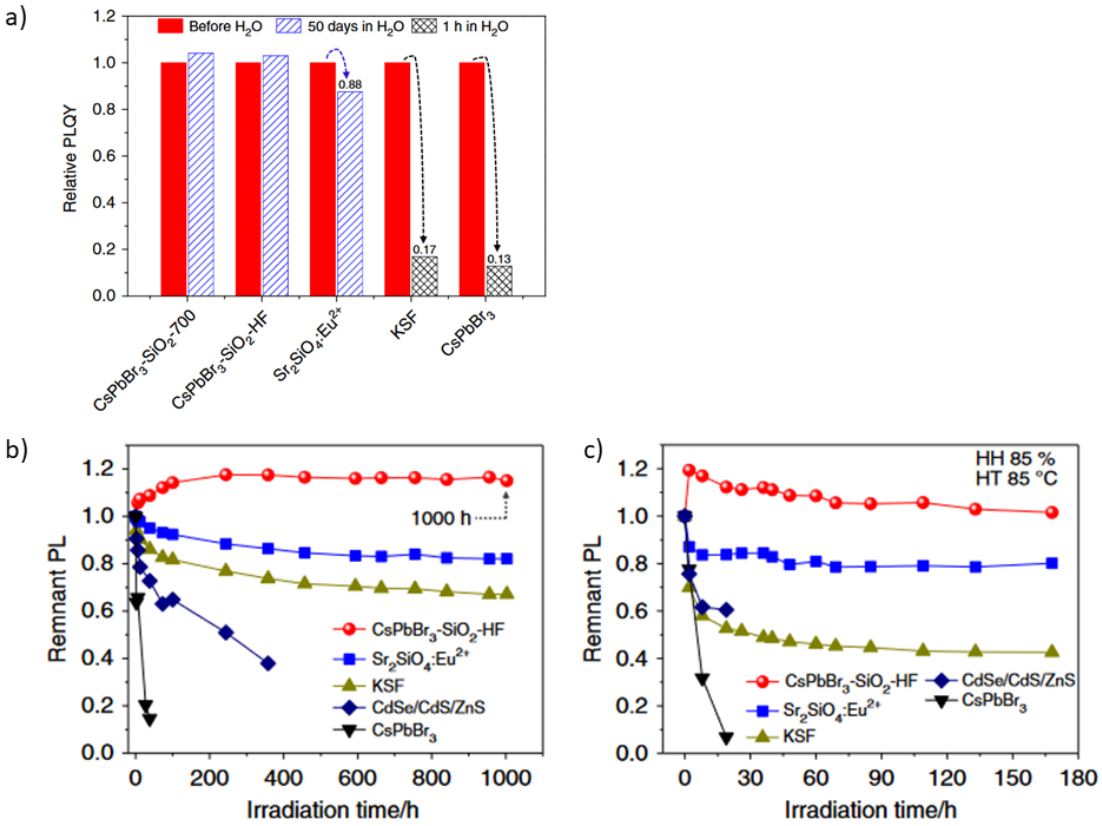

Figure 2.5: a) PLQY of $CsPbBr_3$ in MCM-41 (with and without HF etching) was measured before and after 50 days in water, and compared to green phosphor Sr_2SiO_4:Eu^{2+}, red phosphor KSF and non-encapsulated $CsPbBr_3$, b) PL of $CsPbBr_3$ in molecular sieves, installed on an LED chip (20 mA, 2.7 V), compared to Sr_2SiO_4:Eu^{2+}, KSF, CdSe/CdS/ZnS nanocrystals, and non-encapsulated $CsPbBr_3$, c) PL of $CsPbBr_3$ in molecular sieves, installed on an LED chip (20 mA, 2.7 V), aged at 85°C and 85% humidity. Figures from [18]

An et al. (2021) showed an adapted synthesis by including molten salts [11]. The MCM-41 pores were sealed with a mixture of KNO_3, KBr, and $NaNO_3$, instead of collapsed at high temperature. In this synthesis, a lower annealing temperature of 350°C was required, and a PLQY of up to 89% was measured, with a FWHM of 21.5 nm. However, stability of $CsPbBr_3@SiO_2$ with molten salts was lower compared to the synthesis Zhang et al. (2020) showed [11], [18].

Since then, more papers have been dedicated to using molecular sieves to encapsulate perovskites. Overgrowth steps were taken to lower annealing temperatures [24], Mn^{2+} doped $CsPbBr_3$ was formed in MCM-41 pores [47], alternative molecular sieves like SBA-15 were used [48], and bismuth-halide double perovskites were formed in the sieves [49]. It can be concluded that silica molecular sieves form a good encapsulant for perovskites.

2.3 Eu^{3+} as a red LED phosphor

2.3.1 Lanthanides

Europium is an element in the lanthanide family. These materials are f-block elements, as the f-orbital is partly filled. Lanthanides are often called rare earth elements, but are not as rare as the name would suggest. Europium is the 53rd most prevalent element, making it more prevalent than for example silver. However, it can be difficult to extract lanthanides from the minerals in which they are found [50], and they can only be mined in small mines in the USA, China, Russia, Australia and India. This causes many environmental and socio-economic problems [51]. Therefore, efficient use and design for circularity are critical [51]. Lanthanides are non-toxic, and are often used in lighting, lasers or as catalysts [52], [53]. Most lanthanides are stable in the Ln^{3+} oxidation state. Europium most commonly exists in the Eu^{3+} configuration, although the Eu^{2+} ion is also found [50], [54].

Under illumination, lanthanides can be seen to exhibit sharp emission lines with FWHM $<$ 10 nm [55]. They are characterized by these narrow emission peaks, a small Stokes shift, and long lifetimes. This makes lanthanides very suitable for use as phosphor in wLEDs because a high color purity can be achieved. Furthermore, lanthanides have a high chemical stability and environmentally friendly preparation procedure [17]. Many lanthanides have weak absorption, making direct excitation a challenge [56]. Eu^{3+} can exhibit narrow red emission around 610 nm and forms a good candidate for a red phosphor material [19].

Eu^{3+} is often used as a spectroscopic probe, because its transitions are very sensitive to small changes in the symmetry of the surroundings [54]. A small change in symmetry can be recognized by changes in the peak wavelength, FWHM and number of peaks [57]. This is why Eu^{3+} is used as a security mechanism in EURO notes, that glow red when illuminated with UV light [58].

Much work has been done on incorporating Eu^{3+} in LEDs and phosphors, employing different hosts. As a result, many Eu^{3+} containing phosphors are available. However, most are only excited with UV light, making them incompatible with blue InGaN LED chips [1], [59]–[65].

Some Eu^{3+} phosphors are most efficient upon excitation with blue light, like $La_2Ce_2O_7$:Eu^{3+} [17], $SrAl_2Si_2O_8$:Eu^{3+} [68], and Y_2O_3:Eu^{3+}, one of the most used phosphors [64], [66], [67]. However, the PLQY of these systems is often below 50%. Other phosphors can be excited by blue light, but are many times more efficient on excitation with UV-light, like $BaGe_4O_9$:Eu^{3+} [61], and $Sr_5Nb_4O_{15}$:Eu^{3+} [69].

Incorporating Eu^{3+} in yttria-stabilized zironia enhances Eu^{3+} emission, and ZrO_2 is often used with Eu^{3+} as a spectroscopic or temperature probe [70], [71].

2.3.2 Electron configuration of Eu^{3+}

Eu^{3+} has 54 electrons in closed shells, and 6 electrons in the 4f shell, which means it has electronic configuration [Xe]$4f^6$. The 4f shell is protected from the surroundings by the closed $5s^2$ and $5p^6$ orbitals. Using the binomial coefficient, the degeneracy can be calculated. The electrons can arrange themselves in 3003 different ways [57]. This degeneracy is lifted by electron repulsion, spin-orbit coupling, crystal-field perturbation and the Zeeman effect [72].

The energy levels of Eu^{3+} can be described by $^{2S+1}L_J$ terms. S is the spin quantum number, and the spin multiplicity is given by 2S+1. L is the total orbital angular momentum quantum number, and J is the total angular quantum number. J can range from L+S until |L-S| [73]. In total, Eu^{3+} has 295 $^{2S+1}L_J$ terms. Hund's rules determine the ground state as the state with the highest spin multiplicity and the lowest J number. The highest spin multiplicity is given by 2S+1. Since Eu^{3+} has 6 electrons in the 4f shell, the highest spin multiplicity is $2S+1 = 2\cdot(6\cdot\frac{1}{2})+1 = 7$. The ^7F_J state has multiplicity 7, meaning the ground state of Eu^{3+} is $^7F_0$. With a Hamiltonian the energy levels can be calculated [73].

2.3.3 Judd-Ofelt theory

Eu^{3+} emission is a result of an electric dipole or magnetic dipole transition between states within the 4f shell. The closed $5s^2$ and $5p^6$ orbitals protect the optically active electrons from the crystal field, which gives them characteristic sharp peaks with FWHM<10 nm, and long lifetimes around 1 millisecond [74]–[78].

The Laporte selection rule forbids f-f transitions. According to this rule, electric dipole (ED) transitions of Eu^{3+} are forbidden and have a very low probability of occurring [56]. ED transitions are a consequence of the interaction of the ion with the electric field vector of the light through an electric dipole [72]. Magnetic dipole (MD) transitions are allowed by Laporte selection rule, but generally induce weak emission [76]. They are a result of interaction of the Eu^{3+} ion with the magnetic field component of the light via a magnetic dipole [75]. The location of MD-transitions can be calculated with the wavefunctions of a free Eu^{3+} ion, as the environment does not influence them much [72].

However, the Laporte selection rule is only valid for Eu^{3+} as a free floating ion, and does not take the Eu^{3+} host environment into account. To relax this selection rule, the field cannot be centrosymmetric [72]. Eu^{3+} has to be included in a strongly asymmetric site, or sensitized with organic ligands in order to show ED transitions [1]. The Eu^{3+} ion is affected by surrounding host ions via a static electric field, the crystal field, indicating that the host has a large impact on the location and intensity of ED transitions [53], [74].

Hence, Judd and Ofelt independently proposed a slightly different set of selection rules (see Figure 2.6). These rules take the host matrix of Eu^{3+} into account and are more in accordance with the observed emission from Eu^{3+}. All ED transitions with even ΔJ, and all MD transitions are allowed. Judd-Ofelt theory still forbids some transitions, like $^5D_0 \rightarrow {}^7F_0$ and $^5D_0 \rightarrow {}^7F_J$ (J = 0,1,3,5). These transitions can however be seen in luminescence spectra. Several reasons can be found for this, like J-mixing, the electrostatic interaction between electrons (electron correlation), and dynamic coupling, which is the mutual interaction of the lanthanide ion and the crystal environment [76]. J-mixing is the mixing of different J-levels of the ion, where for example the $^5D_0 \rightarrow {}^7F_0$ transition can borrow intensity from $^5D_0 \rightarrow {}^7F_J$ (J = 2,4,6) transitions [57], [79]. It can arise from spin-orbit coupling and crystal-field perturbations [57].

Selection Rules

	S	L	J (No 0 ↔ 0)
Electric Dipole	$\Delta S = 0$	$\Delta L \leq 6$	$\Delta J \leq 6$ $\Delta J = 2,4,6$ (J or J′ = 0)
Magnetic dipole	$\Delta S = 0$	$\Delta L = 0$	$\Delta J = 0, \pm 1$
Electric quadrupole	$\Delta S = 0$	$\Delta L = 0, \pm 1, \pm 2$	$\Delta J = 0, \pm 1, \pm 2$

Figure 2.6: Selection rules in Judd-Ofelt Theory. Figure adapted from [76]

2.3.4 Emission

Eu^{3+} emission is due to radiative recombination of $^5D_0 \rightarrow {}^7F_J$ transitions. Emission ranges from amber colored to infrared light [75]. $^5D_0 \rightarrow {}^7F_J$ transitions can be seen in Figure 2.7 , typical photoluminescence (PL) emission spectra can be seen in Figure 2.8.

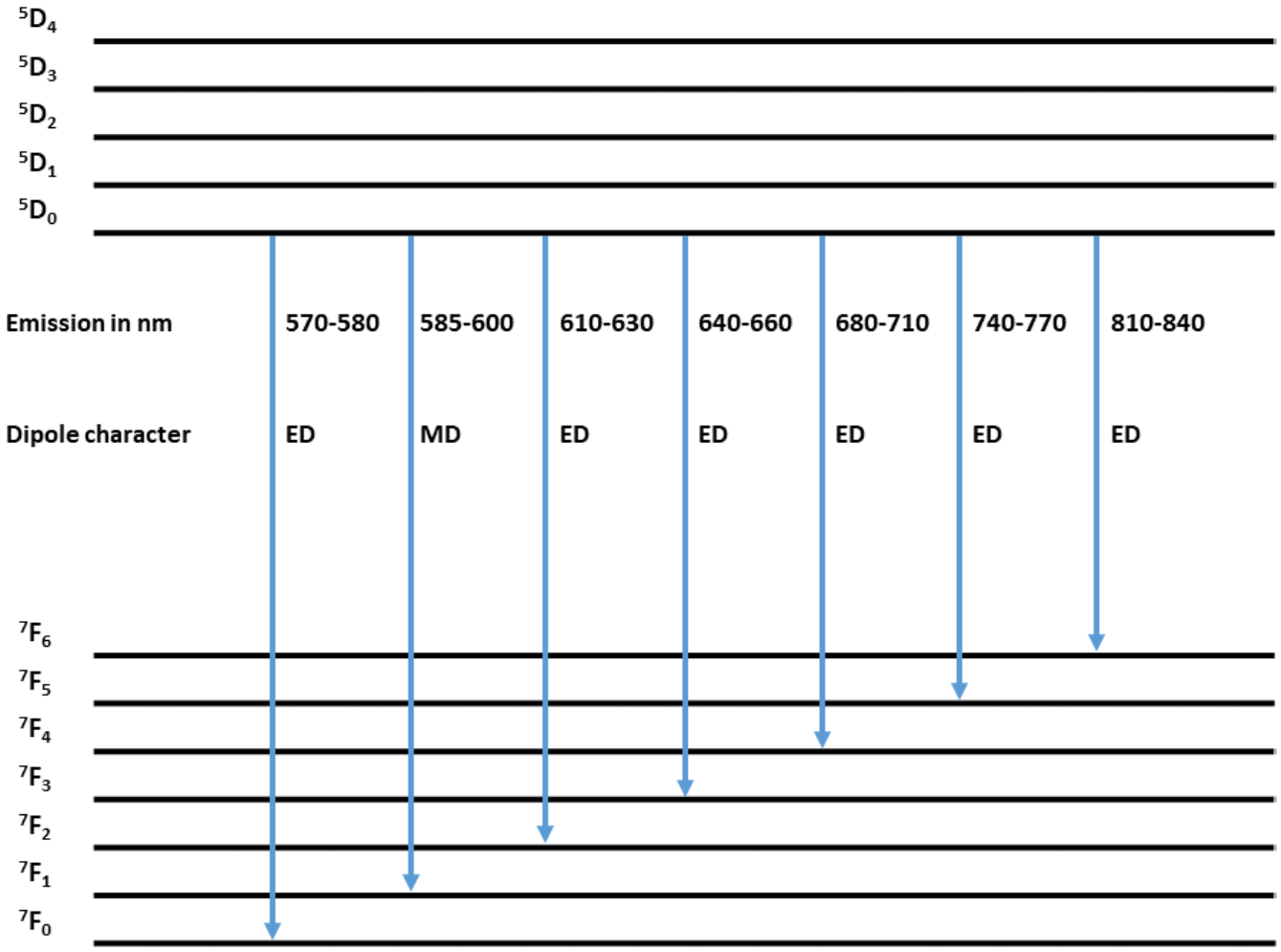

Figure 2.7: $^5D_0 \rightarrow {}^7F_J$ transitions of Eu^{3+} in a host matrix. Data taken from [72]

$^5D_0 \rightarrow {}^7F_0$

The $^5D_0 \rightarrow {}^7F_0$ transition is forbidden according to Judd-Ofelt theory, because it is a J=0 $\rightarrow$ J=0 transition. However, this transition can still be observed in many luminescence spectra, mostly because of J-mixing [79]. This transition has a narrow linewidth, and will only show in low symmetry surroundings [72]. The transition is often weak, but is bright in for example the Y_2O_3:Eu^{3+} complex [72]. This is one of the most narrow linewidth transitions of all lanthanides. The presence of multiple peaks within this transition indicate that Eu^{3+} exists in multiple symmetric host environments [80].

$^5D_0 \rightarrow {}^7F_1$

This transition is an MD transition, and the intensity is mostly independent of the environment, as can be seen in Figure 2.8. However, this level can exhibit splitting, and show multiple peaks. In an environment with low site symmetry, the splitting becomes larger [72]. Splitting is very common in a silica host, because the silica host provides many different crystal-field strengths [81]. This transition can overlap with both the $^5D_0 \rightarrow {}^7F_0$ and $^5D_0 \rightarrow {}^7F_2$ level.

$^5D_0 \rightarrow {}^7F_2$
$^5\mathrm{D}_0 \rightarrow {}^7\mathrm{F}_2$ is the transition which can be the most intense, and it is the transition most often utilized in red phosphors [60]. This transition is hypersensitive, meaning that the environment of the ion has a large impact on the intensity of this transition [53]. Its emission is usually centered around 612 nm, and shows a bright red/pink color. This transition can be used as a measure for the asymmetry of the Eu^{3+} site [72].

This hypersensitive transition is the transition that is most influenced by the local symmetry and ligands of Eu^{3+} [74]. Most ED transitions can have a variation of a factor 3 in intensity, depending on the host environment and ligands. However, a hypersensitive transition shows emission that has a variation in intensity of a factor 100 [72]. This large variation in intensity can be seen in Figure 2.8, where the intensity of the $^5\mathrm{D}_0 \rightarrow {}^7\mathrm{F}_2$ varies depending on the host. A hypersensitive transition behaves like an electrical quadrupole transition, and the dynamic coupling model explains the variation in intensity [53]. The variation can be calculated as a result of Coulomb correlation between the $^5\mathrm{D}_0 \rightarrow {}^7\mathrm{F}_2$ quadrupole moment and the induced dipole moments of the host environment or ligands, caused by incoming light [53]. This indicates that a longer distance between Eu^{3+} and the host environment or ligands results in a lower $^5\mathrm{D}_0 \rightarrow {}^7\mathrm{F}_2$ emission.

This transition is often more intense in complexes, like the Eu^{3+} β-diketonate complexes. In this complex, ligands act as an intensity enhancing mechanism.

$^5D_0 \rightarrow {}^7F_3$
The $^5\mathrm{D}_0 \rightarrow {}^7\mathrm{F}_3$ transition is forbidden by Judd-Ofelt theory, and is only seen as a result of J-mixing. This transition is very weak in most cases [72].

$^5D_0 \rightarrow {}^7F_4$
The $^5\mathrm{D}_0 \rightarrow {}^7\mathrm{F}_4$ transition is an ED transition, and the emission can be seen as a small peak in PL emission spectra. Compared to the $^5\mathrm{D}_0 \rightarrow {}^7\mathrm{F}_2$ hypersensitive transition it has a much lower intensity. This peak occurs around 700 nm, in the deep red. Human eyes can see light up to 740 nm, but the sensitivity of the eye is low from around 700 nm [14], meaning that emission from this transition is not effective for use in wLEDs.

Transitions to higher $^7\mathrm{F}_J$ states can occur, but have a lower intensity [72]. These transitions are often not included in papers, partly due to their limited use in phosphors, as they emit light that is not visible for the human eye. Emission from higher $^5\mathrm{D}_J$ levels is possible, but unlikely, as excitons will mostly relax non-radiatively to the $^5\mathrm{D}_0$ state, and then recombine radiatively.

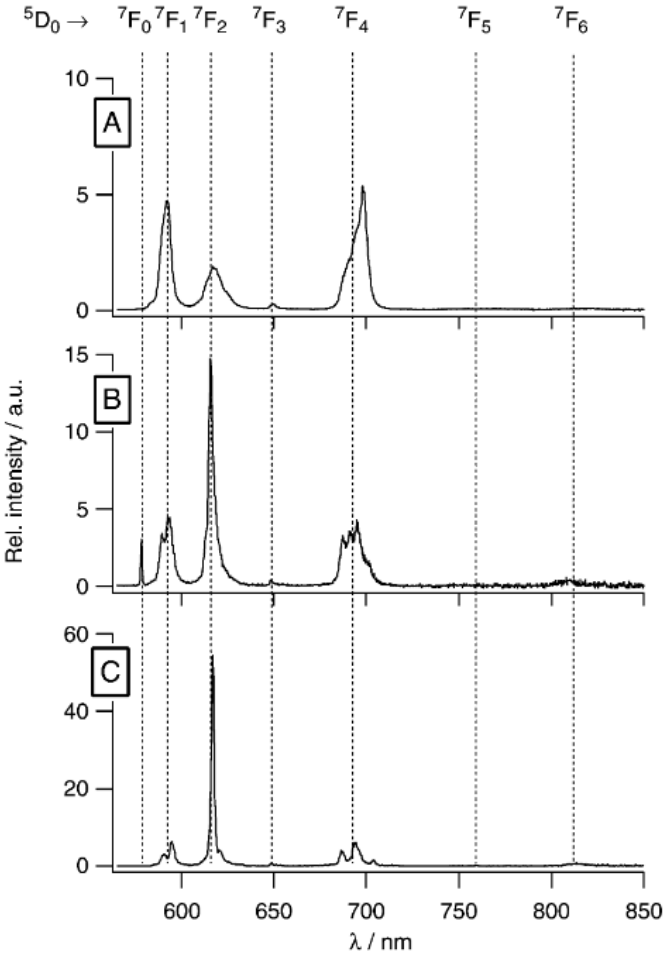

Figure 2.8: PL emission of Eu^{3+} in different hosts, a) Eu^{3+} in water, b) $Eu(DPA)^+$ complex in water, c) $Eu(DPA)_3$ $^{3-}$ complex in water. The intensity of the different emission bands vary significantly depending on the host. Figure from [78]

2.3.5 Absorption

Eu^{3+} is, like all lanthanides, known to be a bad absorber, and most transitions have a molar absorption coefficient smaller than 10 L/mol/cm [77]. Most transitions are very weak, but Eu^{3+} can be effectively excited with UV light [9]. $^7F_{0,1} \rightarrow {}^5D_J$ absorption transitions are shown in Figure 2.9. A typical photoluminescence excitation (PLE) spectrum is shown in Figure 2.10.

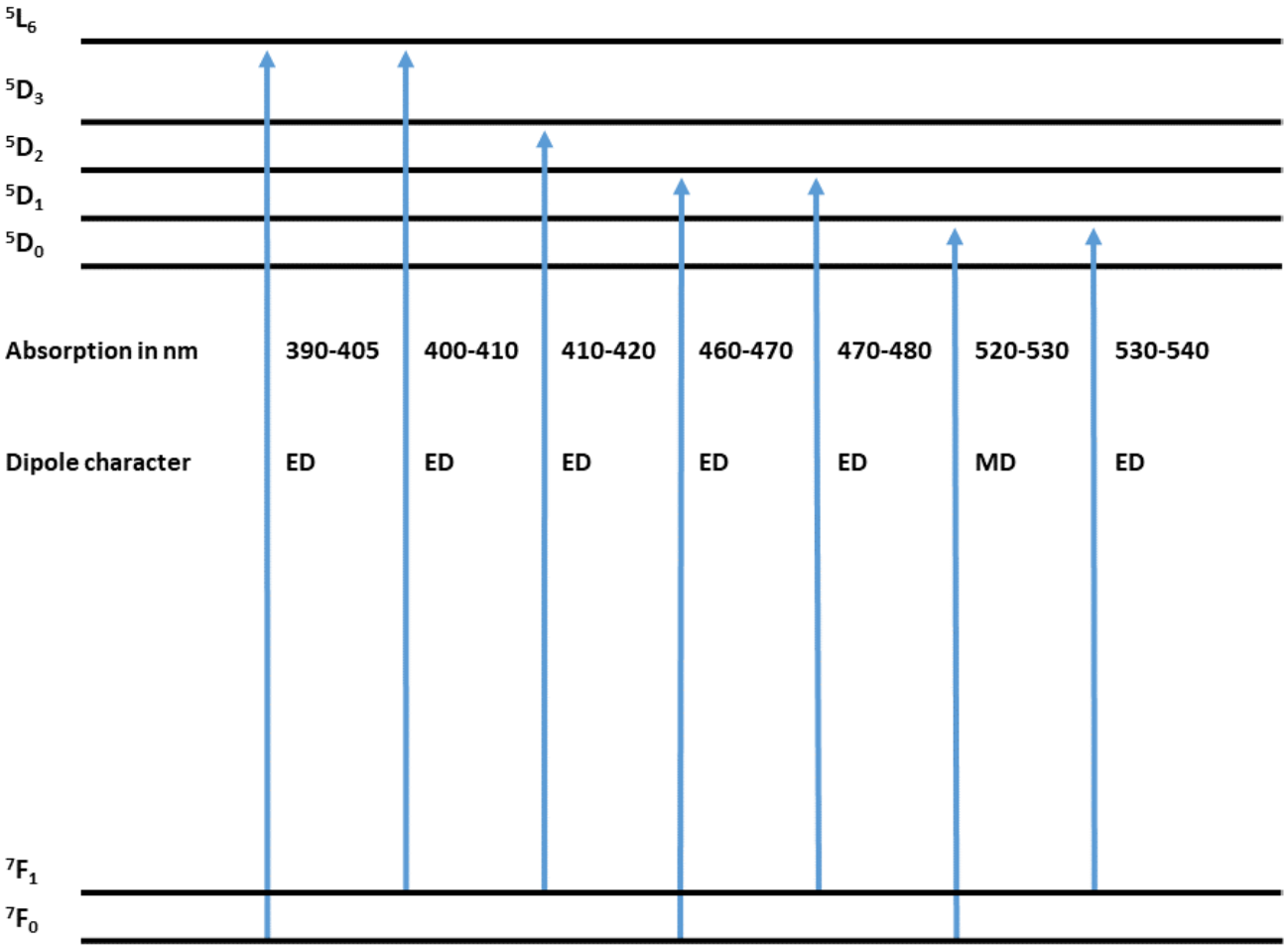

Figure 2.9: $^7F_{0,1} \rightarrow {}^5D_J$ transitions of Eu^{3+} in a host matrix. Data taken from [72]

At room temperature, ground state $^7F_0$ has an occupation of 65% of the Eu^{3+} ions, compared to an occupation of 35% in the $^7F_1$ state. This is due to the Boltzmann distribution [72], [82]. Because of low occupancy, absorption from the $^7F_1$ state is less likely to occur, and transitions from this state are generally very weak. Transitions from higher ^7F_J states are highly unlikely, as they have a $<$1% ion occupation [72].

The most intense absorption transition is the $^7F_0 \rightarrow {}^5L_6$ transition, which absorbs UV light between 390-405 nm [83], as is visible in Figure 2.10. In most hosts $^7F_1 \rightarrow {}^5L_6$ partly overlaps this peak, showing a broader excitation peak. Most Eu^{3+} based phosphors utilize the $^7F_0 \rightarrow {}^5L_6$ transition, as this transition has a strong absorption [1], [54], [59]–[65], as can also be seen in Figure 2.10. However, this transition is not suitable for use in a blue LED-chip based wLED, since the emission of the blue LED-chip lies around 460 nm.

The $^7F_0 \rightarrow {}^5D_3$ transition is forbidden because of Judd-Ofelt theory, and is only present due to J-mixing. It is very weak. While the $^7F_1 \rightarrow {}^5D_3$ transition is not forbidden, it is very weak because of the Boltzmann distribution.

To directly excite Eu^{3+} in a blue LED-chip based wLED, the $^7F_0 \rightarrow {}^5D_2$ transition has to absorb strongly. This absorption band perfectly overlaps with emission from a 460 nm LED-chip. The hypersensitive character of this transition indicates that depending on the host, the transition can be very weak or very absorbing, even similar in strength to the $^7F_0 \rightarrow {}^5L_6$ transition [82]. In contrast, the $^7F_1 \rightarrow {}^5D_2$ transition is very weak.

$^7F_0 \rightarrow {}^5D_1$ transition is a MD transition, which makes the intensity mostly independent to the environment, and weak in absorption [82]. This transition can be used for energy transfer via ligands. In order to have direct energy transfer from $CsPbBr_3$ emission, this transition has to be excited. $^7F_1 \rightarrow {}^5D_1$ is hypersensitive, although it is also not as strongly absorbing due to the Boltzmann distribution.

Around 240-270 nm, Eu^{3+} shows a broad absorption band [84], as can be seen in Figure 2.10. This is due to the Eu-O charge transfer band (CTB), or ligand-to-metal charge transfer band (LMCT). Electron transfer can cause Eu^{3+} to reduce to Eu^{2+}-O^-. Eu^{2+} transitions are f-d transitions, so they are not forbidden according to the Laporte selection rule [85]. They can be very absorbing, and transfer energy to Eu^{3+} in a non-radiative energy transfer process. The exact wavelengths of this band are heavily dependent on the host environment [84].

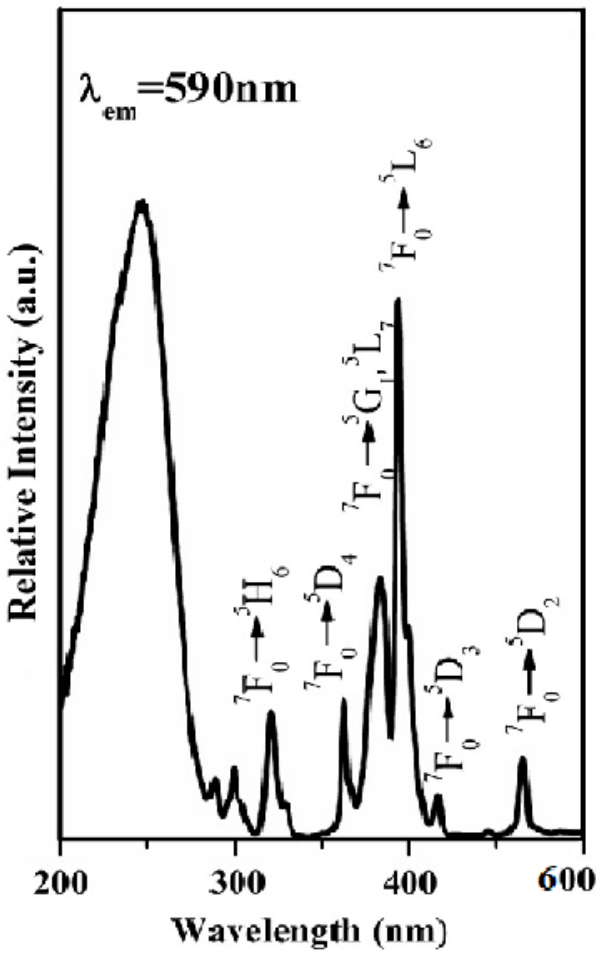

Figure 2.10: Photoluminescence excitation spectrum of $Sr_9Sc(PO_4)_7$:Eu^{3+}. Figure from [86]

2.4 Energy transfer to Eu^{3+}

2.4.1 Dexter energy transfer and Förster Resonance Energy Transfer

Even in an ideal host material, absorption coefficients of Eu^{3+} are low [72]. By combining Eu^{3+} with a well absorbing material, emission of Eu^{3+} can be increased via energy transfer. Energy transfer to Eu^{3+} can occur via Dexter Energy Transfer, or via Förster Resonance Energy Transfer (FRET) [56], [72].

Dexter energy transfer is a process where an excited electron is transferred from a donor to an acceptor (see Figure 2.11). This requires an overlap between the orbitals of the energy donor and the Eu^{3+} ion. A close distance between the donor and acceptor of around 0.5 nm is required [87].

Eu^{3+} can also be sensitized by Förster Resonance Energy Transfer (FRET). FRET happens when the triplet level of an energy donor couples with the dipole moment of the 4f orbital. A donor electron that is excited can recombine non-radiatively, and through resonance excite an acceptor electron, as is shown in Figure 2.11. The electron is not transferred to the acceptor [9], in contrast to a Dexter energy transfer process. The resonance mechanism occurs because of Coulombic interaction between the donor and acceptor [56].

The efficiency of FRET is given by

$$\eta_{FRET} = \frac{1}{1 + (\frac{R}{R_0})^6}$$

R is the donor-acceptor distance, R_0 is the distance where 50% of excited photons in the donor transfer energy to the acceptor [56]. For most donor-acceptor pairs with Eu^{3+} as acceptor R_0 is around 2 to 5 nm [56]. This means that the distance between donor and acceptor must be smaller than 5 nm for FRET to be efficient.

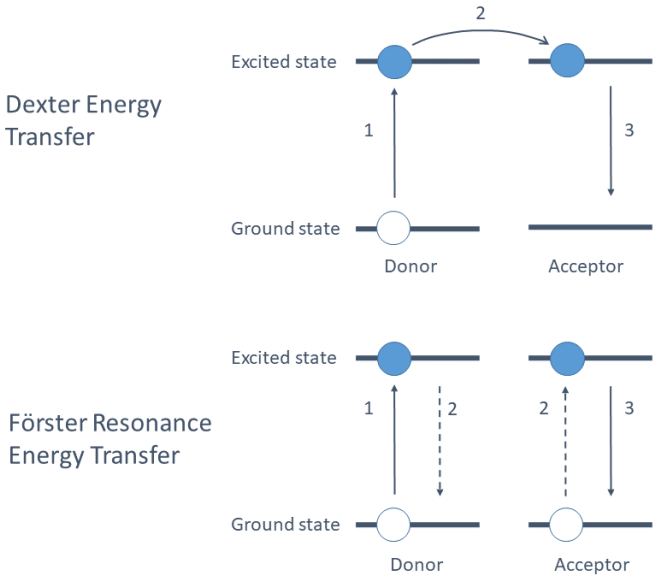

Figure 2.11: Dexter energy transfer. 1. an electron is excited to a higher state, 2. the excited electron transfers from donor to acceptor, 3. the acceptor decays radiatively, b) Förster Resonance Energy Transfer. 1. an electron is excited to a higher state, 2. the excited electron decays non-radiatively, and simultaneously excites the acceptor through resonance, 3. the acceptor decays radiatively. Figure adapted from [88]

2.4.2 Dexter energy transfer in a Eu^{3+} β-diketonate complex

Emission of Eu^{3+} can be improved by adding ligands that can absorb light and transfer energy to the lanthanide ion via intramolecular Dexter energy transfer [77], [89]. The most commonly known ligands for sensitizing lanthanides are β-diketonates (1,3-diketonates) [56].

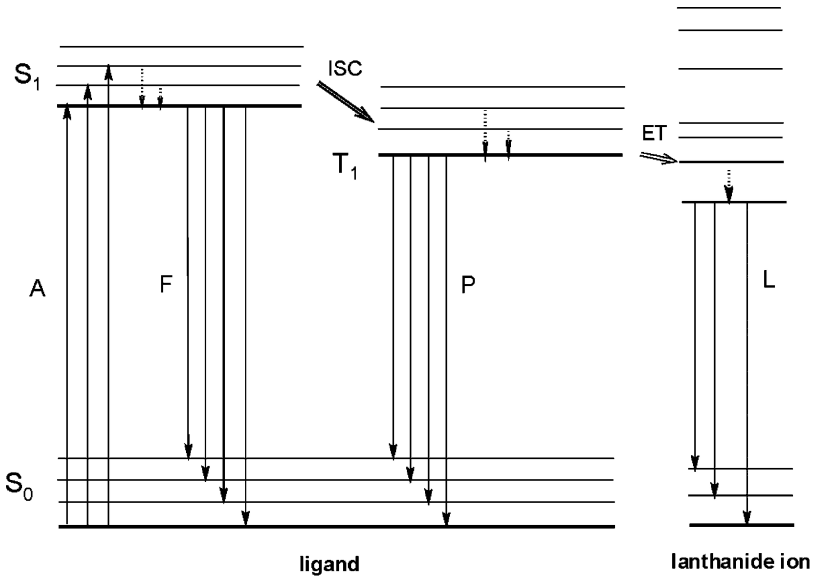

Figure 2.12: The β-diketonate ligand can absorb light and transfer this to the lanthanide ion via the triplet state. A – absorption, F – fluorescence, P – phosphorescence, L – lanthanide luminescence, ISC – intersystem crossing, ET – energy transfer, S – singlet, T – triplet. Figure from [77]

As can be seen in Figure 2.12, the β-diketonate ligand can absorb UV light, and get excited to the S_1 singlet state. Fast internal conversion to a lower S_1 level happens through internal conversion. This light either decays to the S_0 ground state through radiative radiation, or goes through non-radiative intersystem crossing to the triplet state [56]. The triplet state can phosphoresce to the S_0 ground state of the ligand, or transfer energy to an excited state of Eu^{3+} via Dexter energy transfer [77].

This energy transfer is possible because the β-diketonate ligands have a long triplet lifetime, similar to that of Eu^{3+} [56]. The Eu^{3+} $^5D_1$ level is a good acceptor level for Dexter energy transfer [1]. For efficient energy transfer, the triplet state of the antenna should have an energy level that is slightly higher than the resonant acceptor level to prevent back transfer [55]. When energy transfer has occurred, Eu^{3+} will decay non-radiatively to the $^5D_0$ state, and from there decay radiatively to a ^7F_J state.

Tetrakis Eu^{3+} β-diketonate complexes have four tta ligands around Eu^{3+} (Figure 2.13), and are the most efficient complexes at sensitizing Eu^{3+} emission [77]. The ligands have a strong absorption in the UV region, and can transfer energy to the Eu^{3+} $^5D_1$ level via the triplet state [72]. These ligands can absorb UV light, but have weak absorption around 460 nm InGaN emission.

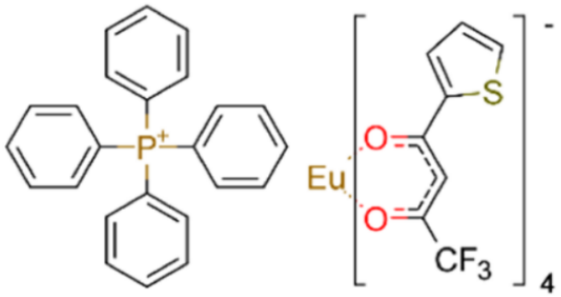

Figure 2.13: Tetrakis Eu^{3+} β-diketonate complex, $Eu(tta)_4P(Ph)_4$. Figure from [44]

Eu^{3+} β-diketonate complexes are not stable under illumination or heat, as the ligands can detach from the Eu^{3+} ion [55]. Different encapsulants have been used to improve stability. Encapsulation in MCM-41 can drastically increase stability of the complex under luminescence and heat [90], and was found to increase PLQY [77]. PMMA is an effective encapsulant that can increase emission intensity and stability under illumination of Eu^{3+} in a β-diketonate complex [91], [92].

The β-diketonate ligands can also be excited via an energy transfer mechanism. A beautiful example is the work of the Petrozza group [1], that sandwiched the $Eu(tta)_4P(Ph)_4$ complex between 2D perovskite NMA_2PbBr_4. In this system, the 2D perovskite absorbs UV light and transfers this to the tta ligands [1].

2.4.3 Förster Resonance Energy Transfer from Tb^{3+} to Eu^{3+}

A much described FRET mechanism is a system with energy transfer from Tb^{3+} to Eu^{3+} [9], [56], [65], [93]–[95]. By co-doping Tb^{3+} and Eu^{3+} in a suitable matrix, enhanced Eu^{3+} emission can be seen. The $^5D_4 \rightarrow {}^7F_5$ Tb^{3+} transition can excite the $^7F_0 \rightarrow {}^5D_1$ transition of Eu^{3+} via resonant Coulombic interaction. Tb^{3+} has a lifetime similar to Eu^{3+}, facilitating energy transfer [94]. Tb^{3+} and Eu^{3+} have been implemented in different hosts, like $CsPbBr_3$ [93], Y_2SiO_5 [94], and PMMA combined with a mixed Tb^{3+}/Eu^{3+} β-diketonate complex [91].

However, Tb^{3+} is a bad absorber that is mostly excited with UV light [94]. Van de Haar et al. (2020) showed a system where Tb^{3+} can be excited with 460 nm light, and energy transfer to Eu^{3+} takes place in an interparticle FRET mechanism, as can be seen in Figure 2.14. This results in red Eu^{3+} emission upon excitation with 460 nm light [9].

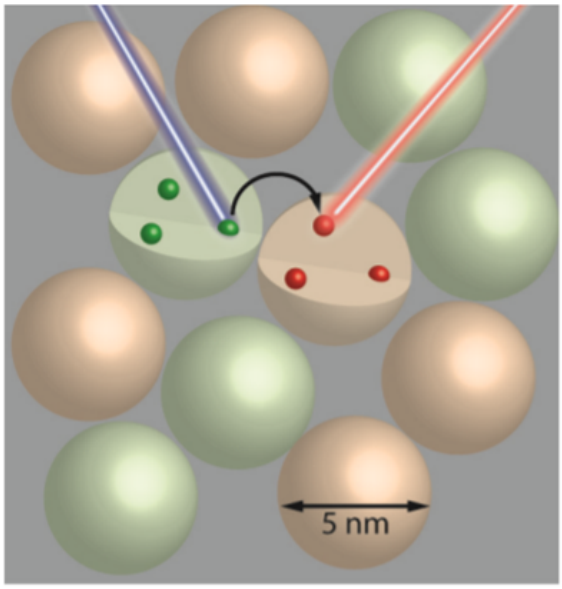

Figure 2.14: Interparticle FRET from Tb^{3+} doped material to Eu^{3+} doped material, resulting in red emission. Tb^{3+} is excited with 460 nm light and transfers energy to Eu^{3+}, which emits red light. Figure from [9]

2.5 Enhanced Eu^{3+} emission by doping in $CsPbBr_3$

In this thesis, $CsPbBr_3$ is investigated as a host matrix and energy donor for Eu^{3+}. $CsPbBr_3$ has high absorption, and a bandgap close to the $^5D_1$ level of Eu^{3+} [23]. These qualities make it a good candidate as a potential energy donor. By incorporating Eu^{3+} in the $CsPbBr_3$ lattice, the donor-acceptor distance is small enough for Dexter energy transfer and FRET.

If $CsPbBr_3$ forms a suited host material, the PLE spectrum would show intense Eu^{3+} excitation peaks, combined with strong UV excitation, as is depicted by the purple line in Figure 2.15. When $CsPbBr_3$ would transfer energy to Eu^{3+}, Eu^{3+} excitation is possible until the bandgap of the perovskite. This is shown by the red line in Figure 2.15.

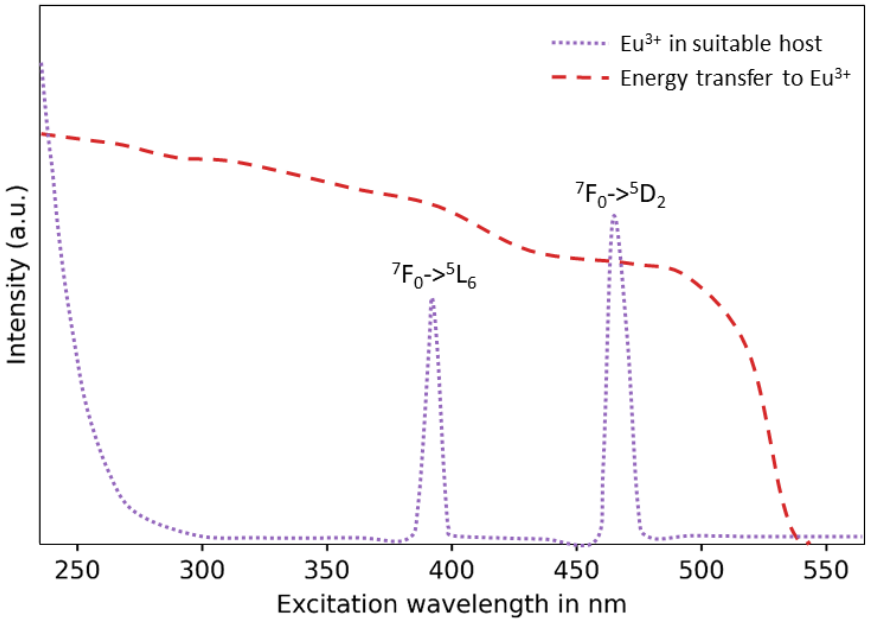

Figure 2.15: PLE of Eu^{3+} peak. The purple line shows Eu^{3+} excitation if the host is suitable for self-excitation. The red line shows Eu^{3+} excitation through energy transfer from $CsPbBr_3$

Inorganic metal lead-halide perovskites can be doped by replacing the Pb^{2+} cation with other materials like lanthanides. Doping can improve PLQY, and broaden the possible emission range [96]. Energy transfer from $CsPbBr_3$ to Yb^{3+} has been shown to enhance Yb^{3+} emission, and induce a quantum cutting effect [97], [106].

Doping $CsPbBr_3$ with Eu^{3+} results in a Eu^{3+}-V_{Pb}-Eu^{3+} structure, with two Eu^{3+} ions and a vacancy in the place of three Pb^{2+} ions, as can be seen in Figure 2.16 [85], [96]. The ionic radius of Eu^{3+} is 1.06 Å [98], compared to an ionic radius of 1.19 Å for Pb^{2+}. These radii are similar enough for the Eu^{3+} ion to be incorporated into the perovskite lattice. Doping of Eu^{3+} increases $CsPbBr_3$ stability and emission, as it can reduce microstrain in the lattice [1], [85], [96]. It can also lead to a blueshift in $CsPbBr_3$ emission because of tilting of the perovskite lattice [96].

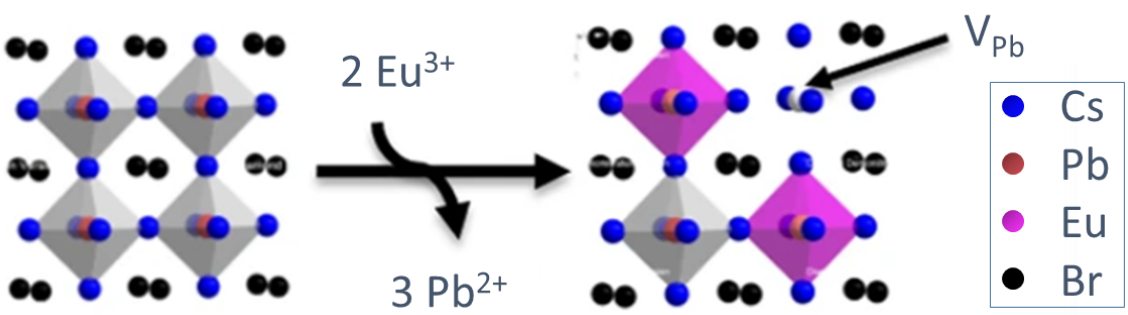

Figure 2.16: Atomic model where 2 Eu^{3+} ions and a vacancy replace 3 Pb^{2+}ions. The pink octahedra represent a replacement of Pb^{2+} with Eu^{3+}. The white sphere corresponds to a Pb^{2+} vacancy. Figure adapted from [99]

When Eu^{3+} is doped in large concentrations, concentration quenching can occur. Eu^{3+} will transfer energy to nearby Eu^{3+} ions, increasing the probability of non-radiative radiation, and quenching emission [56]. The critical distance R_c can be calculated.

$$R_c \approx 2(\frac{3V}{2\pi X_c N})^{1/3}$$

R_c is the distance where the energy transfer probability between Eu^{3+} ions is equal to Eu^{3+} emission probability. For Eu^{3+} ions, $R_c = 5$ Å [100]. V is the volume of the host lattice, X_c the critical doping concentration, and N the number of available sites in the unit cell. For $CsPbBr_3$:10%Eu^{3+}, $R_c = 16$ Å. This indicates that in 10% Eu^{3+} doped $CsPbBr_3$ exchange interaction between Eu^{3+} ions is very unlikely.

Many examples exist of Eu^{3+} doped perovskite nanocrystals embedded in a glass matrix. Different types of glass are used to provide a host that allows both Eu^{3+} and $CsPbBr_3$ emission. However, no clear evidence for energy transfer between Eu^{3+} and $CsPbBr_3$ was found.

A CaO-ZnO-Al_2O_3–B_2O_3–SiO_2–$CsPbBr_3$-Eu^{3+} glass shows high $CsPbBr_3$ emission at 460 nm excitation. However, Eu^{3+} emission is almost negligible at this wavelength [101]. ZnO-SiO_2-B_2O_3 glass with $CsPbBr_3$:Eu^{3+} shows equal $CsPbBr_3$ and Eu^{3+} peaks under 365 nm excitation, with a high PLQY of 74%. However, no Eu^{3+} emission can be shown at higher excitation wavelengths [102]. An example of B_2O_3-SiO_2-ZnO glass with $CsPbBr_3$:Eu^{3+} shows increase of perovskite emission upon doping with Eu^{3+}. However, once again there is no clear Eu^{3+} emission [63].

A very striking example of a Eu^{3+} doped perovskite is shown in a paper by P. Li et al. (2020). A Eu^{3+}-doped $CsPbBr_3$ system is shown where simultaneous blue, green and red emission is produced. Blue emission is caused when Eu^{3+} reduces, and forms $CsEuBr_3$. Green emission originates from $CsPbBr_3$, and red emission from free Eu^{3+} ions, upon UV illumination. They state this is caused by energy transfer [103].

These examples show Eu^{3+} emission at wavelengths where the Eu^{3+} can self-excite, but show no clear signs of energy transfer.

Eu^{3+} emission can be increased by utilizing a two-step annealing process, where a high temperature annealing step is followed by a slow, lower temperature annealing step to alleviate stress in the glass matrix [63], [101]–[103]. Many Eu^{3+} phosphors are fabricated at high temperatures, ranging from 950°C up until 1400°C [16], [17], [60], [68], [69], [104], [105]. High fabrication temperatures are crucial for Eu^{3+} emission, as emission intensities drop significantly at lower fabrication temperatures.

Chapter 3

Methods

Chemicals

$CsPbBr_3$@SiO_2
Caesium bromide (CsBr, >99%) was purchased from Alfa Aesar. Lead(II) bromide ($PbBr_2$, $\geq$ 98%) and hydrochloric acid (HCl, 37%) were purchased from Sigma Aldrich. Molecular sieve MCM-41 type A was purchased from ACS Material, LLC.

Eu^{3+}
Europium(III) bromide hexahydrate ($EuBr_3 \cdot 6H_2O$, 99.99%) and europium(III) chloride ($EuCl_3$, 99.99%) were purchased from Sigma Aldrich. Y_2O_3:15%Eu^{3+} nanoplatelets and silicone gel Momentive IVS9520 were acquired from Seaborough.

Mesoporous yttria-stabilized zirconia
Zirconium(IV) chloride ($ZrCl_4$, >99%) and yttrium(III) chloride (YCl_3, 99.99%) were purchased from Alfa Aesar. Pluronic F127 ($(C_3H_6O \cdot C_2H_4O)$x) was purchased from Sigma Aldrich

Eu^{3+} β-diketonate
Thenoyltrifluoroacetone (Htta or 4,4,4,-trifluoro-1-(2-thienyl)-1,3-butanedione, 99%), tetraphenylphosphonium chloride ($P(Ph)_4Cl$, 98%) and sodium hydroxide (NaOH) were purchased from Sigma Aldrich

All chemicals were used as received without further purification.

Synthesis

Substrates
All substrates used are 1.2 x 1.2 cm quartz substrates. Prior to use, substrates are washed with deionized water and soap and rinsed with isopropanol. For measurements, samples are dropcasted on a substrate.

$CsPbBr_3$@SiO_2
In a ceramic mortar, CsBr and $PbBr_2$ are ground together in a 1:1 molar ratio, typically 1 mmol CsBr:1 mmol $PbBr_2$, together with a 1:3 weight ratio CsPb+$PbBr_2$:MCM-41, in this case 1.739 gram MCM-41. The mixture is ground for 5 minutes, and transferred to a ceramic crucible, which is placed in a quartz tube in a CVD (chemical vapor deposition) oven in air. The powder is heated up to 300°C with a 10°C/min heating ramp, dwelling for 3 minutes, and then heated to 700°C with a 5°C/min heating ramp, dwelling for 30 min. It is then cooled to room temperature.

The powder is washed by mixing with deionized water and sonicating for 5 minutes. The mixture is then centrifuged for 5 min at 2500 rpm, and the water is pipetted off. This is repeated 3 times. Then it is left to dry at 80°C.

This process is shown in Figure 3.1.

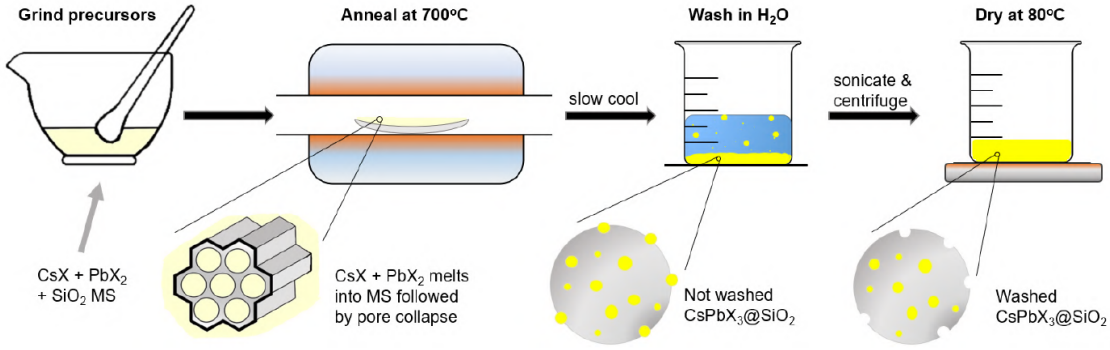

Figure 3.1: Synthesis of $CsPbX_3$ (X = Br) @ SiO_2. Figure from [106]

Stability measurements

For stability measurements, $CsPbBr_3$@SiO_2 is kept in a vial with deionized water. Before measurements, the vial is sonicated, and 100 µL of $CsPbBr_3$@SiO_2 in water is dropcasted on a substrate. This sample is named H_2O .

Two samples are made by encapsulating $CsPbBr_3$@SiO_2 in silicone gel Momentive IVS9520. Part A and part B of the silicone gel are combined in a 1:5 weight ratio. A 1:30 weight ratio $CsPbBr_3$@SiO_2:silicone gel is added. 0.06 g of this mixture is dropcasted on a quartz substrate. The substrate is desiccated for 10 minutes to remove any air bubbles. Then it is cured in the CVD oven in air at 150°C for 90 minutes, with a heating ramp of 5°C/min.

One sample called Ambient is kept in a sample box at room temperature in the dark. The second sample, called Heat & Ill., is kept on a hotplate set at 85°C, illuminated by a laser with a power of 15 mW/cm^2 (see Appendix A.1 for a schematic of the setup). This sample is not further heated and illuminated after 50 days.

$CsPbBr_3$:x%Eu^{3+}@SiO_2 (x = 5%, 10%, 20%, 50%, 100%)

Eu^{3+} doped $CsPbBr_3$@SiO_2 samples are made by grinding 1:1:x (x = 0.05, 0.1, 0.2, 0.5, 1) CsBr:$PbBr_2$:$EuBr_3$ with a 1:1 weight ratio MCM-41:CsBr+$PbBr_2$+$EuBr_3$. After grinding for 5 minutes, this mixture is treated as $CsPbBr_3$@SiO_2, and annealed in the CVD oven. It is heated to 300°C with a 10°C/min heating ramp, dwelling for 3 minutes, and then heated to 700°C with a 5°C/min heating ramp, dwelling for 30 min. Afterwards, it is washed thrice and dried.

$CsPbBr_3$:10%Eu^{3+}@SiO_2 900°

10% Eu^{3+} doped $CsPbBr_3$@SiO_2 was made according to a usual synthesis. After cooling the sample to room temperature, and undertaking washing steps, a second annealing step is done, by heating $CsPbBr_3$:10%Eu^{3+}@SiO_2 to 900°C for 15 minutes with heating ramp 30°C/min. Then, the sample is cooled to room temperature.

$CsPbBr_3$@SiO_2+Y_2O_3:15%Eu^{3+}

A 1:10 weight ratio $CsPbBr_3$@SiO_2:Y_2O_3:15%Eu^{3+} was mixed in H_2O and dropcasted.

Mesoporous yttrium-stabilized zirconia (mYSZ)

A procedure from [107] and [108] is followed. 0.0832 gram Pluronic F127 is dissolved in 33 mL ethanol by stirring at 500 rpm for 10 minutes. 1.192 mmol $ZrCl_4$ and 0.208 mmol YCl_3 are taken out of the glovebox and added to the ethanol mixture whilst stirring. After stirring at 500 rpm for 10 minutes, 1 mL deionized water is added dropwise, and the mixture is stirred for 1 more minute. The mixture is dried in air at room temperature for 1-3 days. The remaining substance is calcined in air by heating it

in the CVD in a ceramic boat, at 600°C for 4 hours, with a heating rate of 1°C/min. It is then cooled to room temperature.

$CsPbBr_3$@mYSZ
Encapsulating $CsPbBr_3$ in mYSZ is done by following the same procedure as used for encapsulation with molecular sieve MCM-41. CsPb and $PbBr_2$ in molar ratio 1:1 are ground together with a 1:1 weight ratio mYSZ:CsBr+$PbBr_2$. The sample is annealed by heating to 300°C with a 10°C/min heating ramp, dwelling for 3 minutes, and then heated to 700°C with a 5°C/min heating ramp, dwelling for 30 min.

mYSZ:10%Eu^{3+}
The procedure for making mYSZ was followed. $EuCl_3$ was added at the same time as $ZrCl_4$ and YCl_3, in molar ratio 1.192 mmol $ZrCl_4$:0.208 mmol YCl_3:0.119 mmol $EuCl_3$.

$CsPbBr_3$@mYSZ:10%Eu^{3+}
$CsPbBr_3$ was encapsulated in mYSZ:10%Eu^{3+} by following the steps for encapsulating in mYSZ, but using a 1:1 weight ratio mYSZ:10%Eu^{3+}:CsBr+$PbBr_2$.

mYSZ:10%Eu^{3+} annealed at x°C (x = 1000, 1300)
mYSZ:10%Eu^{3+} was made according to regular steps, but calcined at 1000°C or 1300°C instead of 600°C for 4 hours with heating rate 1°C/min

Eu^{3+} β-diketonate complex $Eu(tta)_4P(Ph)_4$
A procedure from [1] is followed. A 1M NaOH solution is made by dissolving 0.8 g NaOH in 20 mL demiwater. 6.154 mmol Htta (thenoyltrifluoroacetone) is dissolved in 6.154 mL NaOH solution by stirring at 500 rpm for 10 min. 3.692 mmol $P(Ph)_4Cl$ is dissolved in ethanol by stirring at 500 rpm for 10 min. This is added to the Htta solution. 1.539 mmol $EuCl_3$ is dissolved in 5 mL ethanol by stirring at 500 rpm for 10 min. Dropwise, this is added to the solution, whilst stirring at 60 rpm. The complex precipitates immediately. It is washed with water thrice by adding water to the beaker, sonicating for 5 min, and pipetting the water away. The complex is dissolved with DCM, and either stored in DCM or air dried.

Eu^{3+} β-diketonate + $CsPbBr_3$@SiO_2
Equal weight amounts of Eu^{3+} β-diketonate and $CsPbBr_3$ were dispersed in acetone under vigorous stirring and dropcasted on a substrate.

Instruments

PLQY
Photoluminescence quantum yield measurements were taken with a 405 nm ThorLabs S1FC405 laser and a Labsphere integrating sphere, coupled to an Avantes AvaSpec dual channel spectrometer. A procedure from [15] is followed, as is shown in Appendix A.2. For each PLQY result, three consecutive measurements were averaged. The PLQY setup is accurate within a range of 5%.

Photoluminescence spectra with excitation wavelength 405 nm
PL spectra were taken by exciting a sample with a 405 m Thorlabs S1FC405 diode laser through a WiTEC Alpha300 SR confocal microscope. The laser is focused on the sample with a P5-305A-PCAPC-1 optical fiber. The photoluminescence was measured with a UHTC 300VIS WiTEC spectrometer. The spotsize of the laser is between 2.0 and 2.4 micron in diameter, with a surface between 25 and 40 μm^2. The laser was operated at 150 μW power. Intensity on the sample lies between 3.75 W/mm^2 and 6 W/mm^2

For stability measurements, an image scan was taken of a 20x20 μm surface. The FWHM and center wavelength of all spectra in the image scan were calculated by applying a Jacobian transformation, and fitting a Lorentzian to the emission peak, as can be seen in Appendix A.3. The resulting FWHM and center wavelength were then averaged. Time traces were taken by measuring a spectrum every two seconds, in dark and illuminated periods. The intensity of the total emission peak was then integrated and plotted against the elapsed time.

Photoluminescence spectra with excitation wavelength≠405 nm and photoluminescence excitation spectra
Photoluminescence spectra with excitation wavelength≠405 nm and photoluminescence excitation spectra were taken with a Jobin Yvon FluoroLog spectrofluorometer (Horiba) with a 450 W xenon lamp coupled to a monochormator as an excitation source. All spectra are corrected for the spectral sensitivity of the spectrofluorometer.

Absorbance
Absorbance measurements were taken with a Perkin Elmer LAMBDA 750 UV/Vis/NIR spectrophotometer, with excitation wavelengths between 250 and 800 nm. It has a deuterium and a tungsten lamp with an InGaAs detector. The bandgap of a sample can be calculated by using a Tauc plot, as can be seen in Appendix A.4.

XRD
XRD patterns were measured with a Bruker D2 Phaser with a Cu x-ray source.

TEM
TEM measurements were taken with a FEI Tecnai G2 F20 X-TWIN transmission electron microscope.

Chapter 4

Results and Discussion

$CsPbBr_3$ is encapsulated in molecular sieve MCM-41. Stability is measured under conditions similar to that on an LED-chip for 50 days.

Eu^{3+} is doped in the $CsPbBr_3$ lattice to investigate if the perovskite forms a host where Eu^{3+} emission is enhanced, either because it is incorporated in a suitable host lattice, or because $CsPbBr_3$ can transfer energy to Eu^{3+}. $CsPbBr_3$ is combined with commercial phosphor Y_2O_3:15%Eu^{3+}, to research the possibility of energy transfer from the perovskite to Eu^{3+}.

Eu^{3+} is doped in a mesoporous yttria-stabilized zirconia host. This material is filled with $CsPbBr_3$, to facilitate energy transfer to Eu^{3+} in a host that enhances Eu^{3+} emission. β-diketonate ligands are added to Eu^{3+} to enhance emission under UV light.

4.1 $CsPbBr_3$@SiO_2

$CsPbBr_3$ was encapsulated in molecular sieve MCM-41. After annealing at 700°C, a bright yellow powder is formed that emits green light under UV illumination, as can be seen in Figure 4.1 a). In Figure 4.1 b) the XRD patterns of encapsulated and washed $CsPbBr_3$@SiO_2 can be seen. Comparison with peaks from literature shows that $CsPbBr_3$ has formed in the cubic phase [109]. Small deviations from literature are expected. A broader peak around 2θ/degree can be seen. This peak can be attributed to the molecular sieve formed out of amorphous silica.

$CsPbBr_3$ has formed inside the collapsed pores of MCM-41, as washing samples with water does not quench emission. Non encapsulated perovskite would be destroyed in seconds by washing with water [18].

The absorption spectrum of the sample is shown in Figure 4.1 c). $CsPbBr_3$ can absorb light with wavelength below 530 nm. A small peak in absorption can be seen around 310 nm, this corresponds to absorption by SiO_2. The bandgap is calculated using a Tauc plot, and is set at 530 nm (see Appendix A.4). The PL spectrum in Figure 4.1 d) shows PL emission of $CsPbBr_3$ excited with a 405 nm laser. An emission curve with center wavelength 517 nm and a FWHM of 20 nm can be seen, characteristic for $CsPbBr_3$ [18].

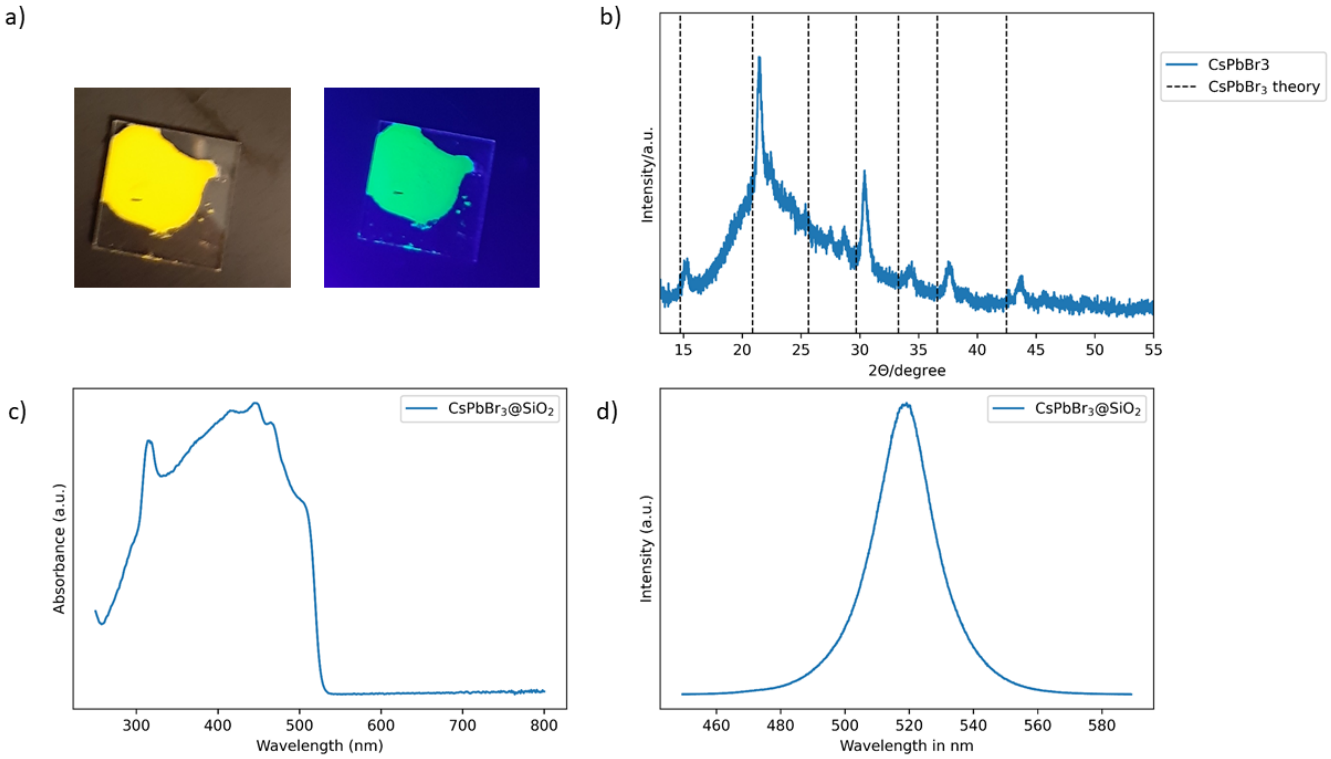

Figure 4.1: $CsPbBr_3$ was encapsulated in molecular sieve MCM-41, a) $CsPbBr_3@SiO_2$, left; ambient lighting, right; excitation at ∼395 nm, b) XRD patterns of $CsPbBr_3@SiO_2$, c) Absorbance of $CsPbBr_3@SiO_2$, d) PL spectrum of $CsPbBr_3@SiO_2$, excitation wavelength = 405 nm

4.2 Stability of $CsPbBr_3@SiO_2$

To investigate the stability of $CsPbBr_3@SiO_2$, 4 parameters were analyzed over a course of 50 days, with additional measurements taken after 184 days. Three different samples were measured, in conditions similar to those on an LED-chip.

The center wavelength of $CsPbBr_3$ emission can undergo a red- or blue shift as a result of changes in particle size, as the particles are quantum confined. Changes in particle size affect the bandgap of the perovskite, and can lead to broadening of the emission peak, which results in an increase in FWHM [18]. Degradation of the perovskite decreases the PLQY [32]. For these reasons, the FWHM, center wavelength, PLQY, and bandgap of the samples was measured.

The center wavelength and FWHM of $CsPbBr_3@SiO_2$ are shown in Figure 4.2 a) and b). Both the center wavelength and FWHM do not shift significantly over this period for $CsPbBr_3@SiO_2$ in ambient conditions, under heat and illumination, and in H_2O. These results indicate that the size of the $CsPbBr_3$ crystals does not change significantly over time under these conditions.

The bandgap as calculated with a Tauc plot is shown in Figure 4.2 d). The bandgap remains constant for all samples.

In the PLQY measurements, a large variation can be seen (see Figure 4.2 c)). This is presumably due to a lack of precision measurements in the setup. However, no significant drop in PLQY can be seen, even after 184 days.

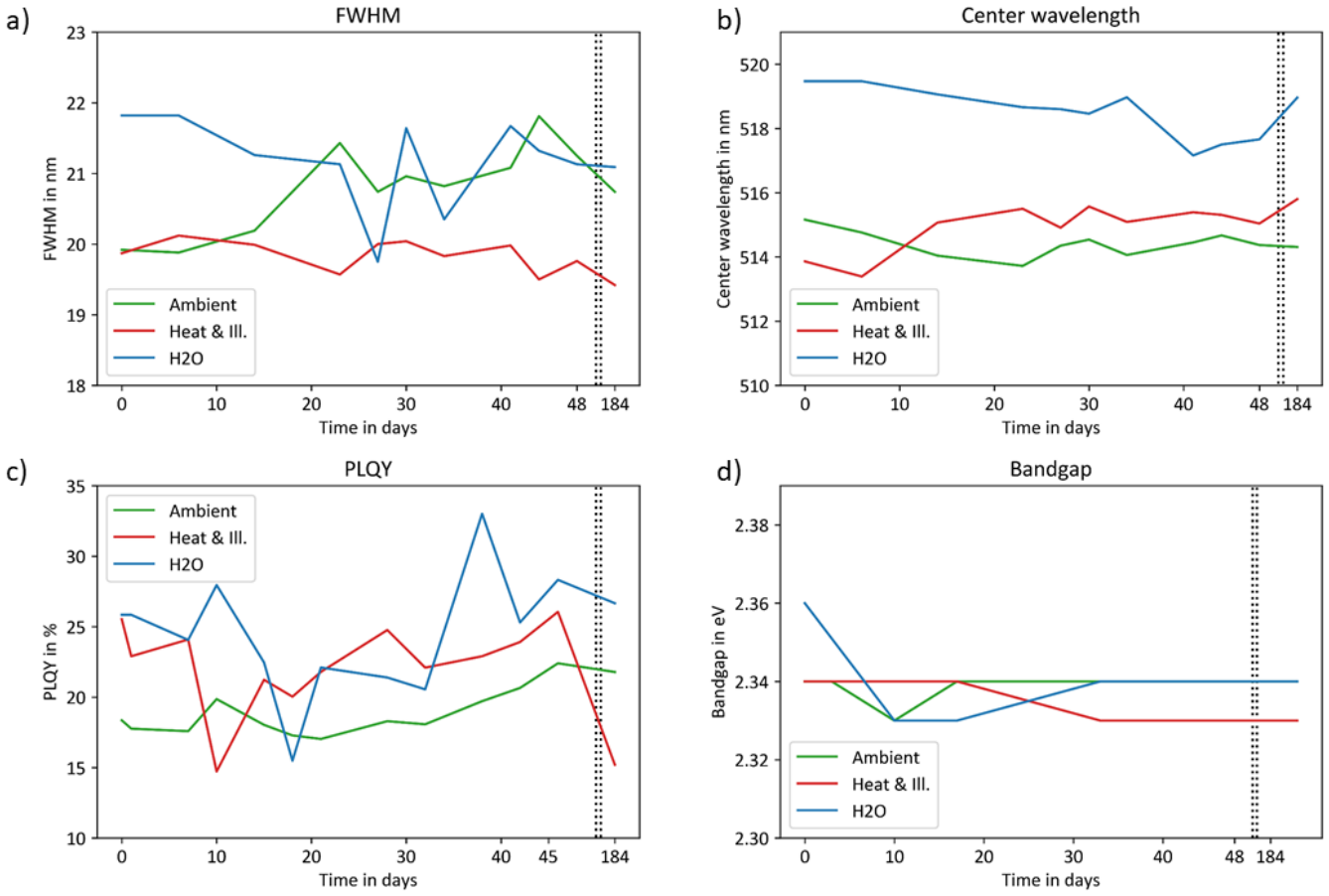

Figure 4.2: Stability of three samples $CsPbBr_3@SiO_2$. Ambient (green line) is stored at room temperature in dark conditions, Heat & Ill. (red line) is kept at 85°C and 15 mW/cm^2 illumination, H_2O (blue line) is stored in water, a) FWHM of PL emission spectra under 405 nm excitation, b) center wavelength of PL emission spectra under 405 nm excitation, c) PLQY, d) bandgap from absorption spectra

4.2.1 Stability of $CsPbBr_3@SiO_2$ under industrial laser power

Stability of $CsPbBr_3@SiO_2$ under a higher power laser was investigated, since a power of 15mW/cm^2 as used in the last section is orders of magnitude smaller than the power of an operating LED-chip [20]. The intensity of $CsPbBr_3@SiO_2$ was measured over 8 minutes of alternated illuminated and dark periods with a laser with power around 5 W/mm^2. The PL emission intensity of $CsPbBr_3$ can be seen to drop (see Figure 4.3 a)). The total emission of the perovskite emission declines, however self-healing behavior can also be observed, as the emission of the perovskite recovers after a dark period.

To analyze the effects of a laser power similar to that in an LED-chip, a 0.8 mW/mm^2 laser was used to excite $CsPbBr_3@SiO_2$. The total emission intensity was measured over the course of 2 minutes, as can be seen in Figure 4.3 b). After a large initial spike in intensity, perovskite emission intensity remains stable, and does not show further decay.

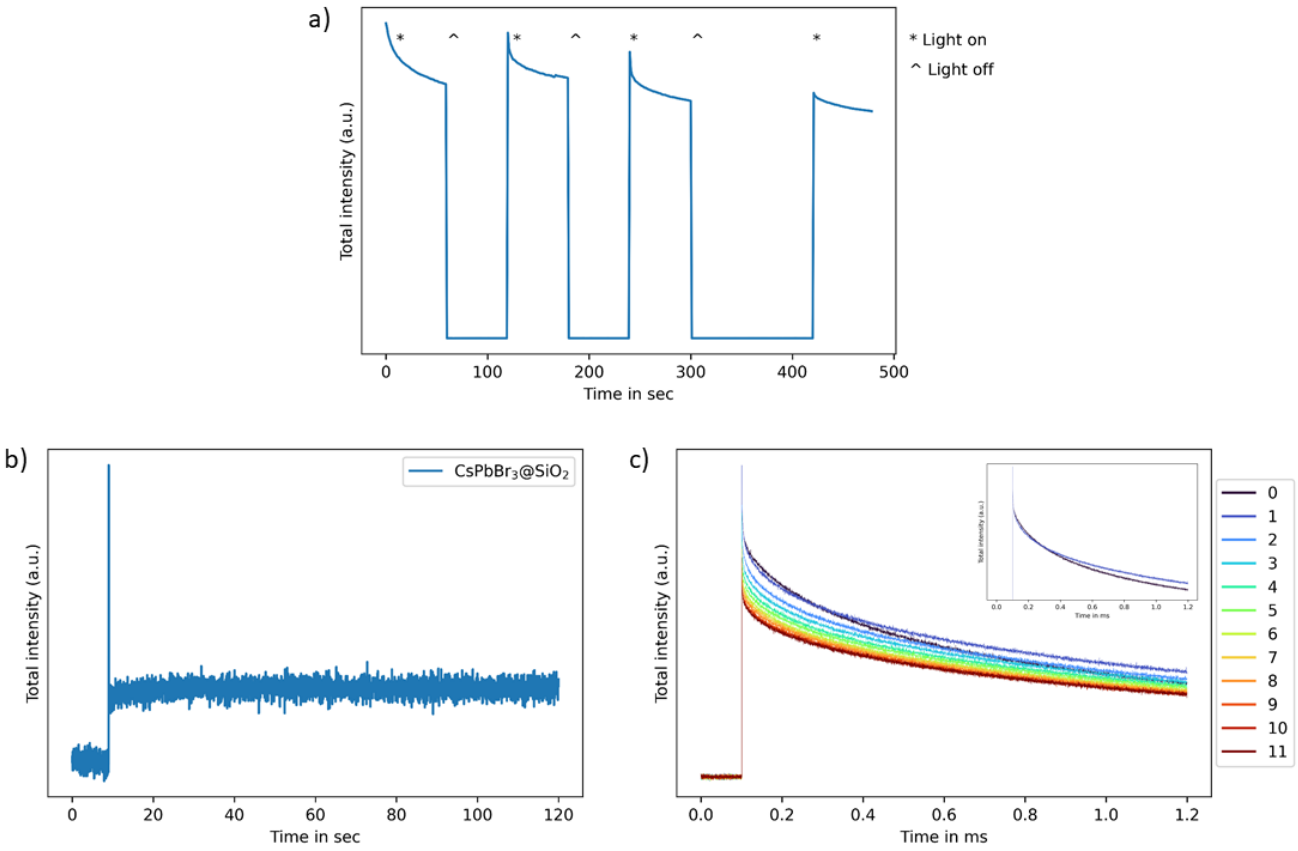

Figure 4.3: Stability of $CsPbBr_3@SiO_2$ under high intensity illumination, a) Total integrated intensity of $CsPbBr_3@SiO_2$ PL emission measured in 8 minutes consecutive illuminated and dark periods, with laser power around 5 W/mm^2, b) total intensity of $CsPbBr_3@SiO_2$ under 0.8 mW/mm^2 laser power for 2 minutes, c) total intensity of $CsPbBr_3@SiO_2$ under 12 consecutive 1 ms pulses of a 0.8 mW/mm^2 laser, with 1 s recovery time between pulses. a), b), c) excitation wavelength = 405 nm

To further examine this fast initial decay, a 0.8 mW/mm^2 laser was pulsed, and $CsPbBr_3$ was excited for 1 millisecond. After each pulse a dark period of 1 second followed. PL intensity declines quickly, but recovers after 1 second in the dark (Figure 4.3 c)). Self-healing behavior is visible between i.a. the first and second pulse, as is shown in the inset of Figure 4.3 c). Over the 12 pulses, a gradual total decline can be seen. After 10 pulses, the intensity traces overlap, and no further overall decline in emission intensity can be seen. The decay of $CsPbBr_3$ can be attributed to light induced stress.

Concluding, encapsulated $CsPbBr_3@SiO_2$ is stable over a long period of time. Encapsulation in molecular sieve MCM-41 effectively protects $CsPbBr_3$ from environmental degradation induced by water, oxygen, heat or weak illumination. However, the perovskite does not retain its full emission under high intensity illumination. This decline in emission does stabilize after a short period of time. $CsPbBr_3$ also exhibits self-healing behavior. For use as a wLED phosphor, stability under high laser power has to be further researched.

4.3 Eu^{3+} doped $CsPbBr_3@SiO_2$

$CsPbBr_3@SiO_2$ was doped with different molar concentrations Eu^{3+}. The XRD patterns in Figure 4.4 a) show that cubic phase $CsPbBr_3$ has formed. A normalized PL spectrum of $CsPbBr_3$:x$Eu@SiO_2$ (x = 5%, 10%, 20%, 50%, 100%) is shown in Figure 4.4 b). A typical $CsPbBr_3$ emission peak can be seen between 520-530 nm. With higher Eu^{3+} doping concentrations, this peak blueshifts. When Eu^{3+} is incorporated into $CsPbBr_3$, there is a strain on the perovskite lattice, and luminescence can blueshift [96]. This indicates that Eu^{3+} gets incorporated into the lattice. A growing blueshift with higher doping concentrations suggests that more Eu^{3+} is incorporated into the lattice at higher doping concentrations.

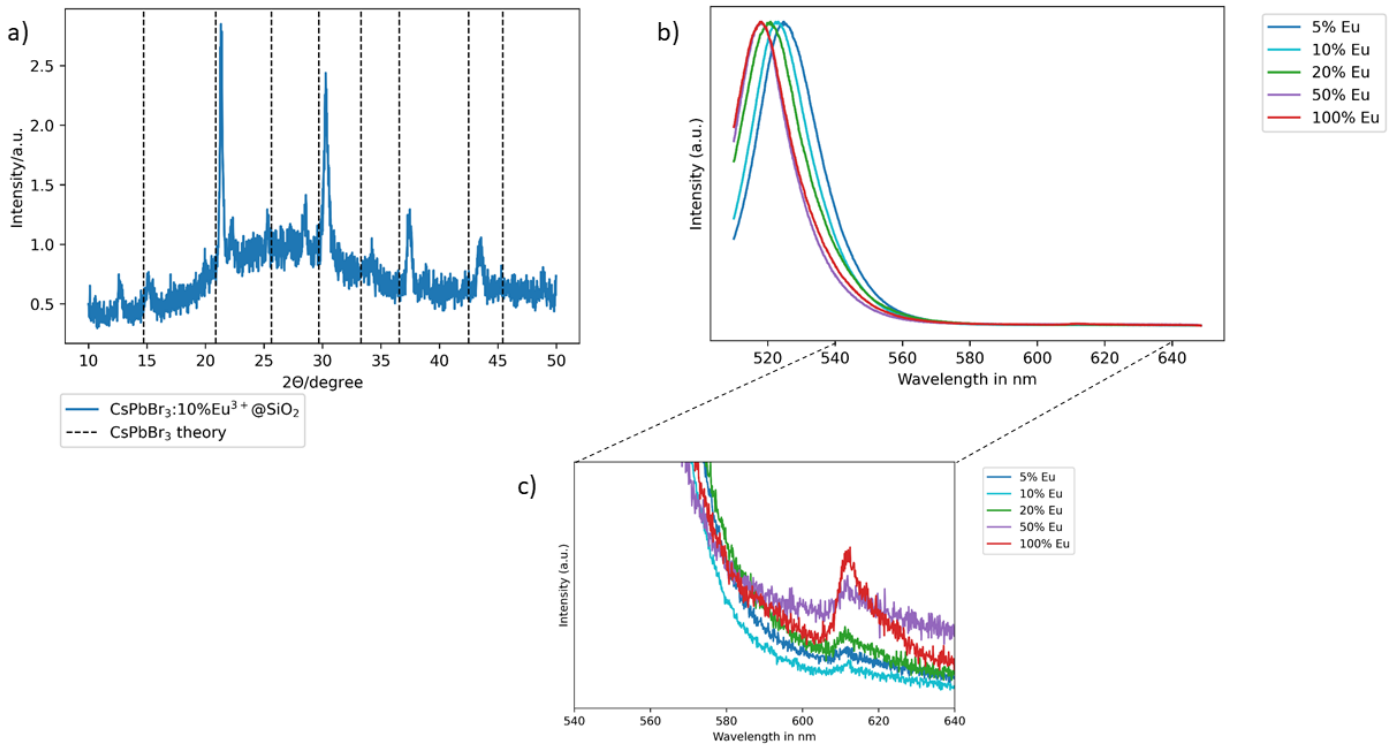

Figure 4.4: $CsPbBr_3@SiO_2$ doped with different concentrations Eu^{3+}, a) XRD patterns of $CsPbBr_3$:10%$Eu^{3+}@SiO_2$, b) normalized PL spectrum of $CsPbBr_3$:x$Eu^{3+}@SiO_2$ (x = 5%, 10%, 20%, 50%, 100%), c) close-up of PL spectrum, b), c) excitation wavelength 405 nm

In all samples, Eu^{3+} emission from the $^5D_0 \rightarrow {}^7F_2$ transition can be seen (see Figure 4.4 c)) when excited with a 405 nm laser. However, this emission is extremely weak in comparison to the perovskite emission. This indicates $CsPbBr_3$ is not a suited host matrix for Eu^{3+} emission.

A PLE spectrum was taken of a 50% doped $CsPbBr_3$:Eu^{3+} spectrum (Figure 4.5), to examine whether energy transfer occurs. Excitation of $CsPbBr_3$ (green line) can be seen to drop after the bandgap of $CsPbBr_3$ at 530 nm. A slight dip in excitation can be seen around 310 nm, this can be attributed to absorption of the light by SiO_2. A large excitation peak can be seen around 514 nm, which is the point where the emission wavelength corresponds to the excitation wavelength. This peak can be ascribed to the lamp saturating the detector. A sideband of the emission of the lamp can be seen between 480 and 500 nm.

The excitation spectrum of Eu^{3+} emission (red line) shows a large excitation peak below 300 nm. This is due to the Eu-O charge transfer band. Two very small excitation bands can be seen at 395 nm and 465 nm. These bands are the $^7F_0 \rightarrow {}^5L_6$ and $^7F_0 \rightarrow {}^5D_2$ transitions, respectively. Around 520 nm, a small rise in excitation can be seen in the Eu^{3+} excitation spectrum. This is due to a sideband of the lamp. No signs of energy transfer can be seen.

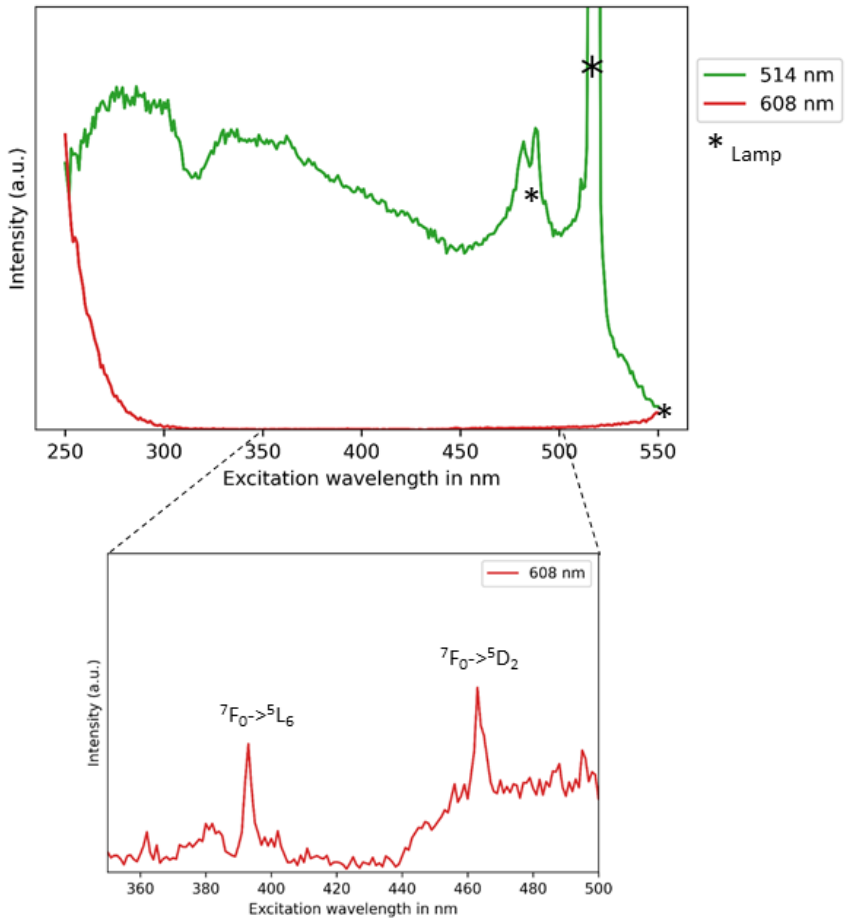

Figure 4.5: PLE spectrum of $CsPbBr_3$:50%Eu^{3+}@SiO_2. The green line is the excitation spectrum of 514 nm $CsPbBr_3$ emission, the red line is the excitation spectrum of 608 nm Eu^{3+} emission. A close-up of the PLE spectrum shows Eu^{3+} excitation bands

4.3.1 $CsPbBr_3$:Eu^{3+}@SiO_2 annealed at 900°C

Many Eu^{3+} phosphors are produced at high temperature to enhance PL intensity [101]-[105]. Hence, $CsPbBr_3$:10%Eu^{3+}@SiO_2 was subjected to a double annealing procedure.

The PL spectrum in Figure 4.6 a) shows $CsPbBr_3$ and Eu^{3+} emission. The perovskite emission is slightly blueshifted compared to regular $CsPbBr_3$:10%Eu^{3+}@SiO_2 as shown in Figure 4.4 b). High temperature annealing could change the pore size of SiO_2, and induce a stronger quantum confinement effect, causing a blueshift in $CsPbBr_3$ emission. The shape of the perovskite emission is distorted when excited at 460 nm. A large peak can be seen at 460 nm, because of direct excitation of the spectrometer by the lamp. The emission around 510 nm is a sideband of the emission of the lamp.

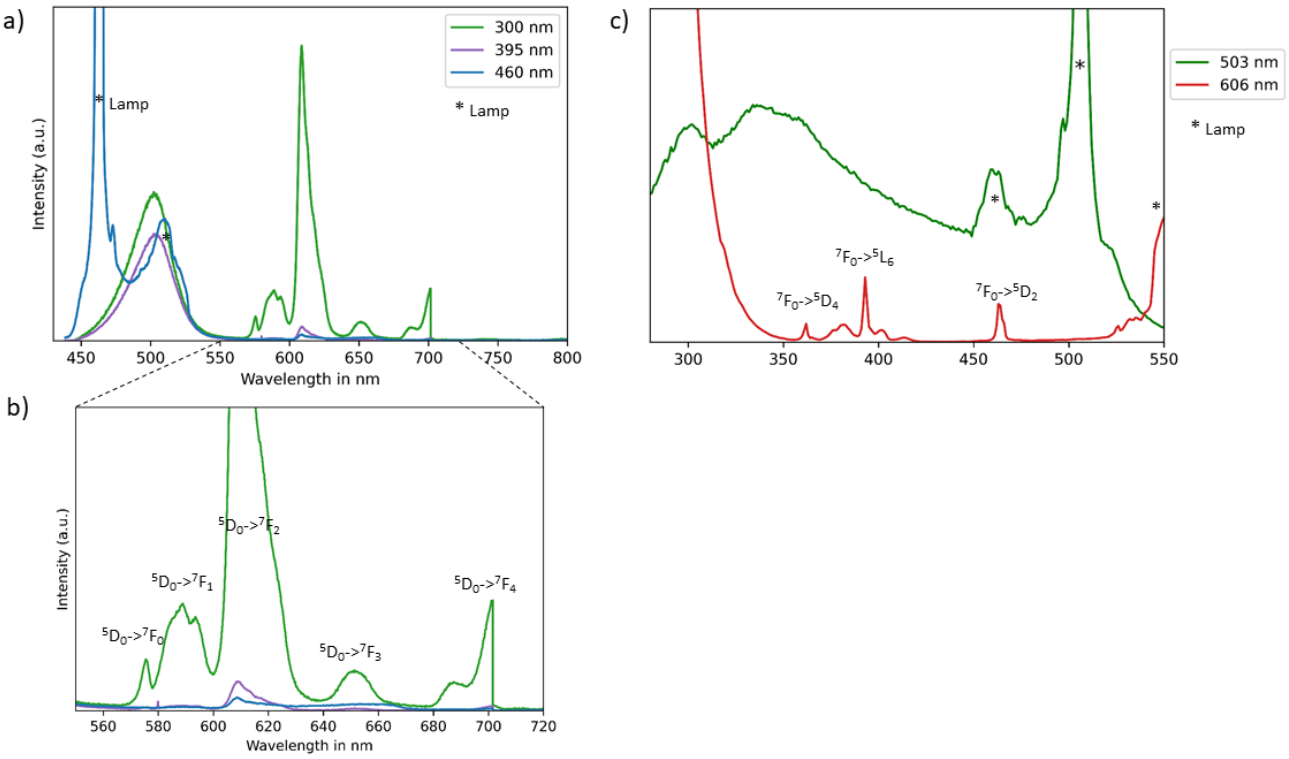

Figure 4.6: $CsPbBr_3$:10%Eu^{3+}@SiO_2 annealed at 900°C, a) PL spectrum excited at 300 nm, 395 nm, 460 nm respectively, b) close-up of PL spectrum, c) PLE spectrum, the green line is the excitation spectrum of 503 nm $CsPbBr_3$ emission, the red line is the excitation spectrum of 606 nm Eu^{3+} emission

In Figure 4.6 a) and b), Eu^{3+} emission can be observed. This emission is strongest with excitation at 300 nm, which indicates self-excitation due to the Eu-O charge transfer band. Multiple Eu^{3+} transitions can be observed. The hypersensitive transition $^5D_0 \rightarrow {}^7F_2$ is the most intense. This indicates Eu^{3+} has an asymmetrical environment. The appearance of the $^5D_0 \rightarrow {}^7F_0$ peak indicates J-mixing. MD transition $^5D_0 \rightarrow {}^7F_3$ is visible. The $^5D_0 \rightarrow {}^7F_4$ ED transition is also present, but is not very bright. This transition is not completely visible due to the range of the spectrofluorometer. The peaks are also visible at 395 and 460 nm excitation, albeit with a much weaker intensity.

From the PLE spectrum in Figure 4.6 c) it can be seen that Eu^{3+} is effectively excited with UV light. This is due to the broad Eu-O charge transfer band. Compared to regular $CsPbBr_3$:10%Eu^{3+}@SiO_2 this charge transfer band is broader, and shows Eu^{3+} excitation up to 350 nm. This indicates Eu^{3+} experiences a different crystal field from the host lattice [72] when annealed at higher temperatures.

The $^7F_0 \rightarrow {}^5D_4$, $^7F_0 \rightarrow {}^5L_6$, and $^7F_0 \rightarrow {}^5D_2$ excitation peaks are visible. The rise in excitation around 520 nm can be ascribed to a sideband of the lamp. There are no signs of energy transfer, the Eu^{3+} emission is most likely due to self-excitation.

Compared to the sample annealed at 700°C, Eu^{3+} emission is much stronger in relation to the perovskite emission. This has two possible reasons. On one hand, the high annealing temperature could partly destroy the $CsPbBr_3$, leading to a decrease in perovskite emission [18]. On the other hand, Eu^{3+} could be in an asymmetric site that allows more effective absorption and emission.

4.3.2 $CsPbBr_3$:Eu^{3+}@SiO_2 combined with red phosphor Y_2O_3:15%Eu^{3+}

The commercially available phosphor Y_2O_3:15%Eu^{3+} was combined with $CsPbBr_3$@SiO_2. The phosphor is a host that is suitable for Eu^{3+} self-excitation [66]. In this system, $CsPbBr_3$ could form an energy donor to transfer energy to Eu^{3+} via a FRET mechanism.

In Figure 4.7 a) the PL spectrum of Y_2O_3:15%Eu^{3+} can be seen. As expected, hypersensitive transition $^5D_0 \rightarrow {}^7F_2$ shows strong emission. Figure 4.7 b) shows the excitation spectrum of Y_2O_3:15%Eu^{3+}, where $^7F_0 \rightarrow {}^5L_6$, and $^7F_0 \rightarrow {}^5D_2$ are the largest excitation peaks. This shows Y_2O_3:15%Eu^{3+} can be excited by both UV light and 460 nm light. These transitions have many sidebands, which indicates splitting of the Eu^{3+} energy levels.

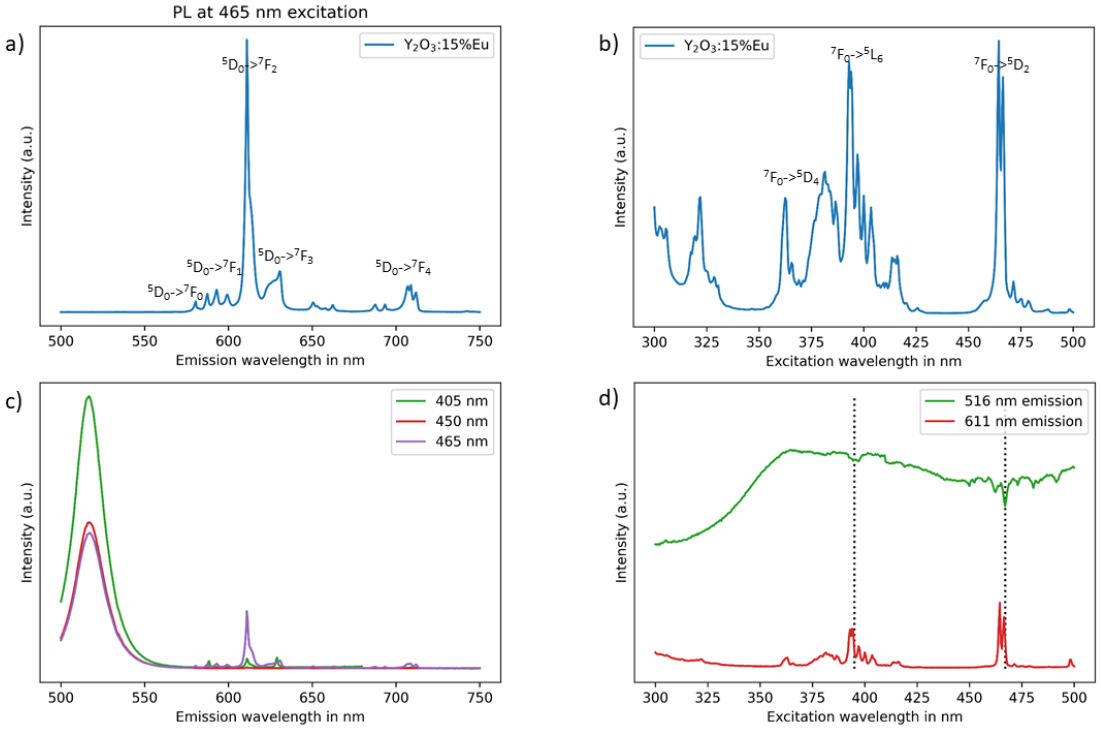

Figure 4.7: $CsPbBr_3$@SiO_2 was combined with Y_2O_3:15%Eu^{3+}, a) PL spectrum of Y_2O_3:15%Eu^{3+}, excited at 465 nm b) PLE spectrum of Y_2O_3:15%Eu^{3+} emission at 611 nm, c) PL spectrum of $CsPbBr_3$@SiO_2 + Y_2O_3:15%Eu^{3+}, excited at 405 nm, 450 nm, and 460 nm, d) PLE spectrum of $CsPbBr_3$@SiO_2 + Y_2O_3:15%Eu^{3+}. The green line is the excitation spectrum of 516 nm $CsPbBr_3$ emission, the red line is the excitation spectrum of 611 nm Eu^{3+} emission

Figure 4.7 c) shows the PL spectrum of $CsPbBr_3$@SiO_2 + Y_2O_3:15%Eu^{3+}. Excitation at 405 nm induces the strongest $CsPbBr_3$ emission peak, and excitation at 465 gives the largest Eu^{3+} $^5D_0 \rightarrow {}^7F_2$ emission peak.

In the PLE spectrum of Y_2O_3:15%Eu^{3+} emission at 611 nm (red line in Figure 4.7 d)) the $^7F_0 \rightarrow {}^5L_6$ and $^7F_0 \rightarrow {}^5D_2$ absorption bands are clearly visible. $CsPbBr_3$ excitation at 516 nm (green line in Figure 4.7 d)) shows two small dips, around 395 nm and 465 nm. This shows that Eu^{3+} absorbs part of the light at that wavelength. There are no clear signs of energy transfer.

Y_2O_3:15%Eu^{3+} was also combined with $CsPbBr_3$ nanocubes (see Appendix A.5), no energy transfer was found.

It can be concluded that Eu^{3+} directly with $CsPbBr_3$ does not induce energy transfer. To enhance this, a different host was found to enhance Eu^{3+} emission.

4.4 Mesoporous yttria-stabilized zirconia

The emission and excitation spectrum of Eu^{3+} is heavily dependent on the environment [72]. To enhance emission intensity, a different host matrix was chosen. Yttria-stabilized zirconia (YSZ) has been used as a host for Eu^{3+}, and it has been shown to enhance Eu^{3+} emission [71], [110]. Mesoporous yttria-stabilized zirconia (mYSZ) was chosen as host material, since $CsPbBr_3$ can be formed in the pores. This results in a small distance between the Eu^{3+} ions in the mYSZ matrix and the $CsPbBr_3$ nanocrystals, increasing FRET efficiency.

Mesoporous yttria-stabilized zirconia is a ceramic material that has high thermal stability, a uniform porous structure, and high chemical stability [107]. The porous structure is stable until about 800°C [111].

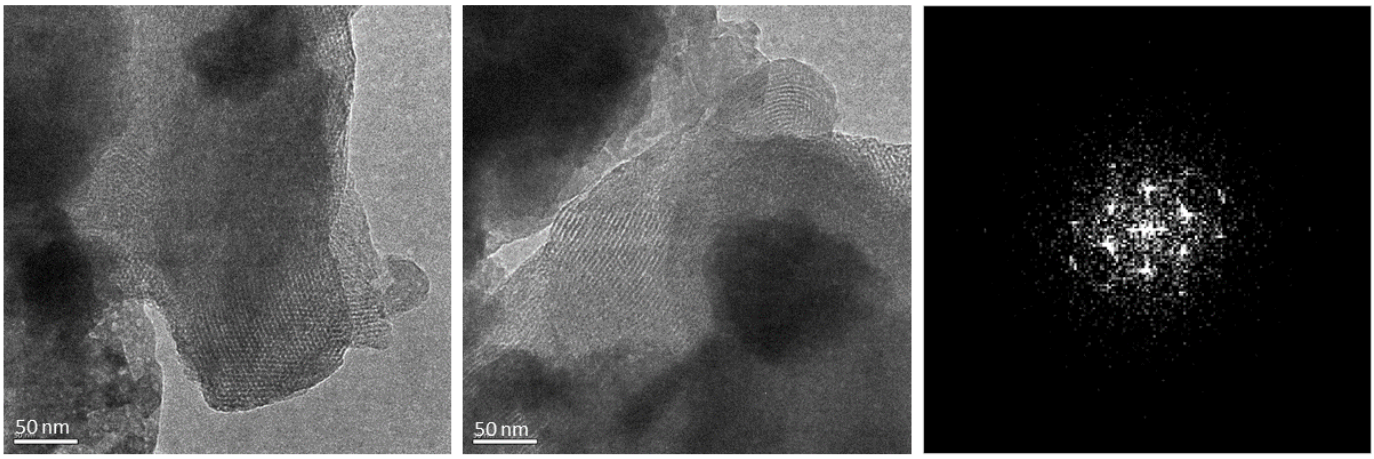

Figure 4.8: TEM images of mesoporous yttria-stabilized zirconia. Right: Fourier transform of TEM image

TEM images of mYSZ in Figure 4.8 show a mesoporous material. The pore size of the material was calculated with a Fourier transform (Figure 4.8; right). The pores have a size between 3 and 4 nm in diameter, with most pores <3.5 nm. This is a pore size similar to MCM-41, which has pore size 3.4 nm [46].

Peaks in the XRD spectrum confirm this is a mesoporous yttria-stabilized zirconia material with comparison to literature as can be seen in Figure 4.10 a) [71], [110], [112] . A broad peak can be seen between 20-30 2θ/degree. This indicates that part of the sample is amorphous. In Figure 4.9 a), the absorption spectrum shows that mYSZ strongly absorbs light below 300 nm.

4.4.1 Encapsulating $CsPbBr_3$ with mesoporous yttria-stabilized zirconia

$CsPbBr_3$ is formed in the mYSZ pores. mYSZ forms a suitable encapsulant for $CsPbBr_3$ because it is impermeable for water or oxygen and has high thermal stability. Upon illumination with ∼395 nm light, green emission can be seen (Figure 4.9 c)). From the XRD pattern in Figure 4.10 b), the presence of mYSZ is confirmed. The peak at 21 2θ/degree can be attributed to the cubic phase of $CsPbBr_3$ [109].

The mYSZ XRD patterns are much more well-defined compared to mYSZ without $CsPbBr_3$ (Figure 4.10 a)), as the broad peak between 20-30 2θ/degree has disappeared. This indicates that additional annealing can improve mYSZ structure.

The absorption spectrum (Figure 4.9 a)) of $CsPbBr_3$@mYSZ shows absorption up until 500 nm. This can be attributed to absorption of $CsPbBr_3$ up until the bandgap, which was calculated to be at 510 nm. This indicates that $CsPbBr_3$ has a slightly smaller crystal size compared to $CsPbBr_3$@SiO_2 [25].

The PL spectrum in Figure 4.9 b) shows typical $CsPbBr_3$ emission, with a FWHM of 23 nm, and a center wavelength of 506 nm. This center wavelength is slightly blueshifted in comparison to $CsPbBr_3$@SiO_2 (see Figure 4.1 d)), also indicating that $CsPbBr_3$ has a slightly smaller crystal size.

$CsPbBr_3$ is protected from the influences of oxygen and water by encapsulation in mYSZ. The perovskite is luminescent, even when dispersed in water or 1M hydrochloric acid (HCl) (see Figure 4.9 c)). After storing in water or 1M HCl for 5 months, the perovskite is still luminescent. Non encapsulated $CsPbBr_3$ emission would be quenched after seconds in water [18], [33]. The center wavelength is stable at 506 nm, with a FWHM of 23 nm, as can be seen in Figure 4.9 d).

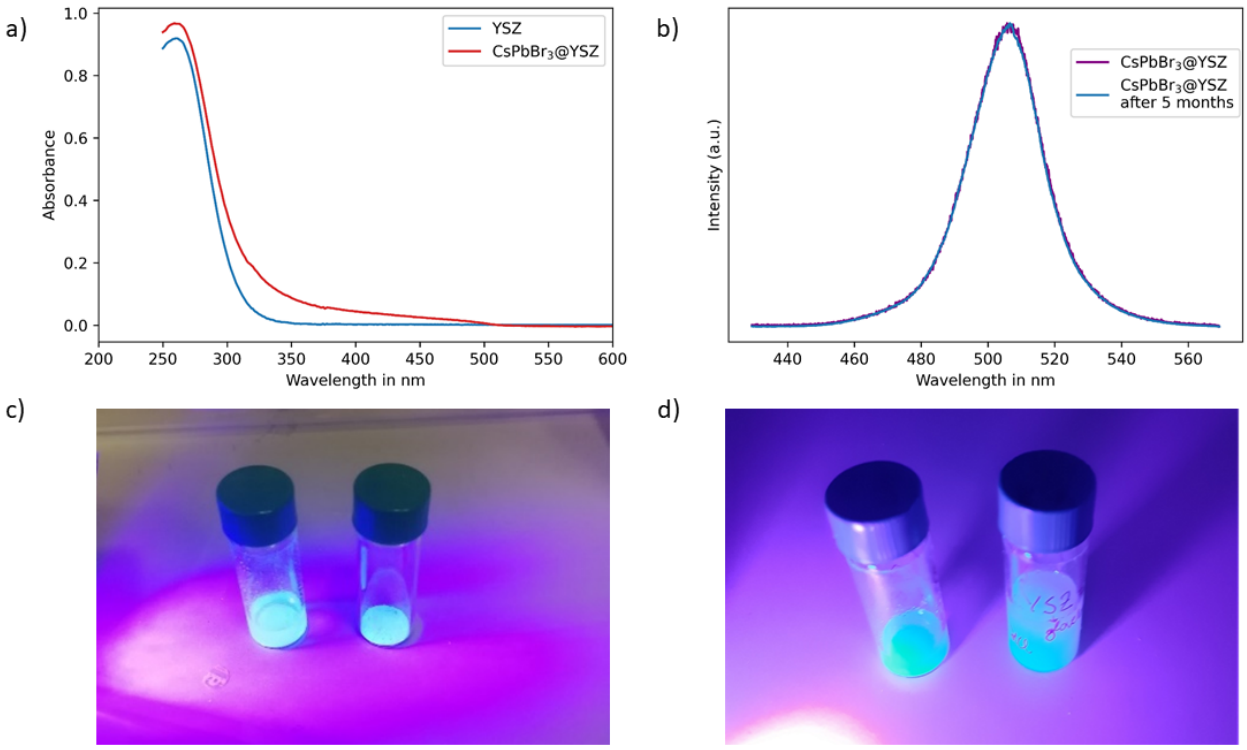

Figure 4.9: $CsPbBr_3$ was encapsulated in mYSZ, a) absorption spectrum of mYSZ and $CsPbBr_3$@mYSZ, b) normalized PL spectrum of $CsPbBr_3$@mYSZ and $CsPbBr_3$@mYSZ after 5 months in H_2O, excited at 405 nm, c) $CsPbBr_3$@mYSZ illuminated with UV light, right; powder in air, left; in water, d) $CsPbBr_3$@mYSZ illuminated with UV light, right; after 5 months in 1M HCl, left; after 5 months in water

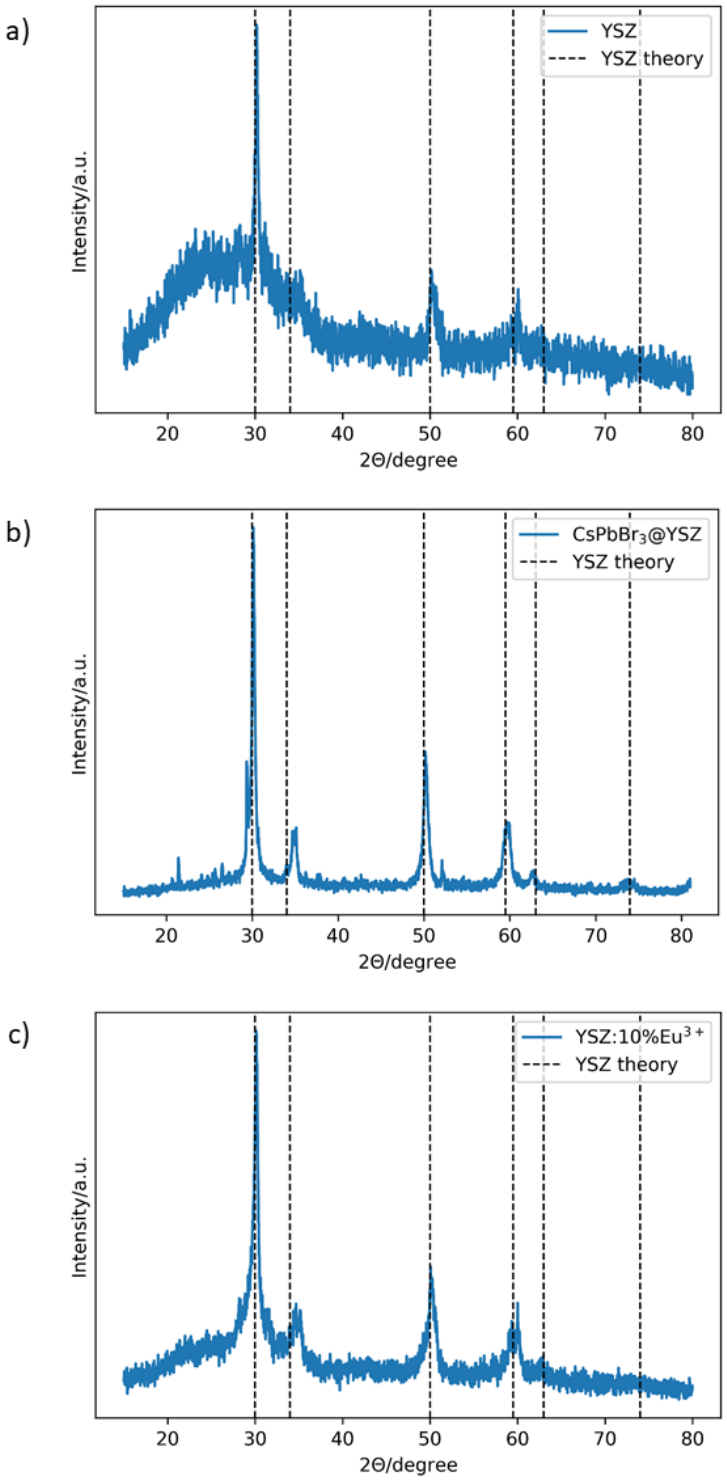

Figure 4.10: a) XRD patterns of mYSZ, b) XRD patterns of $CsPbBr_3$@mYSZ, c) XRD pattern of mYSZ doped with 10% Eu^{3+}

4.4.2 Eu^{3+} doped mesoporous yttria-stabilized zirconia

Eu^{3+} was incorporated in the mYSZ matrix. 10% Eu^{3+} doping (mYSZ:10%Eu^{3+}) results in a weak Eu^{3+} emission (Figure 4.11 a), inset). The structure of mYSZ is preserved, as can be seen from the XRD patterns in Figure 4.10 c), although a slight broadening in peaks can be seen, indicating that the structure is less well-defined.

PL measurements show Eu^{3+} emission (Figure 4.11 a)), mostly upon excitation with UV light, but also under excitation with 460 nm light. The hypersensitive transition $^5D_0 \rightarrow {}^7F_2$ is slightly stronger than other $^5D_0 \rightarrow {}^7F_J$ transitions. However, in an optimal host, this emission would be up to 100 times stronger than other transitions.

The PLE spectrum in Figure 4.11 b) shows effective Eu^{3+} excitation up to 380 nm. This indicates effective excitation of the Eu-O charge transfer band. The band extends up until 380 nm, underlining the sensitive nature of this band to the host environment. In the PLE spectra in Figure 4.5 and Figure 4.6 c) these bands are not as broad. Eu^{3+} emission intensity shows a dip in excitation below 300 nm, which is likely due to strong absorption of the YSZ matrix. The inset shows the $^7F_0 \rightarrow {}^5L_6$ and $^7F_0 \rightarrow {}^5D_2$ transitions.

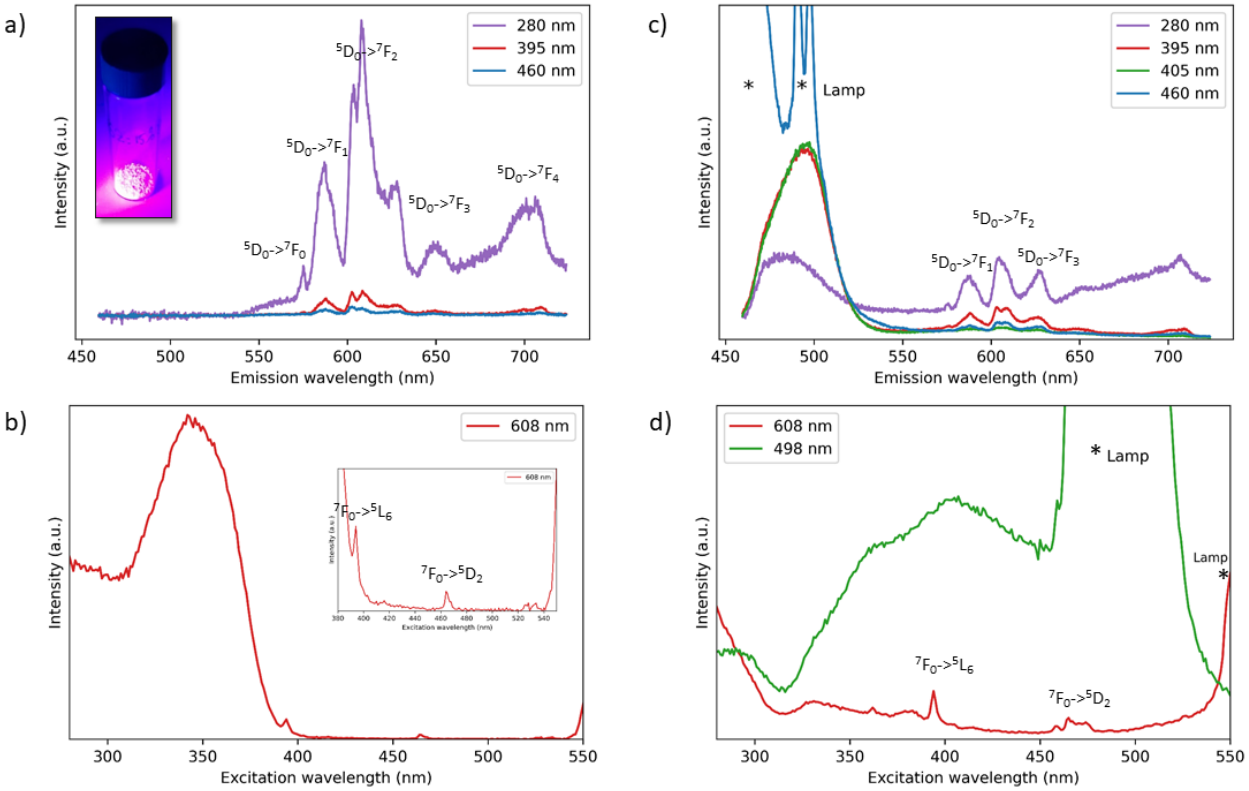

Figure 4.11: mYSZ was doped with 10%Eu^{3+}, and filled with $CsPbBr_3$, a) PL spectrum of mYSZ:10%Eu^{3+}, inset; photo under ~395 illumination, b) PLE spectrum of mYSZ:10%Eu^{3+} emission at 608 nm, c) PL spectrum of $CsPbBr_3$@mYSZ:10%Eu^{3+}, d) PLE spectrum of $CsPbBr_3$@mYSZ:10%Eu^{3+} emission at 608 and 498 nm

$CsPbBr_3$@mYSZ:10%Eu^{3+}

$CsPbBr_3$ was formed inside the pores of mYSZ:10%Eu^{3+}. This sample emits green light under ~395 illumination. After washing the sample with water, it was still emissive. This indicates that mYSZ:10%Eu^{3+} has a mesoporous structure, in which $CsPbBr_3$ can be formed. After storing this material in HCl for 5 months, green emission could still be seen (see A.6 a) and b)). The luminescence of this material was less bright than $CsPbBr_3$@mYSZ, as can be seen in A.6. This could indicate that the pore structure of mYSZ changes when doped with Eu^{3+}, and is less suited for $CsPbBr_3$ encapsulation.

The PL spectrum shows both $CsPbBr_3$ and Eu^{3+} emission (Figure 4.11 c)). The high $^5D_0 \rightarrow {}^7F_1$ and $^5D_0 \rightarrow {}^7F_3$ Eu^{3+} emission peaks indicate strong J-mixing.

In the PLE spectrum in Figure 4.11 d) excitation below 320 nm is weak for both $CsPbBr_3$ and Eu^{3+}, due to strong absorption of mYSZ. The strong Eu-O charge transfer band that extends up to 380 nm in unfilled mYSZ:10%Eu^{3+} is also quenched. The $^7F_0 \rightarrow {}^5L_6$ and $^7F_0 \rightarrow {}^5D_2$ transitions are visible.

4.4.3 mYSZ:10%Eu^{3+} annealed at high temperature

Eu^{3+} doped YSZ has a higher emission after annealing at high temperature as more defects arise [71], [110], [112]. This means Eu^{3+} can occupy more non-symmetric sites in the material, which increases emission intensity [112].

After annealing mYSZ:10%Eu^{3+} at 1000°C, Eu^{3+} emission showed a more narrow $^5D_0 \rightarrow {}^7F_2$ emission (see Figure 4.12 a)). The hypersensitive character of this transition is clear, as its intensity is about 10 times higher than that of the $^5D_0 \rightarrow {}^7F_3$ transition. Annealing at 1300°C does not induce further narrowing of the $^5D_0 \rightarrow {}^7F_2$ transition (see Figure 4.12 a)). Here, the hypersensitivity of the transition is not optimal.

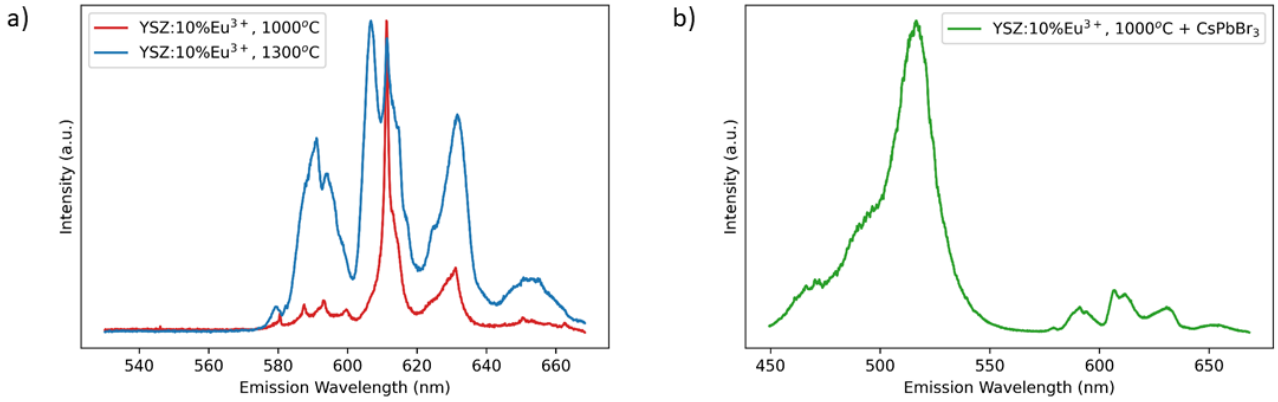

Figure 4.12: mYSZ:10%Eu^{3+} was annealed at higher temperatures and filled with $CsPbBr_3$, a) normalized PL intensity of mYSZ:10%Eu^{3+}, annealed at 1000°C and 1300°C, excited by a 405 nm laser, b) normalized PL intensity of $CsPbBr_3$@mYSZ:10%Eu^{3+} annealed at 1000 °C , excited by a 405 nm laser

$CsPbBr_3$ encapsulated in mYSZ:10%Eu^{3+} annealed at 1000°

mYSZ:10%Eu^{3+} annealed at 1000°C was filled with $CsPbBr_3$. Both perovskite and Eu^{3+} emission could be detected upon excitation with a 405 nm laser, as is shown in Figure 4.12 b). To properly analyze the effect of high temperature annealing of mYSZ:10%Eu^{3+} and $CsPbBr_3$@mYSZ:10%Eu^{3+}, PL measurements at 460 nm excitation wavelength and PLE spectra are needed.

mYSZ proves to be a matrix in which $CsPbBr_3$ is encapsulated, and partially protected from the influence of oxygen and water. Doping the mYSZ matrix with Eu^{3+} provides a good host for self-excitation of Eu^{3+} emission. When annealing at higher temperatures, the hypersensitive character of the $^5D_0 \rightarrow {}^7F_2$ transition can be observed. For use in a wLED, Eu^{3+} emission is not bright enough under illumination with a 460 nm LED-chip. There is no strong evidence for energy transfer between $CsPbBr_3$ and YSZ:Eu^{3+}.

4.5 Eu^{3+} β-diketonate complex

In order to enhance Eu^{3+} emission, the $Eu(tta)_4P(Ph)_4$ β-diketonate complex was formed. This complex produces a bright pink/red color under ~395 nm illumination (see Figure 4.13 c)), characteristic for the hypersensitive $^5D_0 \rightarrow {}^7F_2$ transition. The PL spectrum in Figure 4.13 a) shows an extremely narrow peak with a center wavelength at 613 nm and a FWHM of 3.2 nm upon excitation at 295 nm. This shows the hypersensitive transition of Eu^{3+} has high intensity emission. The PLQY of this complex was measured up to 52% under 405 nm excitation.

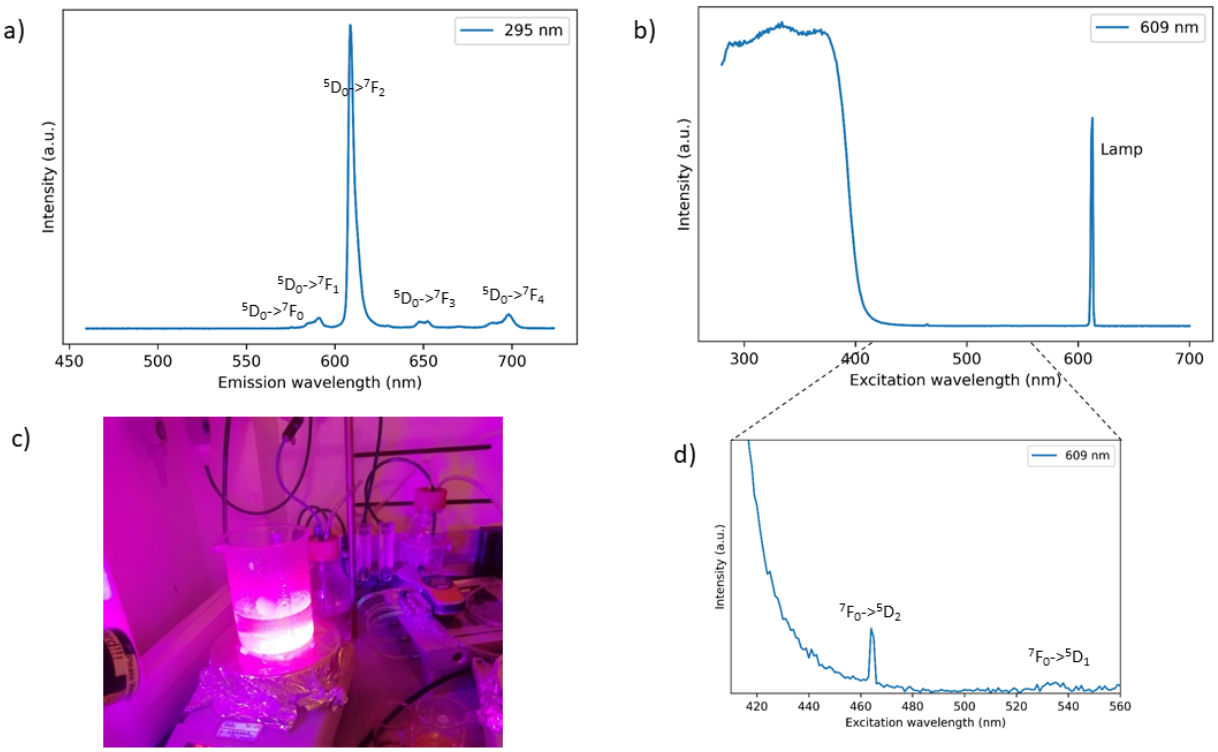

Figure 4.13: Eu^{3+} β-diketonate complex $Eu(tta)_4P(Ph)_4$, a) PL spectrum of Eu^{3+} β-diketonate complex, excited at 295 nm, b) PLE spectrum of Eu^{3+} emission at 609 nm, c) photo of Eu^{3+} β-diketonate complex excited with ~395 nm light, d) close-up of b)

The PLE spectrum in Figure 4.13 b) shows strong UV excitation. The tta ligands of the complex absorb UV light and transfer it to Eu^{3+} via Dexter energy transfer [55]. Efficient UV excitation is extended up until the $^7F_0 \rightarrow {}^5L_6$ transition that absorbs around 395 nm, because of energy transfer from the ligands. Further small excitation peaks can be seen at 460 nm, attributed to the $^7F_0 \rightarrow {}^5D_2$ transfer band, and at around 535 nm. This very small peak indicates excitation through the $^7F_1 \rightarrow {}^5D_1$ transition. However, this excitation is very weak, possibly because of low occupation density of the $^7F_1$ state at room temperature [72]. The PLE shows that although the Eu^{3+} β-diketonate complex has a very bright emission, excitation wavelengths are not compatible with use in a wLED.

The Eu^{3+} β-diketonate complex is not stable under illumination, as is shown in Appendix A.7. However, it shows remarkable self-healing properties. The stability of the complex can be improved by encapsulating it in PMMA (Figure A.7).

4.5.1 $CsPbBr_3$@SiO_2 combined with Eu^{3+} β-diketonate

$CsPbBr_3$@SiO_2 was combined with the Eu^{3+} β-diketonate complex. A photo in Figure 4.14 c) shows a warm white/yellow emission under UV illumination. The PL spectrum in Figure 4.14 a) shows a green $CsPbBr_3$ emission peak and a narrow red Eu^{3+} β-diketonate peak under 405 nm illumination. This PL spectrum is how an emission spectrum for two phosphors should ideally look like [14]. The green emission peak and the red emission peak are displayed in a CIE chromaticity diagram in Figure 4.14 b). It can be seen that combined with a 460 nm InGaN LED-chip a wide color gamut would be achieved.

However, this system is not suited for use in a wLED, as Eu^{3+} emission would be drastically lower under 460 nm excitation.

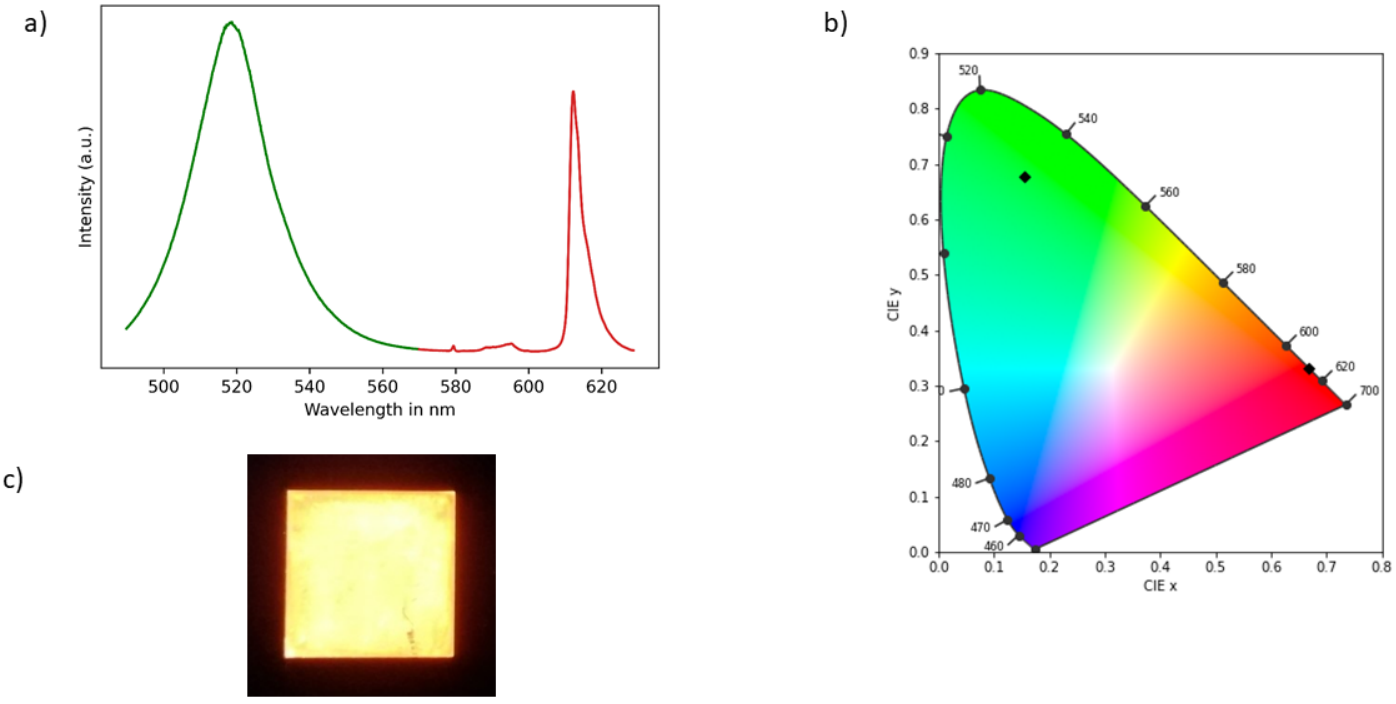

Figure 4.14: Eu^{3+} β-diketonate combined with $CsPbBr_3$@SiO_2, a) Emission of $CsPbBr_3$@SiO_2 mixed with Eu^{3+} β-diketonate complex under 405 nm illumination, b) CIE chromaticity diagram with the two peaks in a) as displayed as $\Diamond$, c) photo of $CsPbBr_3$@SiO_2 mixed with Eu^{3+} β-diketonate complex

Chapter 5

Conclusions and outlook

Eu^{3+} was doped into $CsPbBr_3@SiO_2$ to investigate $CsPbBr_3$ as host for Eu^{3+} self-excitation and energy donor Eu^{3+}. By enhancing Eu^{3+} $^5D_0 \rightarrow {}^7F_2$ emission, Eu^{3+} can be used as a red phosphor. $CsPbBr_3$ can be used as a green phosphor under 460 nm illumination.

Encapsulating $CsPbBr_3$ in silica mesoporous sieve MCM-41 enhances the stability of the perovskite. The $CsPbBr_3$ PL emission peak does not shift or broaden under influence of water, heat, or oxygen for an extended period of time, and the PLQY also remains stable. However, under high laser power, $CsPbBr_3$ emission shows a quick initial decay, followed by a stabilization of intensity. For use on an LED-chip, the influence of high intensity illumination has to be further researched.

Eu^{3+} was successfully doped into the $CsPbBr_3$ lattice. Under 405 nm illumination, a clear $CsPbBr_3$ emission peak could be seen, with an orders of magnitude smaller Eu^{3+} emission peak, suggesting that $CsPbBr_3$ is not a good host for Eu^{3+} self-excitation. The PLE spectrum showed weak Eu^{3+} self-excitation, but no signs of energy transfer. Eu^{3+} emission was slightly enhanced after annealing at high temperature.

A mesoporous YSZ matrix proved to be suited for $CsPbBr_3$ encapsulation, showing $CsPbBr_3$ emission after 5 months in H_2O. Incorporating Eu^{3+} into the mesoporous YSZ matrix yields improved Eu^{3+} emission under 460 nm excitation, especially after annealing at 1000°C. However, this emission was not yet strong enough for use as an LED phosphor. Combining Eu^{3+} doped YSZ with $CsPbBr_3$ results in both Eu^{3+} emission and $CsPbBr_3$ emission, but no signs of energy transfer between the two were found.

By synthesising an Eu^{3+} β-diketonate complex, Eu^{3+} emission with PLQY up to 52% under 405 nm excitation was achieved. Emission was very strong under excitation up to 410 nm, and drastically declined upon excitation with higher wavelengths.

In this thesis, energy transfer from $CsPbBr_3$ to Eu^{3+} could not be definitively proven. For future research, a mixed halide $CsPbCl_{3-x}Br_x$ perovskite can be employed. Matching the bandgap of of the perovksite to the resonance $^5D_1$ level of Eu^{3+} could optimize the energy transfer. In this way, back transfer can be prevented.

Energy transfer could be improved by matching the lifetime of the perovskite energy donor to that of Eu^{3+}. Using an intermediate with a lifetime similar to that of Eu^{3+} could help to increase energy transfer probability. A co-dopant that is able to accept energy transfer from $CsPbBr_3$ should be investigated.

By attaching Eu^{3+} to ligands that can effectively absorb light at 460 nm and then transfer it to the $^5D_1$ resonance level of Eu^{3+}, a complex can be made that can absorb light at 460 nm, without the need for an energy donor.

Another pathway to a red phosphor would be to optimize perovskite red emitters without Eu^{3+}. $CsPbI_3@SiO_2$ is an effective absorber and red emitter, and would make a good candidate as red phosphor, even though the FWHM of $CsPbI_3@SiO_2$ is not as narrow as that of Eu^{3+}. $CsSnBr_3@SiO_2$ is similarly a good option, although PLQY is still low.

Acknowledgements

The last year has been a great experience thanks to all the amazing people at AMOLF. It has been a pleasure to be able to be here (both in person and online).

I would like to express my thanks to my supervisor Erik Garnett, for an unbelievable amount of ideas, inspiration, and optimism. Thanks to Bruno Ehrler for being my second examiner.

Thank you Eitan Oksenberg, for the countless conversations with advice about research, europium and life in general. Thanks to the amazing Susan Rigter, who not only helped an incredible amount in writing my thesis, but also kept me from many breakdowns.

Marc Duursma, thanks for fixing every problem imaginable. Sarah Gillespie, I am eternally happy we became such great friends and I'm going to miss not seeing you every day. A huge thank you goes to everyone in the Nanoscale Solar Cells group. Elaina, thanks for being amazing. Thanks to Rohit for many laughs (and making fun of my dance moves). Daan, it was great fun to be in the same office as you. You taught me the true meaning of progress (because yesterday you said tomorrow). Thank you Hongyu, for being such a nice person. Also many thanks to Julia, Sven, Francesca and Maryam.

Seaborough made this entire project possible, and I would like to thank Marie Anne van de Haar, Federico Montanarella, Anne Berendse, Atul Sontakke and Mohamed Tachikirt for all the help and inspiration.

Then, last but certainly not least, I would like to thank everyone else. Of course all my amazing friends and family, but also my violin teacher, Chris Duindam, and the amazing members of my string quartet. Thank you, Maartje, Gabriël and Laurence, for always wanting to rehearse at the weirdest possible times, and for supporting me so much.

Bibliography

[1] D. Cortecchia et al., "Layered Perovskite Doping with Eu3+and β-diketonate Eu3+ Complex," *Chem. Mater.*, vol. 33, no. 7, pp. 2289–2297, 2021, doi: 10.1021/acs.chemmater.0c04097.

[2] P. Stott, "How climate change affects extreme weather events," *Science (80-.).*, vol. 352, no. 6293, pp. 1517–1518, 2016, doi: 10.1126/science.aaf7271.

[3] IPCC, "Global warming of 1.5°C. An IPCC Special Report on the impacts of global warming of 1.5°C above pre-industrial levels and related global greenhouse gas emission pathways, in the context of strengthening the global response to the threat of climate change," *Ipcc - Sr15*, vol. 2, no. October, pp. 17–20, 2018, [Online]. Available: www.environmentalgraphiti.org.

[4] A. Borunda, "The science connecting wildfires to climate change," *National Geographic*, 2020. https://www.nationalgeographic.com/science/article/climate-change-increases-risk-fires-western-us (accessed Feb. 13, 2022).

[5] "Tienduizenden mensen bij klimaatmars in Amsterdam," *ANP/Het Parool*, 2019.

[6] K. Zhang, N. Zhu, M. Zhang, L. Wang, and J. Xing, "Opportunities and challenges in perovskite LED commercialization," *J. Mater. Chem. C*, vol. 9, no. 11, pp. 3795–3799, 2021, doi: 10.1039/d1tc00232e.

[7] M. A. Van De Haar, M. Tachikirt, A. C. Berends, M. R. Krames, A. Meijerink, and F. T. Rabouw, "Saturation Mechanisms in Common LED Phosphors," *ACS Photonics*, vol. 8, no. 6, pp. 1784–1793, 2021, doi: 10.1021/acsphotonics.1c00372.

[8] A. De Almeida, B. Santos, P. Bertoldi, and M. Quicheron, "Solid state lighting review - Potential and challenges in Europe," *Renew. Sustain. Energy Rev.*, vol. 34, pp. 30–48, 2014, doi: 10.1016/j.rser.2014.02.029.

[9] M. A. Van De Haar, A. C. Berends, M. R. Krames, L. Chepyga, F. T. Rabouw, and A. Meijerink, "Eu 3+ Sensitization via Nonradiative Interparticle Energy Transfer Using Inorganic Nanoparticles," pp. 3–9, 2020, doi: 10.1021/acs.jpclett.9b03764.

[10] A. Smets, O. Isabella, R. Van Swaaij, M. Zeman, and K. Jäger, *Solar Energy - The Pysics and Engineering of Photovoltaic Conversion, Technologies and Systems.* 2016.

[11] M. N. An et al., "Low-Temperature Molten Salts Synthesis: CsPbBr3Nanocrystals with High Photoluminescence Emission Buried in Mesoporous SiO2," *ACS Energy Lett.*, vol. 6, no. 3, pp. 900–907, 2021, doi: 10.1021/acsenergylett.1c00052.

[12] R. Comerford, "LED Specs - Understanding the Color White," *Electronic Products*, 2011. https://www.digikey.be/nl/articles/led-specs—understanding-the-color-white.

[13] E. Taylor, P. R. Edwards, and R. W. Martin, "Colorimetry and efficiency of white LEDs: Spectral width dependence," *Phys. Status Solidi Appl. Mater. Sci.*, vol. 209, no. 3, pp. 461–464, 2012, doi: 10.1002/pssa.201100449.

[14] J. H. Oh, Y. J. Eo, H. C. Yoon, Y. D. Huh, and Y. R. Do, "Evaluation of new color metrics: Guidelines for developing narrow-band red phosphors for WLEDs," *J. Mater. Chem.* C, vol. 4, no. 36, pp. 8326–8348, 2016, doi: 10.1039/c6tc02387h.

[15] J. C. de Mello, H. F. Wittmann, and R. H. Friend, "An Improved Experimental Determination of External Photoluminescence Quantum Efficiency," *Adv. Mater.*, vol. 9, no. 3, pp. 230–232, 1997, doi: 10.1201/b10862-5.

[16] X. Yin, Y. Wang, F. Huang, Y. Xia, D. Wan, and J. Yao, "Excellent red phosphors of double

perovskite Ca2LaMO 6:Eu (M=Sb, Nb, Ta) with distorted coordination environment," *J. Solid State Chem.*, vol. 184, no. 12, pp. 3324–3328, 2011, doi: 10.1016/j.jssc.2011.10.032.

[17] S. Shi et al., "Blue-light excitable La2Ce2O7:Eu3+ red phosphors for white light-emitting diodes," *J. Alloys Compd.*, vol. 814, p. 152226, 2020, doi: 10.1016/j.jallcom.2019.152226.

[18] Q. Zhang et al., "Ceramic-like stable CsPbBr3 nanocrystals encapsulated in silica derived from molecular sieve templates," *Nat. Commun.*, vol. 11, no. 1, pp. 1–9, 2020, doi: 10.1038/s41467-019-13881-0.

[19] M. A. Van De Haar et al., "Increasing the effective absorption of Eu3+-doped luminescent materials towards practical light emitting diodes for illumination applications," *Appl. Phys. Lett.*, vol. 112, no. 13, pp. 1–5, 2018, doi: 10.1063/1.5016948.

[20] Y. Tian, "Development of phosphors with high thermal stability and efficiency for phosphor-converted LEDs," *J. Solid State Light.*, vol. 1, no. 1, pp. 1–15, 2014, doi: 10.1186/s40539-014-0011-8.

[21] J. K. Ling et al., "A Perspective on the Commercial Viability of Perovskite Solar Cells," *Sol. RRL*, vol. 5, no. 11, pp. 1–48, 2021, doi: 10.1002/solr.202100401.

[22] M. A. Green, A. Ho-Baillie, and H. J. Snaith, "The emergence of perovskite solar cells," *Nat. Photonics*, vol. 8, no. 7, pp. 506–514, 2014, doi: 10.1038/nphoton.2014.134.

[23] L. Protesescu et al., "Nanocrystals of Cesium Lead Halide Perovskites ($CsPbX_3$, X = Cl, Br, and I): Novel Optoelectronic Materials Showing Bright Emission with Wide Color Gamut," *Nano Lett.*, vol. 15, no. 6, pp. 3692–3696, 2015, doi: 10.1021/nl5048779.

[24] Q. Zhang et al., " Confined Synthesis of Stable and Uniform CsPbBr 3 Nanocrystals with High Quantum Yield up to 90% by High Temperature Solid-State Reaction ," *Adv. Opt. Mater.*, vol. 2002130, p. 2002130, 2021, doi: 10.1002/adom.202002130.

[25] J. Butkus et al., "The Evolution of Quantum Confinement in CsPbBr3 Perovskite Nanocrystals," *Chem. Mater.*, vol. 29, no. 8, pp. 3644–3652, 2017, doi: 10.1021/acs.chemmater.7b00478.

[26] O. H. C. Cheng, T. Qiao, M. Sheldon, and D. H. Son, "Size-and temperature-dependent photoluminescence spectra of strongly confined CsPbBr3 quantum dots," *Nanoscale*, vol. 12, no. 24, pp. 13113–13118, 2020, doi: 10.1039/d0nr02711a.

[27] A. Dey et al., "State of the Art and Prospects for Halide Perovskite Nanocrystals," *ACS Nano*, vol. 15, no. 7, pp. 10775–10981, 2021, doi: 10.1021/acsnano.0c08903.

[28] D. N. Dirin et al., "Harnessing Defect-Tolerance at the Nanoscale: Highly Luminescent Lead Halide Perovskite Nanocrystals in Mesoporous Silica Matrixes," Nano Lett., vol. 16, no. 9, pp. 5866–5874, 2016, doi: 10.1021/acs.nanolett.6b02688.

[29] H. Huang, M. I. Bodnarchuk, S. V. Kershaw, M. V. Kovalenko, and A. L. Rogach, "Lead Halide Perovskite Nanocrystals in the Research Spotlight: Stability and Defect Tolerance," *ACS Energy Lett.*, vol. 2, no. 9, pp. 2071–2083, 2017, doi: 10.1021/acsenergylett.7b00547.

[30] L. Protesescu et al., "Dismantling the 'red Wall' of Colloidal Perovskites: Highly Luminescent Formamidinium and Formamidinium-Cesium Lead Iodide Nanocrystals," *ACS Nano*, vol. 11, no. 3, pp. 3119–3134, 2017, doi: 10.1021/acsnano.7b00116.

[31] Quantum Solutions, "QDOT TM Perovskite ABX3 Quantum Dots," 2022.

[32] G. Grancini et al., "One-Year stable perovskite solar cells by 2D/3D interface engineering," *Nat. Commun.*, vol. 8, pp. 1–8, 2017, doi: 10.1038/ncomms15684.

[33] C. Zhang et al., "Thermal stability of CsPbBr3 perovskite as revealed by in situ transmission

electron microscopy," *APL Mater.*, vol. 7, no. 7, pp. 1–7, 2019, doi: 10.1063/1.5108849.

[34] M. Imran et al., "Switchable Anion Exchange in Polymer-Encapsulated APbX3Nanocrystals Delivers Stable All-Perovskite White Emitters," *ACS Energy Lett.*, vol. 6, no. 8, pp. 2844–2853, 2021, doi: 10.1021/acsenergylett.1c01232.

[35] G. Mensitieri et al., "Improving the Lifetime of CsPbBr 3 Perovskite in Water Using Self-Healing and Transparent Elastic Polymer Matrix," *Front. Chem.*, vol. 8, p. 766, 2020, doi: 10.3389/fchem.2020.00766.

[36] D. R. Ceratti et al., "Self-Healing Inside APbBr3 Halide Perovskite Crystals," *Adv. Mater.*, vol. 30, no. 10, pp. 1–7, 2018, doi: 10.1002/adma.201706273.

[37] X. Jiang et al., "Dion-Jacobson 2D-3D perovskite solar cells with improved efficiency and stability," *Nano Energy*, vol. 75, no. March, p. 104892, 2020, doi: 10.1016/j.nanoen.2020.104892.

[38] J. Kim, A. Ho-Baillie, and S. Huang, "Review of Novel Passivation Techniques for Efficient and Stable Perovskite Solar Cells," *Sol. RRL*, vol. 3, no. 4, pp. 1–16, 2019, doi: 10.1002/solr.201800302.

[39] Z. J. Li et al., "Photoelectrochemically active and environmentally stable cspbbr3/tio2 core/shell nanocrystals," *Adv. Funct. Mater.*, vol. 28, no. 1, 2018, doi: 10.1002/adfm.201704288.

[40] A. Loiudice, S. Saris, E. Oveisi, D. T. L. Alexander, and R. Buonsanti, " CsPbBr 3 QD/AlO x Inorganic Nanocomposites with Exceptional Stability in Water, Light, and Heat ," *Angew. Chemie*, vol. 129, no. 36, pp. 10836–10841, 2017, doi: 10.1002/ange.201703703.

[41] E. Erol, O. Kıbrıslı, M. Çelikbilek Ersundu, and A. E. Ersundu, "Size-controlled emission of long-time durable CsPbBr3 perovskite quantum dots embedded tellurite glass nanocomposites," *Chem. Eng. J.*, vol. 401, p. 126053, Dec. 2020, doi: 10.1016/J.CEJ.2020.126053.

[42] H. Liu et al., "Fabricating $CsPbX_3$-Based Type i and Type II Heterostructures by Tuning the Halide Composition of Janus $CsPbX_3$/ZrO2 Nanocrystals," *ACS Nano*, vol. 13, no. 5, pp. 5366–5374, 2019, doi: 10.1021/acsnano.9b00001.

[43] Y. Duan et al., "Meeting High Stability and Efficiency in Hybrid Light-Emitting Diodes Based on SiO2/ZrO2 Coated CsPbBr3 Perovskite Nanocrystals," *Adv. Funct. Mater.*, vol. 30, no. 40, pp. 1–10, 2020, doi: 10.1002/adfm.202005401.

[44] K. Wang, R. Yao, P. Shen, Y. Fang, L. Chen, and H. Wang, "Quantum Dots Encapsulated by ZrO2 Enhance the Stability of Perovskite Solar Cells," *Adv. Mater. Interfaces*, vol. 8, no. 19, pp. 1–7, 2021, doi: 10.1002/admi.202100776.

[45] D. Kumar, K. Schumacher, C. F. Von Hohenesche, and M. Gru, "MCM-41 , MCM-48 and related mesoporous adsorbents: their synthesis and characterisation," vol. 188, pp. 109–116, 2001.

[46] ACS Material, "MCM-41," 2022. https://www.acsmaterial.com/mcm-41.html.

[47] Z. Li, L. Li, H. Liu, F. Li, J. Zhao, and Y. Wang, "Strongly quantum-confined Mn2+-doped CsPbBr3 nanocrystals in MCM-41 with pure blue emission," *New J. Chem.*, vol. 44, no. 7, pp. 2980–2985, 2020, doi: 10.1039/c9nj06053g.

[48] H. Chen, Y. Wang, J. Wang, and W. Liu, "Thermal stability of cspbbr3 perovskite quantum dots assembled with sba-15," *Coatings*, vol. 11, no. 8, pp. 1–12, 2021, doi: 10.3390/coatings11080953.

[49] Y. Q. Hu, L. J. Fan, H. Y. Hui, H. Q. Wen, D. S. Yang, and G. D. Feng, "Monodisperse bismuth-halide double perovskite nanocrystals confined in mesoporous silica templates," *Inorg. Chem.*, vol. 58, no. 13, pp. 8500–8505, 2019, doi: 10.1021/acs.inorgchem.9b00798.

[50] D. A. Atwood, *The Rare Earth Elements: Fundamentals and Applications*. John Wiley & Sons,

2013.

[51] Q. C. Wang, P. Wang, Y. Qiu, T. Dai, and W. Q. Chen, "Byproduct surplus: Lighting the depreciative europium in China's rare earth boom," *Environ. Sci. Technol.*, vol. 54, no. 22, 2020, doi: 10.1021/acs.est.0c02870.

[52] A. Martin and A. Iles, "The ethics of rare earth elements over time and space," *Ethics Chem.* From Poison Gas To Clim. Eng., vol. 26, no. 2020, pp. 317–346, 2021, doi: 10.1142/97898112335480012.

[53] M. Hatanaka and S. Yabushita, "Mechanisms of f–f hypersensitive transition intensities of lanthanide trihalide molecules: a spin–orbit configuration interaction study," *Theor. Chem. Acc.*, vol. 133, no. 8, pp. 1–15, 2014, doi: 10.1007/s00214-014-1517-2.

[54] F. Steudel, J. A. Johnson, C. E. Johnson, and S. Schweizer, "Characterization of luminescent materials with 151Eu Mössbauer spectroscopy," *Materials (Basel).*, vol. 11, no. 5, pp. 1–27, 2018, doi: 10.3390/ma11050828.

[55] K. Nehra et al., "Lanthanides β-diketonate complexes as energy-efficient emissive materials: A review," *J. Mol. Struct.*, vol. 1249, p. 131531, 2022, doi: 10.1016/j.molstruc.2021.131531.

[56] J. C. G. Bünzli and C. Piguet, "Taking advantage of luminescent lanthanide ions," *Chem. Soc. Rev.*, vol. 34, no. 12, pp. 1048–1077, 2005, doi: 10.1039/b406082m.

[57] J. Bünzli, "The europium(III) ion as spectroscopic probe in bioinorganic chemistry," *Inorganica Chim. Acta*, vol. 139, no. 1–2, pp. 219–222, 1987, doi: 10.1016/S0020-1693(00)84084-0.

[58] F. Suyver and A. Meijerink, "Europium beveiligt de Euro," *Chemisch2Weekblad*, vol. 98, no. 4, pp. 12–13, 2002.

[59] S. Y. Kim, K. Woo, K. Lim, K. Lee, and H. S. Jang, "Highly bright multicolor tunable ultrasmall β-Na(Y,Gd)F 4:Ce,Tb,Eu/β-NaYF4 core/shell nanocrystals," *Nanoscale*, vol. 5, no. 19, pp. 9255–9263, 2013, doi: 10.1039/c3nr02591h.

[60] Q. Sun et al., "Double perovskite Ca2LuTaO6:Eu3+ red-emitting phosphors: Synthesis, structure and photoluminescence characteristics," *J. Alloys Compd.*, vol. 804, pp. 230–236, Oct. 2019, doi: 10.1016/J.JALLCOM.2019.06.260.

[61] C. Ji et al., "Synthesis and photoluminescence properties of a novel BaGe4O9:Eu3+ red emitting phosphor for warm white LEDs," *Dye. Pigment.*, vol. 160, no. August 2018, pp. 772–778, 2019, doi: 10.1016/j.dyepig.2018.09.012.

[62] Y. Yu et al., "Ultra-stable Eu3+-doped CsPbCl2Br1 perovskite quantum dots glass for optical temperature sensing," *J. Rare Earths*, no. xxxx, pp. 1–9, 2020, doi: 10.1016/j.jre.2020.11.010.

[63] R. Yuan et al., "Eu3+-doped CsPbBr1.5I1.5 quantum dots glasses: A strong competitor among red fluorescence solid materials," *J. Am. Ceram. Soc.*, vol. 101, no. 11, pp. 4927–4932, 2018, doi: 10.1111/jace.15933.

[64] A. P. Jadhav, A. U. Pawar, U. Pal, and Y. S. Kang, "Red emitting Y2O3:Eu3+ nanophosphors with >80% down conversion efficiency," *J. Mater. Chem. C*, vol. 2, no. 3, pp. 496–500, 2014, doi: 10.1039/c3tc31939c.

[65] S. Fischer and T. Jüstel, "Effective Sensitization of Eu3+ with Ce3+ by suppression of metal-to-metal charge transfer in composite structured TbF3 fluoride particles," *J. Lumin.*, vol. 223, no. March, p. 117232, 2020, doi: 10.1016/j.jlumin.2020.117232.

[66] C. De Mayrinck et al., "Spherical-shaped Y2O3:Eu3+ nanoparticles with intense photoluminescence emission," *Ceram. Int.*, vol. 41, no. 1, pp. 1189–1195, 2015, doi: 10.1016/j.ceramint.2014.09.047.

[67] S. Takemura, K. C. Mishra, J. Collins, and K. Ogasawara, " First-Principles Calculations of Charge Transfer Transitions of Eu 3+ in Y2O3 and Y2O2S ," *ECS J. Solid State Sci. Technol.*, vol. 9, no. 6, p. 066005, 2020, doi: 10.1149/2162-8777/aba765.

[68] X. Li, C. Yang, Q. Liu, X. Wang, and X. Mi, "Enhancement of luminescence properties of SrAl2Si2O8: Eu3+ red phosphor," *Ceram. Int.*, vol. 46, no. 11, pp. 17376–17382, 2020, doi: 10.1016/j.ceramint.2020.04.027.

[69] Q. Tang, T. Yang, B. Guo, B. Peng, H. Huang, and J. Ao, "Synthesis and photoluminescence properties of Eu3+ doped Sr5Nb4O15 red-emitting phosphors for white LEDs," *Optik (Stuttg).*, vol. 224, no. July, p. 165770, 2020, doi: 10.1016/j.ijleo.2020.165770.

[70] Y. Hui et al., "Fluorescence of Eu3+ as a probe of phase transformation of zirconia," *J. Alloys Compd.*, vol. 573, pp. 177–181, 2013, doi: 10.1016/j.jallcom.2013.03.248.

[71] J. P. Feist and A. L. Heyes, "Europium-doped yttria-stabilized zirconia for high-temperature phosphor thermometry," *Proc. Inst. Mech. Eng. Part L J. Mater. Des. Appl.*, vol. 214, no. 1, pp. 7–12, 2000, doi: 10.1177/146442070021400102.

[72] K. Binnemans, "Interpretation of europium(III) spectra," *Coord. Chem. Rev.*, vol. 295, pp. 1–45, 2015, doi: 10.1016/j.ccr.2015.02.015.

[73] D. J. Griffiths, *Introduction to quantum mechanics*, vol. 193, no. 2. Prentice Hall, Inc., p. 394, 1995.

[74] M. Hatanaka and S. Yabushita, "Theoretical study on the f-f transition intensities of lanthanide trihalide systems," *J. Phys. Chem. A, vol. 113, no. 45*, pp. 12615–12625, 2009, doi: 10.1021/jp9049507.

[75] C. Görller-Walrand and K. Binnemans, "Spectral intensities of f-f transitions," in Handbook on the physics and chemistry of rare earths, J. K.S. Gschneider and L. Eyring, Eds. Elsevier Science, 1998, pp. 101–264.

[76] B. M. Walsh, "Judd-Ofelt theory: Principles and practices," in *Advances in Spectroscopy for Lasers and Sensing*, no. May, Springer, 2006, pp. 403–433.

[77] K. Binnemans, "Lanthanide-based luminescent hybrid materials," *Chem. Rev.*, vol. 109, no. 9, pp. 4283–4374, 2009, doi: 10.1021/cr8003983.

[78] M. H. V. Werts, R. T. F. Jukes, and J. W. Verhoeven, "The emission spectrum and the radiative lifetime of Eu3+ in luminescent lanthanide complexes," *Phys. Chem. Chem. Phys.*, vol. 4, no. 9, pp. 1542–1548, 2002, doi: 10.1039/b107770h.

[79] M. Tanaka, G. Nishimura, T. Kushida, and T. J-mixing, "Contribution of J mixing to the 5D0-7F0 transition of Eu3+ ions in several host matrices," *Phys Rev B Condes Matter.*, vol. 49, no. 24, 1994.

[80] P. A. Tanner, "Some misconceptions concerning the electronic spectra of tri-positive europium and cerium," *Chem. Soc. Rev.*, vol. 42, no. 12, pp. 5090–5101, 2013, doi: 10.1039/c3cs60033e.

[81] M. J. Weber, J. A. Paisner, S. S. Sussman, W. M. Yen, L. A. Riseberg, and C. Brecher, "Spectroscopic studies of rare-earth ions in glass using fluorescence line narrowing techniques," *J. Lumin.*, vol. 12–13, no. C, pp. 729–735, 1976, doi: 10.1016/0022-2313(76)90168-X.

[82] K. Binnemans, K. Van Herck, and C. Görller-Walrand, "Influence of dipicolinate ligands on the spectroscopic properties of europium(III) in solution," *Chem. Phys. Lett.*, vol. 266, no. 3–4, pp. 297–302, 1997, doi: 10.1016/S0009-2614(97)00012-2.

[83] W. T. Carnall, P. R. Fields, and K. Rajnak, " Electronic Energy Levels of the Trivalent Lanthanide Aquo Ions. IV. Eu 3+ ," *J. Chem. Phys.*, vol. 49, no. 10, pp. 4450–4455, 1968, doi: 10.1063/1.1669896.

[84] A. K. Parchur and R. S. Ningthoujam, "Behaviour of electric and magnetic dipole transitions of Eu3+, 5D0 → 7F0 and Eu-O charge transfer band in Li+ co-doped YPO4:Eu3+," RSC Adv., vol. 2, no. 29, pp. 10859–10868, 2012, doi: 10.1039/c2ra22144f.

[85] A. Bala and V. Kumar, "A Study of Eu Doping in Nanolayers of CsPbBr3using Ab Initio Calculations to Understand f-f Transitions in Eu3+-Doped Nanocrystals for Light-Emitting Diodes," *ACS Appl. Nano Mater.*, vol. 3, no. 5, pp. 4437–4444, 2020, doi: 10.1021/acsanm.0c00536.

[86] X. Dong, J. Zhang, X. Zhang, Z. Hao, and Y. Luo, "New orange-red phosphor Sr9Sc(PO4) 7:Eu3+ for NUV-LEDs application," *J. Alloys Compd.*, vol. 587, pp. 493–496, 2014, doi: 10.1016/j.jallcom.2013.10.116.

[87] D. L. Dexter, "A theory of sensitized luminescence in solids," *J. Chem. Phys.*, vol. 21, no. 5, pp. 836–850, 1953, doi: 10.1063/1.1699044.

[88] "Dexter Energy Transfer," *Chemistry LibreTexts*, 2021. https://bit.ly/3t2KZ3X.

[89] S. I. Weissman, "Intramolecular energy transfer the fluorescence of complexes of Europium," *J. Chem. Phys.*, vol. 10, no. 4, pp. 214–217, 1942, doi: 10.1063/1.1723709.

[90] Q. Xu, L. Li, X. Liu, and R. Xu, "Incorporation of rare-earth complex Eu(TTA)4C5H5NC16H33 into surface-modified S-MCM-41 and its photophysical properties," *Chem. Mater.,* vol. 14, no. 2, pp. 549–555, 2002, doi: 10.1021/cm0102234.

[91] J. Kai, M. C. F. C. Felinto, L. A. O. Nunes, O. L. Malta, and H. F. Brito, "Intermolecular energy transfer and photostability of luminescence-tuneable multicolour PMMA films doped with lanthanide-β-diketonate complexes," *J. Mater. Chem.*, vol. 21, no. 11, pp. 3796–3802, 2011, doi: 10.1039/c0jm03474f.

[92] L. H. C. Francisco, M. C. F. C. Felinto, H. F. Brito, E. E. S. Teotonio, and O. L. Malta, "Development of highly luminescent PMMA films doped with Eu3+ β-diketonate coordinated on ancillary ligand," *J. Mater. Sci. Mater. Electron.*, vol. 30, no. 18, pp. 16922–16931, 2019, doi: 10.1007/s10854-019-01639-9.

[93] Y. Cheng, C. Shen, L. Shen, W. Xiang, and X. Liang, "Tb 3+ , Eu 3+ Co-doped CsPbBr 3 QDs Glass with Highly Stable and Luminous Adjustable for White LEDs," 2018, doi: 10.1021/acsami.8b05003.

[94] X. Zhang, L. Zhou, Q. Pang, J. Shi, and M. Gong, "Tunable luminescence and Ce3+ → Tb3+ → Eu3+ energy transfer of broadband-excited and narrow line red emitting Y2SiO5:Ce3+, Tb3+, Eu 3+ phosphor," *J. Phys. Chem. C*, vol. 118, no. 14, pp. 7591–7598, 2014, doi: 10.1021/jp412702g.

[95] T. K. Anh et al., "Nanomaterials containing rare-earth ions Tb, Eu, Er and Yb: preparation, optical properties and application potential," *J. Lumin.*, vol. 102–103, no. SPEC, pp. 391–394, May 2003, doi: 10.1016/S0022-2313(02)00531-8.

[96] X. L. Quinn et al., "Europium Addition Reduces Local Structural Disorder and Enhances Photoluminescent Yield in Perovskite CsPbBr3," *Adv. Opt. Mater.*, vol. 2002221, pp. 1–8, 2021, doi: 10.1002/adom.202002221.

[97] W. J. Mir et al., "Postsynthesis Doping of Mn and Yb into $CsPbX_3$ (X = Cl, Br, or I) Perovskite Nanocrystals for Downconversion Emission," *Chem. Mater.*, vol. 30, no. 22, pp. 8170–8178, 2018, doi: 10.1021/acs.chemmater.8b03066.

[98] G. Vinothkumar, S. Rengaraj, P. Arunkumar, S. W. Cha, and K. Suresh Babu, "Ionic Radii and Concentration Dependency of RE3+ (Eu3+, Nd3+, Pr3+, and La3+)-Doped Cerium Oxide Nanoparticles for Enhanced Multienzyme-Mimetic and Hydroxyl Radical Scavenging Activity," *J. Phys. Chem. C*, vol. 123, no. 1, pp. 541–553, 2019, doi: 10.1021/acs.jpcc.8b10108.

[99] W. J. Mir, T. Sheikh, H. Arfin, Z. Xia, and A. Nag, "Lanthanide doping in metal halide perovskite

nanocrystals: spectral shifting, quantum cutting and optoelectronic applications," *NPG Asia Mater.*, vol. 12, no. 1, 2020, doi: 10.1038/s41427-019-0192-0.

[100] G. Blasse, "Energy transfer in oxidic phosphors," Phys. Lett. A, vol. 28, no. 6, pp. 444–445, 1968, doi: 10.1016/0375-9601(68)90486-6. [101] E. Erol, O. Kibrisli, M. Çelikbilek Ersundu, and A. E. Ersundu, "Color tunable emission from Eu 3+ and Tm 3+ co-doped CsPbBr 3 quantum dot glass nanocomposites," *Phys. Chem. Chem. Phys.*, vol. 24, no. 3, pp. 1486–1495, 2022, doi: 10.1039/d1cp05016h.

[102] R. Yuan et al., "CsPbBr3:: X Eu3+ perovskite QD borosilicate glass: A new member of the luminescent material family," *Chem. Commun.*, vol. 54, no. 27, pp. 3395–3398, 2018, doi: 10.1039/c8cc00243f.

[103] P. Li et al., "Nanocrystalline structure control and tunable luminescence mechanism of Eu-doped CsPbBr3 quantum dot glass for WLEDs," *Nanoscale*, vol. 12, no. 12, pp. 6630–6636, 2020, doi: 10.1039/d0nr01207f.

[104] A. B. S. Garcia, A. G. Bispo-Jr, S. A. M. Lima, and A. M. Pires, "Effects of the Pechini's modified synthetic route on structural and photophysical properties of Eu3+ or Tb3+-doped LaAlO3," Mater. Res. Bull., vol. 143, no. April, p. 111462, 2021, doi: 10.1016/j.materresbull.2021.111462.

[105] C. Zhang, W. Li, and L. Li, "Metal Halide Perovskite Nanocrystals in Metal–Organic Framework Host: Not Merely Enhanced Stability," *Angewandte Chemie - International Edition.* Wiley-VCH Verlag, 2020, doi: 10.1002/anie.202006169.

[106] S. Gillespie, "Encapsulating Metal Halide Perovskite Nanocrystals in Silica Molecular Sieves," Universiteit van Amsterdam, 2021.

[107] I. M. Hung, K. Z. Fung, D. T. Hung, and M. H. Hon, "Thermal stability of ordered mesoporous yttria-stabilized zirconia," *J. Eur. Ceram. Soc.*, vol. 28, no. 6, pp. 1161–1167, 2008, doi: 10.1016/j.jeurceramsoc.2007.09.044.

[108] I. M. Hung, D. T. Hung, K. Z. Fung, and M. H. Hon, "Highly-ordered mesoporous nanocrystalline yttria-stabilized zirconia synthesized through evaporation-induced self-assembly method," *Mater. Lett.*, vol. 62, no. 6–7, pp. 1147–1150, 2008, doi: 10.1016/j.matlet.2007.07.070.

[109] Materials Project, "CsPbBr3," 2022. https://materialsproject.org/materials/mp-600089/ (accessed Feb. 22, 2022).

[110] S. Stepanov, O. Khasanov, E. Dvilis, V. Paygin, D. Valiev, and M. Ferrari, "Luminescence performance of yttrium-stabilized zirconia ceramics doped with Eu3+ ions fabricated by Spark Plasma Sintering technique," *Ceram. Int.*, vol. 47, no. 5, pp. 6608–6613, 2021, doi: 10.1016/j.ceramint.2020.10.250.

[111] M. Mamak, N. Coombs, and G. Ozin, "Self-Assembling Solid Oxide Fuel Cell Materials: Mesoporous Yttria-Zirconia and Metal-Yttria-Zirconia Solid Solutions," no. 6, pp. 8932–8939, 2000.

[112] L. Huangqing, W. Lingling, C. Shuguang, Z. Bingsuo, and P. Zhiwei, "Effect of annealing temperature on luminescence of Eu 3+ ions doped nanocrystal zirconia," *Appl. Surf. Sci.*, vol. 253, no. 8, pp. 3872–3876, 2007, doi: 10.1016/j.apsusc.2006.08.009.

Appendix A

Appendix

A.1 Setup for testing stability of $CsPbBr_3@SiO_2$ under heat and illumination

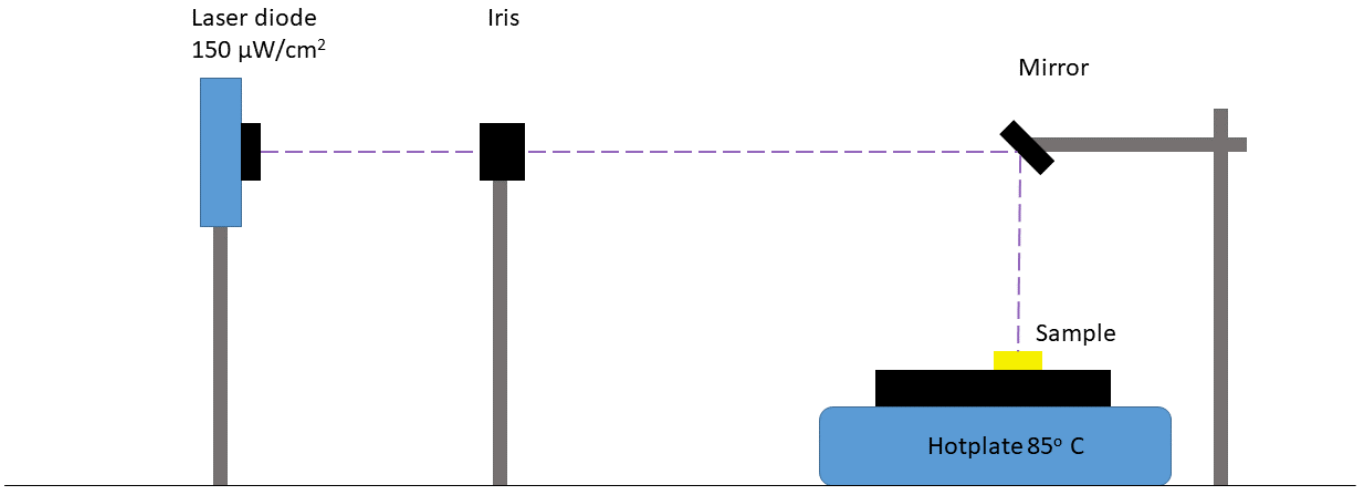

Figure A.1: Setup for testing stability of $CsPbBr_3@SiO_2$ under 150 $\mu W/cm^2$ 405 nm illumination and 85°C

A.2 PLQY measurements

To calculate PLQY, three measurements were taken with the integrating sphere and laser according to a procedure described in [15].

Measurement 1: The laser was focused in the integrating sphere without sample.
Measurement 2: The laser was focused in the integrating sphere, with the sample (the laser is not focused on the sample).
Measurement 3: The laser was focused on the sample in the integrating sphere.

An emission pattern is shown in Figure A.2. Two peaks per measurement can be seen. The peak around 450 nm is the result of the laser, the broad peak around 600 nm is the result of emission of the sample.

Curves L_1, L_2, L_3 correspond to the total intensity of the peaks around 450 nm of respectively the 1^{st}, 2^{nd}, and 3^{rd} measurement.
Curves P_2, and P_3 correspond to the total intensity of the peaks around 600 nm of respectively the 2^{nd} and 3^{rd} measurement. These are calculated by integrating over the peak.

The PLQY is given by

$$\eta = \frac{P_3 - (1 - A)P_2}{L_1 A}$$

with

$$A = 1 - \frac{L_3}{L_2}$$

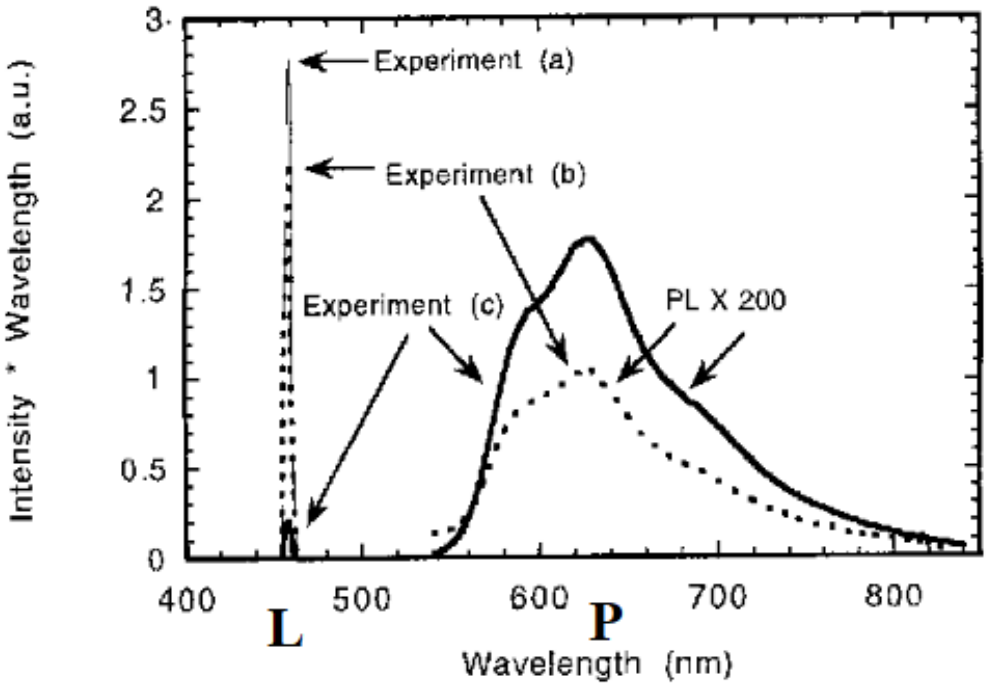

Figure A.2: PLQY measurements of MEH PPV. The dashed line is the result of measurement 1, the dotted line the result of measurement 2, the solid line the result of measurement 3. Figure from [15]

A.3 Lorentzian fit of $CsPbBr_3@SiO_2$

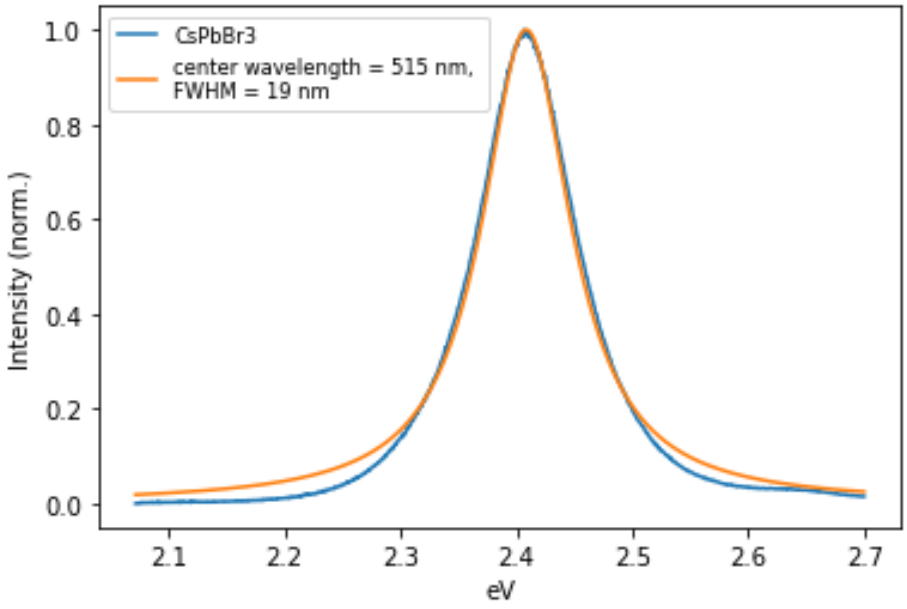

Figure A.3: Lorentzian fit of $CsPbBr_3@SiO_2$

A.4 Tauc plot of $CsPbBr_3@SiO_2$

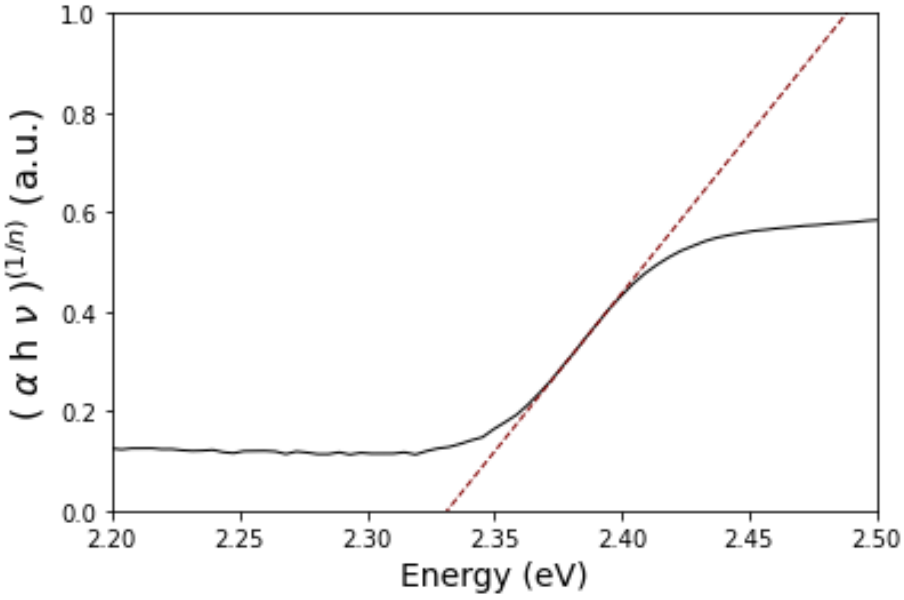

Figure A.4: Tauc plot of $CsPbBr_3@SiO_2$

A.5 Y_2O_3:15%Eu^{3+} on $CsPbBr_3$ nanocubes

Y_2O_3:15%Eu^{3+} was dissolved in toluene and dropcasted on a substrate covered with $CsPbBr_3$ nanocubes. The PL spectrum is shown in Figure A.5 a). Both $CsPbBr_3$ emission and Y_2O_3:15%Eu^{3+} emission can be seen. The PLE spectrum in Figure A.5 b) shows clear self-excitation of Eu^{3+}, and $CsPbBr_3$ excitation. No energy transfer can be seen.

Here, Eu^{3+} is intense compared to $CsPbBr_3$ emission. Large spatial variation of $CsPbBr_3$ emission could be seen on the sample. This indicates that Y_2O_3:15%Eu^{3+} is not evenly distributed on the sample.

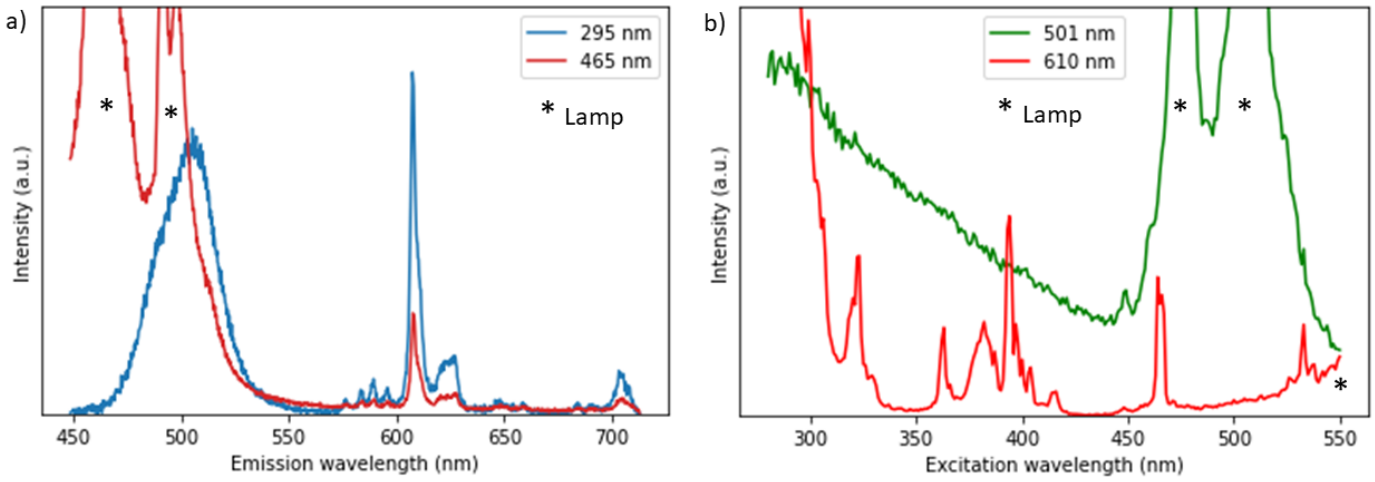

Figure A.5: Y_2O_3:15%Eu^{3+} on $CsPbBr_3$ nanocubes, a) PL spectrum under 295 and 465 nm excitation, b) PLE spectrum of 501 nm $CsPbBr_3$ emission (green line) and 610 nm Y_2sO_3:15%Eu^{3+} emission (red line)

A.6 Luminescence of $CsPbBr_3$@mYSZ and mYSZ:10%Eu^{3+} in 1M HCl

$CsPbBr_3$ was encapsulated in mYSZ and mYSZ:10%Eu^{3+}. Figure A.6 a) shows that both samples are luminescent after immersion in 1M HCl, although $CsPbBr_3$@mYSZ has brighter emission. This indicates that the perovskite is protected from the environment, as unencapsulated $CsPbBr_3$ emission would be quenched after seconds in 1M HCl. After 5 months in HCl, both samples were still luminescent, as can be seen in A.6 b).

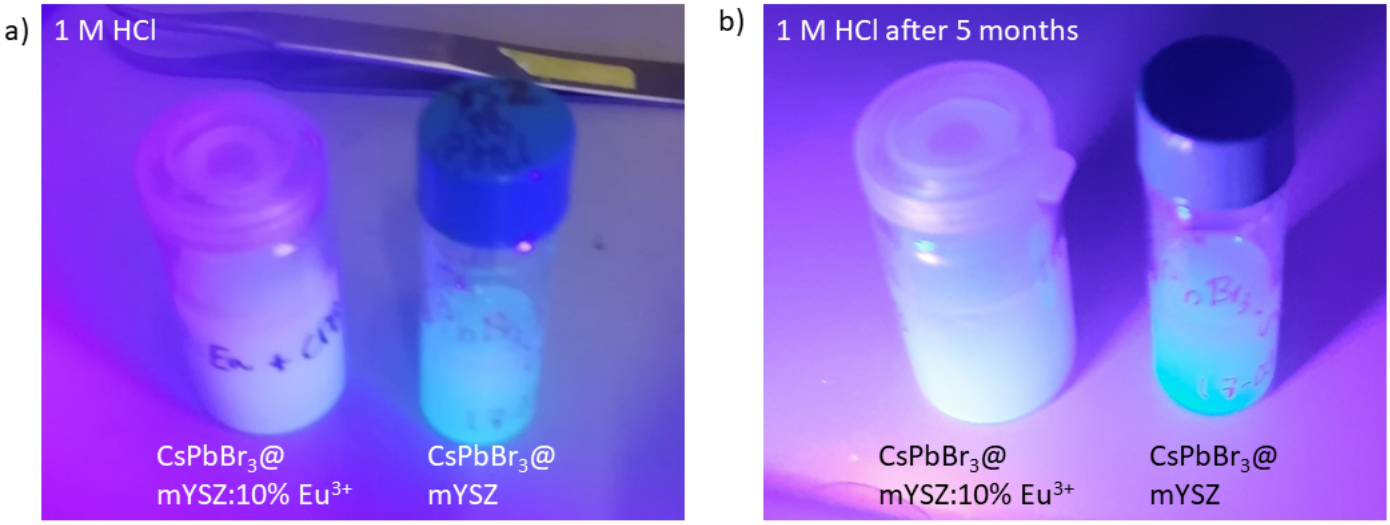

Figure A.6: Luminescence of $CsPbBr_3$@mYSZ and mYSZ:10%Eu^{3+} in HCl, a) photo of $CsPbBr_3$@mYSZ in HCl (right) and mYSZ:10%Eu^{3+} in HCl (left), b) photo of $CsPbBr_3$@mYSZ in HCl after 5 months (right) and mYSZ:10%Eu^{3+} in HCl after 5 months (left). All photos taken under ~395 nm illumination

A.7 Stability of the Eu^{3+} β-diketonate complex

This complex is stable in water, but not under illumination or heat, as the ligands will detach [55]. The PL intensity of complex was measured under ~5 W/mm^2 illumination over time, as shown in Figure A.7 a). Emission declines rapidly, but the complex also shows remarkable self-healing behavior after time in the dark. After 5 minutes in the dark emission skyrockets and saturates the detector.

Multiple encapsulation methods were used to improve the stability of the complex. An encapsulation method that could stabilize the complex was PMMA. Under illumination, stability was improved significantly (see Figure A.7 b)).

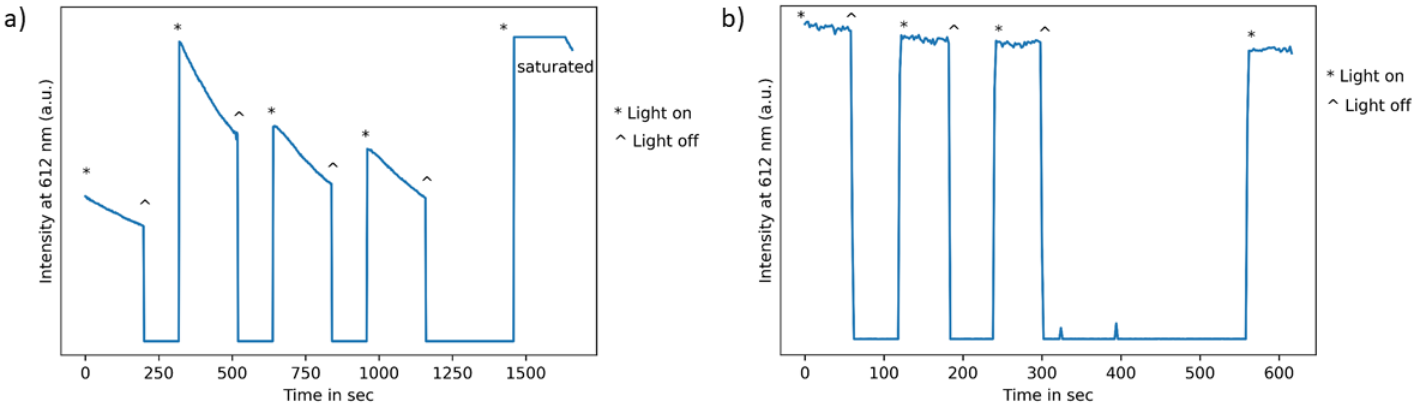

Figure A.7: a) Stability of Eu^{3+} β-diketonate complex under ~5 W/mm^2 405 nm illumination, b) Stability of Eu^{3+} β-diketonate complex encapsulated in PMMA under ~5 W/mm^2 405 nm illumination